

ABSTRACT

CRIMI, CHRISTINA MARIE. Stresses in the Cranial Cruciate Ligament Deficient Canine Stifle Following Three Tibial Osteotomy Procedures: A Finite Element Analysis. (Under the direction of Dr. Andre Mazzoleni and Dr. Ola Harrysson.)

Cranial cruciate rupture remains one of the most widely diagnosed and threatening conditions to stifle stability and rear limb function in dogs. The objective of this research was to evaluate the post-operative effects of three commonly practiced corrective surgeries for a CCL deficient canine stifle. A fully three-dimensional, anatomically accurate, quasi-static, nonlinear computer model of the left hind limb of a healthy dog was analyzed via finite element analysis. This model was then modified to simulate CCL deficiency and subsequent treatment by means of three different surgical procedures: the Tibial Plateau Leveling Osteotomy (TPLO), Tibial Tuberosity Advancement (TTA) and the Triple Tibial Osteotomy (TTO). Analysis was carried out for three stifle positions (75° , 113° , 148°) representing the normal range of motion of a large-breed dog. An increase in stress on the CaCL was apparent in flexion and in good accordance with literature and physical testing. The results of the models suggest that throughout the range of motion the TPLO increased the stress in the patellar ligament to a higher degree than did the TTA or TTO. Additionally, the TTA appeared to increase the stress of the CaCL more than the TPLO or TTO did at 75° of stifle flexion and, overall, the TTO resulted in a more consistent stress distribution. These results will give veterinary orthopedic surgeons a better understanding of the effects of these procedures on the geometry and function of the canine stifle throughout a normal range of motion.

Stresses in the Cranial Cruciate Ligament Deficient Canine Stifle Following
Three Tibial Osteotomy Procedures: A Finite Element Analysis

by
Christina Marie Crimi

A thesis submitted to the Graduate Faculty of
North Carolina State University
in partial fulfillment of the
requirements of the Degree of
Master of Science

Mechanical Engineering

Raleigh, North Carolina

2008

APPROVED BY:

Dr. Denis J. Marcellin-Little

Dr. Kara Peters

Dr. Andre P. Mazzoleni
Chair of Advisory Committee

Dr. Ola L. A. Harrysson
Co-Chair of Advisory Committee

DEDICATION

This thesis is dedicated to my husband and family. And to my Grandma and Grandpa Whelan whom I will miss very much.

BIOGRAPHY

Christina Marie Crimi was raised in Palm Harbor, FL by her parents, Ron and Clarice Montgomery. She began pursuing her engineering career at the University of Florida where she received her B.S degree in Mechanical Engineering in December 2005. She moved to North Carolina in August of 2006 to pursue her Masters degree in ME at North Carolina State University. After attaining her graduate degree she hopes to work for a company who specializes in medical manufacturing.

ACKNOWLEDGEMENTS

I would like to express my gratitude to Dr. Anke Langenbach, Dr. Tibor Lazar and Dr. Denis Marcellin-Little for their orthopedic expertise and contributions to this project. I would also like to thank my advisory committee for their support and understanding and acknowledge all the teachers and mentors throughout my life who have taken the time to answer my questions and feed my enthusiasm for learning. I would especially like to extend my thanks and appreciation to my parents, Ron and Clarice Montgomery, for their continual love, support and words of wisdom, and to my little brother, Adam, of whom I am always so proud. Above all, I would like to thank my wonderful husband, Christopher, for being my friend, my teammate and the love of my life.

TABLE OF CONTENTS

LIST OF FIGURES.....	ix
LIST OF TABLES	xvii
1. DATA PROCESSING AND MODEL DESIGN.....	1
1.1 INTRODUCTION	1
1.2 BACKGROUND INFORMATION	4
1.2.1 Cranial Cruciate Ligament Rupture	4
1.2.3 Patella Alta and Patella Baja (Infera).....	5
1.2.3 Finite Element Analysis	5
1.3 REVIEW OF LITERATURE AND RESEARCH	7
1.3.1 Anatomy of the Stifle Joint.....	7
1.3.1.1 The Stifle Ligaments, Muscles and Patellar Tendon.....	8
1.3.1.2 Joint Motion and Gait Analysis	11
1.3.1.3 The CCL deficient stifle	13
1.3.2 Patellar Articulation	15
1.3.2.1 Vertical Patellar Position	15
1.3.2.2 Patella Alta and Patella Baja (Infera).....	18
1.3.2.3 Patellafemoral Contact	19
1.3.3 Medical Imaging	20
1.3.3.1 CT technology.....	20
1.3.3.2 Concerns with CT technology.....	22

1.3.4	Finite Element Analysis	23
1.3.4.1	Modeling in Humans and Canines	23
1.3.4.2	FEA of Ligaments	26
1.3.5	Summary.....	27
1.4	STATEMENT OF THE PROBLEM.....	30
1.5	MATERIALS AND METHODS	31
1.5.1	Subject Specifics	31
1.5.2	CT to 3D Modeling: Pre-processing	31
1.5.3	Convergence Analysis & Final Mesh Preparation.....	32
1.5.5	Modeling the Meniscus	39
1.5.6	Measuring Patellar Location.....	42
1.5.7	Measuring the Stifle Angles	43
1.5.8	Ligaments	46
1.5.9	Model Assembly in ABAQUS.....	50
1.5.9.1	Material Properties and Mesh Assignment.....	51
1.5.9.2	Contact and Surface Interaction.....	55
1.5.9.3	Loads and Boundary Conditions.....	59
1.5.9.4	Testing Procedure.....	60
1.6	RESULTS.....	61
1.6.1	75 Degree Results	61
1.6.2	113 Degree Results	64
1.6.3	148 Degree Results	67

1.7	DISCUSSION.....	70
1.8	CONCLUSION.....	74
2.	SURGICAL PROCEDURES AND TESTING.....	75
2.1	INTRODUCTION	75
2.2	BACKGROUND INFORMATION	78
2.2.1	Intra-Articular and Extra-Articular Techniques.....	78
2.2.2	Tibial Osteotomy Procedures: A Novel Approach to CCL Deficiency	79
2.3	REVIEW OF LITERATURE AND RESEARCH	82
2.3.1	The Cruciate Ligaments	82
2.3.2	CCL Rupture.....	84
2.3.3	Tibial Plateau	87
2.3.3.1	Steep tibial plateaus.....	88
2.3.3.2	Tibial Plateau Measurement Concerns	89
2.3.4	Tibial Osteotomies	91
2.3.4.1	TPLO	92
2.3.4.2	TTA	100
2.3.4.3	TTO	103
2.3.5	Summary.....	104
2.4	STATEMENT OF THE PROBLEM.....	107
2.5	MATERIALS AND METHODS	108
2.5.1	Tibial Plateau Leveling Osteotomy.....	108
2.5.2	Tibial Tuberosity Advancement	111

2.5.3	Triple Tibial Osteotomy	115
2.5.4	Testing Procedure.....	119
2.6	RESULTS.....	120
2.6.1	75 Degree Results	120
2.6.2	113 Degree Results	123
2.6.3	148 Degree Results	126
2.6.4	Changes in Tibial Long Axis and Tibial Plateau Slope	130
2.7	DISCUSSION.....	132
2.7	CONCLUSION.....	136
3.	FUTURE RESEARCH	138
4.	REFERENCES	139
	APPENDICES	154
	APPENDIX A.....	155
	APPENDIX B	161

LIST OF FIGURES

Figure 1.3.1: The components of the canine stifle. Used with permission of the publisher [Carpenter, Cooper 27].....	8
Figure 1.3.2: Diagram for measuring patellar location. Used with permission from the publisher [Johnson <i>et al.</i> , 34].....	17
Figure 1.5.1: Isolation of bony structures in Mimics 11.11 [Materialise, Leuven, Belgium].....	32
Figure 1.5.2: Global remesh parameters. [Magics, Materialise, Leuven, Belgium]	33
Figure 1.5.3: Selection of femoral shaft for localized re-meshing.....	34
Figure 1.5.4: Variation of femur meshes for convergence test. (a) coarse (b) medium (c) fine.....	34
Figure 1.5.5: Load application and boundary condition for convergence test.....	35
Figure 1.5.6: Resulting stress distribution for each mesh type. (a) coarse (b) medium (c) fine.....	35
Figure 1.5.7: Final tibia mesh. Coarse tibial shaft and fine mesh around articulating surfaces.....	37
Figure 1.5.8: Boolean operation to separate phalanges at metatarsal-phalangeal joints.....	38
Figure 1.5.9: Illustration of angled proximal interphalangeal joint to 110°.....	39
Figure 1.5.10: Meniscus created using boolean operations in Magics. (a) first boolean operation (b) further removal of interior.....	40

Figure 1.5.11: Final model-ready meniscus. (a) top view of meniscus (b) meniscal boundary between articulating surfaces of tibia and femur.....	41
Figure 1.5.12: Patellar and patellar ligament lengths via two different measurement methods. (a) Lengths according to Johnson <i>et al.</i> [34] (b) Lengths according to Mostafa <i>et al.</i> [81].....	43
Figure 1.5.13: Illustration of the determination of the femoral long axis.....	44
Figure 1.5.14: Lateral view showing the original stifle angle from CT data.	45
Figure 1.5.15: Stifle orientations for models. (a) stifle angle of 75° (b) stifle angle of 113° (c) stifle angle of 148°.....	45
Figure 1.5.16: Anatomical models used to determine ligament origins and insertions. (a) dog leg model with painted attachment points (b) cadaver dog leg used to reproduce ligaments.....	46
Figure 1.5.17: Origins and insertions for all stifle ligaments. (a) caudal view (b) cranial view (c) lateral view (d) medial view.....	47
Figure 1.5.18: Measurement of the patellar ligament from CT scans. (a) craniocaudal view (b) mediolateral view.....	48
Figure 1.5.19: The creation of the CaCL in SolidWorks (Dassault Systemes S.A.). (a) using the loft feature with information from CT scans (b) final 3D CaCL.....	49
Figure 1.5.20: Caudal view of the stifle in extension with 3D ligaments attached.....	50
Figure 1.5.21: Local coordinate system for orthotropic property definitions of the hock.....	51

Figure 1.5.22: Ligament meshes for stifle angle of 113°. (a) CaCL (b) CCL (c) MCL (d) LCL (e) PL.....53

Figure 1.5.23: Views of the rigid attachment of the stifle ligaments. (a) caudal view with femur and meniscus removed (b) cranial view of intact stifle (c) medial view showing MCL.....54

Figure 1.5.24: Contact pairs and articulating surfaces. (a) patellofemoral (b) femur and meniscus (c) femur and tibia (d) meniscus and tibia (e) tibia and tarsus.....56

Figure 1.5.25: Attachment of the meniscal horns to the tibial plateau by linear springs.....57

Figure 1.5.26: Gastrocnemius and quadriceps muscles modeled as linear springs.58

Figure 1.5.27: Final assembly of model with muscles, ligaments, and attachment springs....59

Figure 1.5.28: Application of a concentrated compressive load to the femoral head.....60

Figure 1.6.1: Visual stress output of the PS Intact stifle ligaments at 75°. From left to right: CaCL, LCL, MCL, PL, CCL.....61

Figure 1.6.2: Several images of the PS Intact stifle joint with ligaments in place at 75°.....61

Figure 1.6.3: Visual stress output of the PS transected stifle ligaments at 75°. From left to right: CaCL, LCL, MCL, PL.....62

Figure 1.6.4: Several images of the PS transected stifle joint with ligaments in place at 75°62

Figure 1.6.5: Graph of stress (MPa) in each of the ligaments of the PS intact and PS transected models at a stifle angle of 75°63

Figure 1.6.6: Visual stress output of the PS Intact stifle ligaments at 113°. From left to right: CaCL, LCL, MCL, PL, CCL.....64

Figure 1.6.7: Several images of the PS Intact stifle joint with ligaments in place at 113°...	64
Figure 1.6.8: Visual stress output of the PS transected stifle ligaments at 113°. From left to right: CaCL, LCL, MCL, PL, CCL.....	65
Figure 1.6.9: Several images of the PS transected stifle joint with ligaments in place at 113°.....	65
Figure 1.6.10: Graph of stress (MPa) in each of the ligaments of the PS intact and PS transected models at a stifle angle of 113°.....	66
Figure 1.6.11: Visual stress output of the PS Intact stifle ligaments at 148°. From left to right: CaCL, LCL, MCL, PL, CCL.....	67
Figure 1.6.12: Several images of the PS Intact stifle joint with ligaments in place at 148°...	67
Figure 1.6.13: Visual stress output of the PS transected stifle ligaments at 148°. From left to right: CaCL, LCL, MCL, PL, CCL.....	68
Figure 1.6.14: Several images of the PS transected stifle joint with ligaments in place at 148°.....	68
Figure 1.6.15: Graph of stress (MPa) in each of the ligaments of the PS intact and PS transected models at a stifle angle of 148°.....	69
Figure 2.3.1: Illustrations of the conventional TPS measurement method and that proposed by Baroni, Marcellin-Little <i>et al.</i> Used with permission from the publisher [12].....	90
Figure 2.3.2: Schematic showing tibial axial rotation. Used with permission from the publisher [Warzee <i>et al.</i> , 121].....	95

Figure 2.3.3: Chart showing change in osteophyte score over six months. Used with permission from the publisher [Rayward <i>et al.</i> , 90].....	98
Figure 2.5.1: Tool used to Boolean a 30mm radial cut from the proximal tibia.....	108
Figure 2.5.2: Ventral rotation of the proximal tibia by 12mm.....	109
Figure 2.5.3: CCL deficient rear limb with TPLO corrective surgery at various stifle angles. (a) stifle angle of 75° (b) stifle angle of 113° (c) stifle angle of 148°.....	110
Figure 2.5.4: Medial view of TPLO procedures for comparison. (a) physical RP model [30] (b) FEA model.....	111
Figure 2.5.5: Boolean tool used to create tibial crest osteotomy on the proximal tibia.....	111
Figure 2.5.6: Proximal advancement of the tibial tuberosity with 9mm cage.....	112
Figure 2.5.7: TTA procedure and hardware. (a) physical RP model (b) FE model.....	113
Figure 2.5.8: Tie constraint added to distal plate to rigidly attach it to the tibial body.....	114
Figure 2.5.9: TTA procedure and ligament attachments at various stifle angles. (a) 75° (b) 113° (c) 148°.....	114
Figure 2.5.10: Boolean tool used to create tibial crest osteotomy.	115
Figure 2.5.11: Performing a wedge osteotomy of FE models in software. a) boolean tools for cutting the 19° wedge b) boolean operation with wedge tool.....	116
Figure 2.5.12: TTO procedure on FE model with 19° wedge osteotomy and a tibial crest osteotomy of 60mm in length.....	117
Figure 2.5.13: TTO performed on two different models. (a) RP model [30] (b) FE model	118

Figure 2.5.14: Assembled TTO models at three stifle angles. (a) 75° (b) 113° (shown here without surface interactions) (c) 148°.....	118
Figure 2.6.1: Visual stress output of the TPLO ligaments at 75°. From left to right: CaCL, LCL, MCL, PL.....	120
Figure 2.6.2: Several images of the TPLO stifle joint with ligaments in place at 75°.....	120
Figure 2.6.3: Visual stress output of the TTA stifle ligaments at 75°. From left to right: CaCL, LCL, MCL, PL.....	121
Figure 2.6.4: Several images of the TTA stifle joint with ligaments in place at 75°.....	121
Figure 2.6.5: Visual stress output of the TTO stifle ligaments at 75°. From left to right: CaCL, LCL, MCL, PL.....	121
Figure 2.6.6: Several images of the TTO stifle joint with ligaments in place at 75°.....	122
Figure 2.6.7: Graph of stress (MPa) in each of the ligaments at a stifle angle of 75°.....	122
Figure 2.6.8: Visual stress output of the TPLO ligaments at 113°. From left to right: CaCL, LCL, MCL, PL.....	123
Figure 2.6.9: Several images of the TPLO stifle joint with ligaments in place at 113°.....	124
Figure 2.6.10: Visual stress output of the TTA stifle ligaments at 113°. From left to right: CaCL, LCL, MCL, PL.....	124
Figure 2.6.11: Several images of the TTA stifle joint with ligaments in place at 113°.....	124
Figure 2.6.12: Visual stress output of the TTO stifle ligaments at 113°. From left to right: CaCL, LCL, MCL, PL.....	125
Figure 2.6.13: Several images of the TTO stifle joint with ligaments in place at 113°.....	125
Figure 2.6.14: Graph of stress (MPa) in each of the ligaments at a stifle angle of 113°.....	126

Figure 2.6.15: Visual stress output of the TPLO ligaments at 148°. From left to right: CaCL, LCL, MCL, PL.....	127
Figure 2.6.16: Several images of the TPLO stifle joint with ligaments in place at 148°.....	127
Figure 2.6.17: Visual stress output of the TTA stifle ligaments at 148°. From left to right: CaCL, LCL, MCL, PL.....	127
Figure 2.6.18: Several images of the TTA stifle joint with ligaments in place at 148°.....	128
Figure 2.6.19: Visual stress output of the TTO stifle ligaments at 148°. From left to right: CaCL, LCL, MCL, PL.....	128
Figure 2.6.20: Several images of the TTO stifle joint with ligaments in place at 148°.....	128
Figure 2.6.21: Graph of stress (MPa) in each of the ligaments at a stifle angle of 148°.....	129
Figure 2.6.22: Pre-surgical tibial plateau slope.	130
Figure 2.6.23: Tibial slope and long axis shift resulting from the TPLO procedure.....	130
Figure 2.6.24: Tibial slope and long axis shift resulting from the TTO procedure.	131
Figure A.1: Mesh quality and appearance of the patella.	155
Figure A.2: Meshed hock with 110° proximal interphalangeal joint.....	155
Figure A.3: Final meshed meniscus after boolean operations, shrink-wrap and remeshing	156
Figure B.1: Mediolateral radiograph of physical model used for TPLO pre-surgical planning [30].....	161
Figure B.2: Mediolateral radiograph of extended stifle and TTA plate template (Kyon)	162
Figure B.3: TTO cutting jig used to perform the tibial crest osteotomy.....	162

Figure B.4: Resulting TTO, secured with 3.5mm broad TPLO plate (Synthes, Inc.).....163

LIST OF TABLES

Table 1.5.1:	Mesh information and output maximum stresses.....	36
Table 1.5.2:	Final mesh information for hind leg components.....	41
Table 1.5.3:	Linearly elastic, orthotropic properties for the human femur and tibia [38]...	52
Table 1.5.4:	Neo-Hookean constants for ligament property definitions, from literature [113].....	53
Table 1.6.1:	Table of the percent difference between the PS intact model and the PS transected model at a stifle angle of 75°.....	63
Table 1.6.2:	Table of the percent difference between the PS intact model and the PS transected model at a stifle angle of 113°.....	66
Table 1.6.3:	Table of the percent difference between the PS intact model and the PS transected model at a stifle angle of 148°.....	69
Table 2.6.1:	Table of the percent difference between the PS intact model of the stifle and the other models at 75°.....	123
Table 2.6.2:	Table of the percent difference between the PS intact model of the stifle and the other models at 113°.....	126
Table 2.6.3:	Table of the percent difference between the PS intact model of the stifle and the other models at 148°.....	129
Table A.1:	Comparison of coarse and medium meshes to the finest mesh.....	155
Table A.2:	Ligament geometry obtained from CT data.	156

Table A.3:	Stress (MPa) in each of the modeled ligaments of the PS intact and PS transected stifle joints at an angle of 75°	156
Table A.4:	Stress (MPa) in each of the modeled ligaments of the PS intact and PS transected stifle joints at an angle of 113°	157
Table A.5:	Stress (MPa) in each of the modeled ligaments of the PS intact and PS transected stifle joints at an angle of 148°	157
Table A.6:	Stress (MPa) in each of the modeled ligaments at a stifle angle of 75°	157
Table A.7:	Stress (MPa) in each of the modeled ligaments at a stifle angle of 113°	158
Table A.8:	Stress (MPa) in each of the modeled ligaments at a stifle angle of 148°	158
Table A.9:	Displacement measurements between tibia and femur nodes for all models	159
Table A.10:	Final calculations for subluxation measurements.....	160
Table A.11:	Guide for determining any present subluxation based on values in Table A.10.....	160
Table B.1:	Excerpt of TPLO ventral rotation guide for TPA of 25°-30° [30].....	161

1. DATA PROCESSING AND MODEL DESIGN

1.1 INTRODUCTION

The stifle is possibly the most complex joint in the dog, depending on the collective efforts of several major ligaments, muscle groups, cartilaginous fiber materials and a host of other components. One of the main stifle ligaments, the cranial cruciate ligament (CCL), plays a significant role in providing functional stability to the canine stifle joint. Several research experiments have concluded that the cranial cruciate ligament is the primary component opposing cranial tibial thrust and aids in limiting tibial internal rotation and hyperextension of the stifle [25,27,33,121]. Rupturing of the CCL, however, remains one of the most common orthopedic conditions in dogs and afflicts a wide range of weights and breeds. In the CCL-deficient stifle, the joint is subjected to a severely destabilizing cranial tibial shear force with no mechanism to act as the resistive component. Cranial cruciate disease is a degenerative condition which can lead to serious complications such as osteoarthritis, meniscal injury and severe rear limb lameness [8,45,54].

Despite being one of the most widely examined and researched joints in the dog, there is still much to be discovered about the canine stifle. Much of what is used today to evaluate stifle joint mechanics still comes from analysis of human anatomy. Although certain aspects of mammalian anatomy and function are similar, species-specific studies would help to fill the extensive gap of knowledge regarding canine joint mechanics and material properties. With

the advent of advanced medical imaging techniques, such as Computed Tomography, a more thorough knowledge of both normal and afflicted stifle anatomy is possible.

A number of experimental studies have been done to describe the forces, strains and failure of stifle ligaments and surrounding components. Experimental studies, however, are inherently complicated and carry several limitations. A noteworthy alternative is the use of computer models and, in particular, finite element analysis. FEA allows a three-dimensional structure to be analyzed and the mechanical response to be visualized anywhere within the model. Several finite element models have been developed for human anatomy and this method has been equally useful in estimating the mechanical response of certain canine joint structures, such as meniscal response, that are difficult or impossible to measure by other means. However, there remain very few fully three-dimensional models of the canine knee and several issues that would benefit from the implementation of such technology.

The purpose of this study was to create an anatomically accurate, three-dimensional finite element model of the canine hind limb, loaded by physiologic forces that affect it during weight bearing, and to determine the stress distribution in an intact and CCL deficient stifle. Finite element analysis has been utilized by several researchers and proves to be an efficient tool for predicting joint kinematics for given parameters [38,83]. In addition, FEA is much more cost effective and repeatable than in vivo or in vitro experimentation. Analysis of these models will provide data regarding ligament behavior, contact interaction and stifle joint

mechanics that are at this time unavailable to veterinary orthopaedic surgeons, engineers and researchers.

The accuracy of the finite element model depends heavily on the given physical parameters and initial conditions. Therefore, reliable material properties, boundary conditions and constraints and applied loads are necessary to produce reliable outputs. Adequate validation of finite element models has been attained by several means including comparison with literature and cadaveric experiments. This study combines literature comparison and a more modern approach for validating the computer model. Various components of the FE model of this project will be validated with a physical model from a parallel research experiment based on the same CT data used to produce the FE model [Crimi CS, 30]. A model with an intact stifle and one with a CCL deficient stifle will be tested and the geometric data gathered from testing will help provide a sound comparison for the results of the finite element analyses.

Cranial cruciate rupture remains one of the most widely diagnosed and threatening conditions to stifle stability and rear limb function. While several research projects have been done on the human knee joint, very little has been done on modeling the canine stifle using finite element analysis. Furthermore, no known studies have modeled the entire canine limb including all major ligaments, muscles and bony structures or determined the effects of cranial cruciate deficiency to the level of detail proposed by this project. Understanding this condition and its effect on joint mechanics will aid in injury prevention and future efforts to develop new methods of treatment for ligament rupture.

1.2 BACKGROUND INFORMATION

1.2.1 Cranial Cruciate Ligament Rupture

The canine stifle joint is a complex, synovial joint allowing motion in three planes. Due to its complexity and the cooperation of all of the ligaments, muscle groups, cartilage and bony structures, treatment of injury to any of its components becomes an involved, complicated task. The cruciate ligaments are particularly important to joint function, acting as constraints of craniocaudal motion. The cranial cruciate ligament prevents cranial displacement of the tibia and limits excessive internal tibial rotation. It also aids in preventing hyperextension of the joint [8]. The caudal cruciate ligament prevents caudal tibial translation and also helps to limit tibial internal rotation.

There is a high prevalence of CCL insufficiency among dogs. The economic impact of treating dogs with CCL insufficiency in the US was projected at just over \$1 billion in 2003 [57]. Diagnosis of complete CCL rupture is made by detection of joint laxity, seen as craniocaudal instability after applying a cranially directed load on the proximal tibia. Other methods have also been developed to test for ligament insufficiency. Cruciate ligament injury can be related to their function and possibly caused by excessive loads during extreme conditions or actions. Complete rupture of the CCL has been shown to cause progression of degenerative joint disease, meniscal injury, joint instability and is one of the largest sources of chronic rear limb lameness in dogs.

1.2.3 Patella Alta and Patella Baja (Infera)

The location of the patella within the trochlear groove plays an important role in canine stifle joint stability [34,49,55,61,81]. A patella that is displaced too proximally, known as patella alta, loses the buttressing effect of the trochlear groove and will be more prone to luxation [34,55,61]. Conversely, studies have shown that a patella located too distally, known as patella baja (infera), is associated with chondromalacia, a degenerative condition afflicting the articular cartilage of the caudal surface of the patella [61]. The issue of patellar location has historically been focused on human subjects, however, extrapolating the findings to dogs must be done with caution because of the species-specific anatomy. Due to the fact that the canine stifle is the most frequently afflicted joint of the dog, the issue of patellar location with respect to the trochlear groove is of clinical importance and in need of further research.

1.2.3 Finite Element Analysis

There are generally two types of analysis that are used in industry and research: 2-D modeling, and 3-D modeling. Two-dimensional modeling allows for simple analyses that are computationally efficient. However, 2-D models tend to yield less accurate results due to assumptions and over-simplifications. Three-dimensional computer modeling produces more accurate results while sacrificing the ability to run on all but the fastest computers effectively. Both linear and nonlinear analyses can be run on most available FEA packages. Linear systems are far less complex and generally don't account for plastic deformation. Nonlinear systems include plastic deformation, and many also can determine fracture of the material. Finite element analysis implements a complex system of nodes that make up a

mesh. The meshed model can then be programmed with material and structural properties which define how it will react to certain loading conditions. Nodes and subsequent mesh sizes are assigned depending on the anticipated stress levels of a particular region. There are various types of analyses one can perform. The most often used is structural analysis which consists of linear (simple parameters and no plastic deformation) and nonlinear (materials stressed past their elastic capabilities) models. Finite element is currently used in several industries and research environments to determine material behavior, assist in the development of new products and make design modifications or verify an existing design based on structure performance predictions.

1.3 REVIEW OF LITERATURE AND RESEARCH

Advancements in medical technology and computer software have helped researchers make significant strides in modeling and predicting joint behavior. What has long been difficult to visualize is becoming tangible and thus more comprehensible. This section presents a brief overview of the research and literature related to stifle joint mechanics as well as the data processing and model design aspects of this thesis. The literature on this subject is expansive so a concentrated selection of significant work was chosen to provide a clear understanding of imaging techniques, useful technological tools, related anatomical issues and advancements in computer and physical modeling.

1.3.1 Anatomy of the Stifle Joint

The canine stifle joint has been the focus of much orthopedic interest in the veterinary community, the biomechanics of which has been the subject of many recent investigations. Determining how the different components of the stifle are loaded during various activities is important for the understanding of normal joint function as well as gaining insight into the mechanisms responsible for common injuries such as cranial cruciate ligament rupture [103]. To properly correct an injury to any component of the stifle joint by returning normal stifle motion and minimizing further degeneration, an understanding of the normal anatomy of the entire stifle is essential [27].

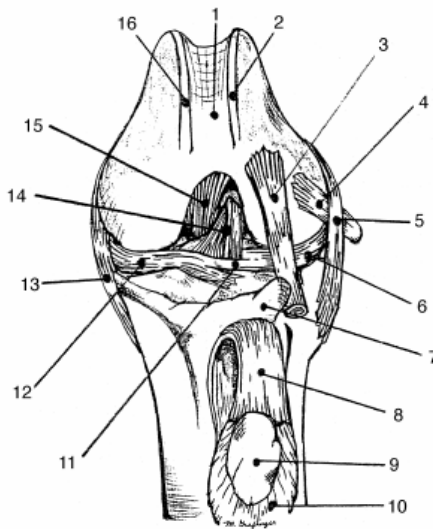


Fig. 1. Cranial view of the left stifle showing associated ligaments and structures. 1, femoral trochlea; 2, lateral ridge of femoral trochlea; 3, tendon of long digital extensor; 4, tendon of popliteus; 5, lateral collateral ligament; 6, lateral meniscus; 7, tibial tuberosity; 8, patellar ligament; 9, patella; 10, parapatellar fibrocartilage; 11, intermeniscal ligament; 12, medial meniscus; 13, medial collateral ligament; 14, cranial cruciate ligament; 15, caudal cruciate ligament; 16, medial ridge of the trochlea.

Figure 1.3.1: The components of the canine stifle. Used with permission of the publisher.

[Carpenter, Cooper 27].

The following sections outline some of the most prominent work regarding the biomechanics and function of the stifle joint as well as its reaction to one of the most frequently occurring orthopedic conditions: cranial cruciate ligament rupture.

1.3.1.1 The Stifle Ligaments, Muscles and Patellar Tendon

There are four primary ligaments critical to stifle joint stability [25,27]. These are the cranial cruciate, caudal cruciate, medial collateral, and lateral collateral ligaments. The combined forces of the two main muscles groups (quadriceps and gastrocnemius) are also responsible

for joint articulation and stability during weight bearing. The biomechanical properties of the stifle ligaments are crucial to their function and thus the focus for many experimental studies. Through a 3-dimensional mathematical model, Shahar and Banks-Sills described the variation in forces in the various ligaments of the intact stifle during the stance phase of a slow walk [103]. They determined that the cranial cruciate ligament is loaded throughout most of the stance phase and reaches a peak at about 40% of this phase. Peak loading for the other ligaments, such as the lateral collateral ligament, were also determined. According to this study, the medial collateral and caudal cruciate ligaments are not loaded at all during the stance phase of a slow walk. In the CCL-transected model the LCL is loaded throughout the stance phase, the caudal is loaded throughout the first 70% of the stance phase and the MCL is not loaded. At the time of this study, there were no in vivo measurements of joint reaction forces or stifle ligament forces to compare their results. The authors stated that many of their assumptions oversimplified the model which may have produced results that do not represent the true physiology of the canine stifle. Later studies confirmed that their estimation of ligament behavior, especially the collateral ligaments, during the stance phase was inaccurate. Vasseur and Arnoczky examined the collateral ligaments in cadaveric canine stifles and determined that the MCL was taut in extension and only partially lax during flexion [120]. Also, the LCL was found to be only engaged (taut) during extension and completely lax when the joint was flexed. Both ligaments were found to play an integral role in the rotational behavior of the joint, working together to prevent varus-valgus angulation in extension and allowing internal tibial rotation during flexion. These conclusions are similar to studies on the collateral ligaments of human knee joints [71,123].

In situ forces and strains have been measured, though inconsistently, for the human knee and very little has been done with respect to canines. Monahan *et al.* measured the strains of all of the canine stifle ligaments *in vivo* by use of mercury strain gages [77]. Each ligament, however, was measured from a different dog due to strain gage attachment issues. Combined with other uncertainties pertaining to gage function and reliability, their results may not be entirely accurate or consistent. Their study also included only varus-valgus loading and did not take into account muscle contraction. Mathematical models, such as that proposed by Blankevoort and Huiskes [19], provide additional insight into the ligament forces and joint mechanics for certain ranges of motion. These models also significantly simplified the complex anatomy of the knee joint but, as the model by Blankevoort and Huiskes showed, can still realistically simulate characteristics of joint biomechanics. For their study, the geometry and function of the menisci was not included which led the authors to believe the resulting ligament forces were overestimated.

Several research studies have been done on the properties of the patellar tendon because it has been used as a graft for replacing ruptured cranial cruciate ligaments in the past. A study by Cabaud *et al.* analyzed the effects of removing a section of the patellar ligament for placement as an artificial CCL [24]. Their study showed the collagen fibers of the tendon to be normal after surgery and that the strength and stiffness in the host tendon actually increased. Burks *et al.* showed contradictory results and a decrease in similar parameters [21]. Linder *et al.* followed a procedure similar to Burks *et al.* and determined that removal of the medial third of the patellar tendon in dogs caused a decrease in stiffness, failure load

and modulus as well as a significant difference when compared with control tendons [66]. Shahar and Banks-Sills assumed in their mathematical model that the patellar ligament was inextensible based on the geometric properties of being much stiffer and thicker than the other knee ligaments [103]. Some have disagreed with this assumption, but Johnson *et al.* determined through physical testing and comparison between ratios of ligament to patellar length that this is a reasonable assumption from 75° of flexion to 148° of extension [34]. Their study only included 13 dogs, however, and solely from large-breeds.

Studies on the meniscus and articular cartilage have also been reported. In a study by Jurvelin *et al.*, a variation of Poisson's ratio of the articular cartilage in the canine knee joint was identified [56]. Donahue *et al.* showed that the tibiofemoral contact pressure was highly sensitive to the circumferential, axial and radial modulus of the menisci as well as the horn stiffness [37]. This information may be influential in the accuracy of advanced models of the stifle joint in that an invalid attachment of the menisci may cause contact and joint motion predictions to be erroneous.

1.3.1.2 Joint Motion and Gait Analysis

Kinematics help describe features of normal motion of the dog during activities such as walking. It has also been useful in identifying changes in joint motion and elucidating anomalies in joint composition [40,68]. Several different techniques have been used in research. Feeney *et al.* investigated the variability and reliability in 2-dimensional kinematic analysis of digitized tapes as a possible diagnostic tool in clinical settings [40]. They found

that this method offered acceptable intra- and inter-observer repeatability for both the normal gait and sit-to-stand motions. Reliabilities were highest for the lower limb joints (carpal, tarsal and stifle) because of more easily identifiable markers. This study did not provide insight into the neck motion during these activities as potential head movement caused their measurements to be unreliable. They were not able to measure accuracy directly but had good agreement with other studies on the joint motion of the hind limb joints. Dogs with clinical lameness were not assessed so there was no conclusion as to whether this method would be helpful in identifying clinical lameness.

Goniometry is another tool widely used to evaluate joint motion in dogs. This measurement technique was validated in a study by Jaegger, Marcellin-Little and Levine [51]. Measurements using a universal plastic goniometer were not significantly different to radiographic measurements. Sedation was also found to have little influence on the joint position. Only Labrador Retrievers were tested and the authors cautioned against potential invalidity of the results if extrapolated to dog breeds with significantly different structure. A study on the comparison of electrogoniometry and the common universal plastic goniometer (UG) found that the use of an electrogoniometer (EG) results in higher variability as compared to both UG and radiographic measurements for a majority of the joint positions tested [117]. Measurements taken with an EG were significantly different for the carpus (when in flexion) and the elbow (in both flexion and extension) joints. Intra-observer variability was concluded to be of low impact to the variability of the different methods. Only German Shepherds were tested but comparison to measurements obtained for Labrador

Retrievers [51] suggested that significant differences for certain joint measurements existed and might be attributable to differences in joint shape, muscle mass and general biomechanics.

Marsolais *et al.* provided information for joint range of motion and limb motion for dogs during swimming [68]. Significant differences were detected for extension and flexion capabilities of the lower limb joints, such as the hip and stifle, as compared with slow or fast walking and an overall increase in the range of motion during swimming was concluded. The authors extended this study to dogs that had undergone extracapsular stabilization treatment for CCL rupture and found that those dogs also had an increased range of motion during swimming. This, as the authors proposed, suggests that swimming may be beneficial during rehabilitation after surgical treatment.

1.3.1.3 The CCL deficient stifle

Since the first clinical attempts to surgically rectify the cranial cruciate ligament deficient stifle in 1952, this orthopedic condition has received more attention than any other musculoskeletal problem in the dog [8]. The surgical treatment for CCL rupture continues to be a subject of investigation in the veterinary and research communities. The purpose of this section is to review the literature regarding cranial cruciate ligament rupture and its impact on the stifle joint.

In a paper regarding CCL rupture, Hayashi *et al.* report that the cellular changes in the canine ruptured CCL are associated with extensive disruption of the ligamentous matrix.

Progressive mechanical overloading is also apparent and there was no correlation found between these changes and variables such as age, sex, body weight, or duration of lameness [45]. Other studies have suggested, however, that characteristics such as breed, age and existence of conformational abnormalities are risk factors for developing cranial cruciate disease [54].

Slocum and Slocum were the first to describe a more active model of the biomechanics of the canine stifle incorporating not only the ligaments, but also the forces created during weight bearing as well as the musculature of the pelvic limb [109]. This was the first model to recognize the force called cranial tibial thrust. They determined that the magnitude of this thrust is dependent on both the tibial compression during weight bearing as well as the slope of the tibial plateau. This means of describing the biomechanical function of the canine stifle has assisted veterinary surgeons in understanding both intact and CCL deficient stifles. In this paper, Slocum and Slocum also confirmed that hyperextension of the stifle deforms the CCL to the point of injury.

Schwandt *et al.* compared the angles between the patellar ligament and the tibial plateau in canine stifle joints with an intact CCL as well as those suffering from a ruptured CCL. Their study focused only on partial CCL rupture. They found that larger patellar tendon angles exist in stifles with a partially ruptured CCL as compared to those with an intact CCL. They also determined that a greater shear force affects the CCL in stifle joints with partial ruptures [98]. Ralphs and Whitney detected a positive correlation between complete rupture in the

CCL and medial meniscal damage [89]. Lateral meniscal injuries as a result of CCL injury were also evident and may be more commonly associated with CCL injury than previously recognized.

Using computer assisted kinematic gait analysis, DeCamp *et al.* demonstrated that the movement of the coxofemoral, tarsal and femorotibial joints during the normal canine gait are affected by cranial cruciate ligament rupture [35]. Another gait analysis was done by Tashman *et al.* and they confirmed that a cranial tibial translation as well as instability increased immediately after loss of CCL. They confirmed a degradation of these changes with an increase in duration of lameness [114].

1.3.2 Patellar Articulation

Patella alta has been considered a significant cause of recurrent dislocation of the patella [49,55,61,81]. Thus, the issue of patellar location within the trochlear groove is of clinical importance and in need of further research as it pertains to the canine stifle.

1.3.2.1 Vertical Patellar Position

In 1971 Insall and Salvati developed a method for defining patellar position by relating the greatest diagonal length of the patella to the length of the patellar ligament [50]. They found that in human subjects this ratio is approximately 1.0 in the normal knee joint and that a deviation of 0.2 or more represents an abnormal patellar position. The calculation was found to be easy to make and independent of the degree of knee flexion. Miller *et al.* applied this

method to sagittal MR images of the fully extended knee and found it to be a reliable method [74]. Blackburne *et al.* later developed another method for determining patellar height in humans by defining the ratio of the articular patellar length to the height of the distal pole of the patella above the tibial plateau [17]. They claim this method removes the variability resulting from the tibial tubercle not being a standard distance below the tibial plateau. A study by Berg *et al.* compares these two methods and others to determine which is the most reliable and reproducible method of measuring patellar height in humans [16]. They found the method by Blackburn *et al.* to be the most reproducible in a study of 15 patients measured by 3 observers. A similar study by Seil *et al.* also compared several patellar height ratios and recommended the Blackburne-Peel method because of its low inter-observer variability and ability to discriminate between patella alta, baja, and norma [99].

One cause for concern in attempting to extend the aforementioned methods to dogs is that they do not precisely relate the location of the patella to the trochlear groove over a range of angles. Additionally, they were not specifically designed to account for procedures which alter the tibial tubercle as it relates to the tibial plateau in the canine stifle. After using a variation of the Insall-Salvati method to verify that the patellar ligament is inextensible in canines over a passive range of motion, Johnson *et al.* developed a method that relates the proximal and distal aspects of the patella to its location within the trochlear groove (Figure 1.3.2) [34].

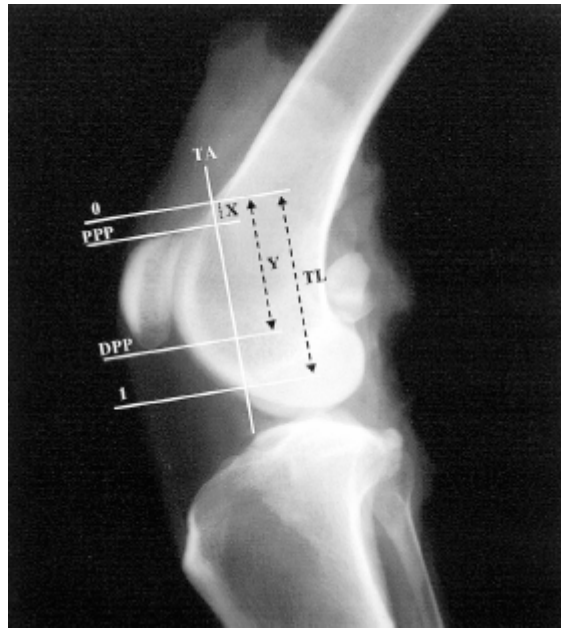


Figure 1.3.2: Diagram for measuring patellar location. Used with permission from the publisher [Johnson *et al.*, 34].

Although more precise in relating the patellar position within the trochlear groove, this new method was involved and time consuming to perform. Extrapolating data between patients was technically difficult due to the fact that the technique required a precise angle of examination and that the proximal and distal aspects of the trochlear groove may be defined differently between subjects. Their stifle joint angle measurement method was close to the measurement method used in a gait analysis study by both Hottinger *et al.* [47] and Feeney *et al.* [40]. Thus, the extrapolation of kinematic analysis angles to anatomic angles was logical and the comments regarding the 96° to 148° range at a trot also appeared to be logical.

In another paper by Mostafa *et al.*, a similar method for defining patellar height in canines was used. The authors defined a ratio between the greatest length of the patella and the length of the patellar ligament from the most proximal extent of the tibial tuberosity to the distal aspect of the patella [81]. They covered a region of flexion from 43 to 134 degrees and found an association between medial patellar luxation (MPL), patella alta, and an increased length of the patellar ligament. The patellar ligament length in was only constant throughout a relatively limited portion of the range of motion (70 - 110°) with a maximal value occurring at approximately 90°. They provided an equation to allow for correction of the ligament length based on joint angle. For their study, an unconventional method for measuring stifle angles was used, relying on limited measurements of the distal portion of the femur and proximal portion of the tibia, due to the fact that they did not have complete radiographs of the legs. Consequently, the angles in the Johnson *et al.* and Mostafa *et al.* studies are not analogous. Compared with the widely recognized measurement methods stated by Jaegger *et al.* [51], the measurement method by Johnson *et al.* would overestimate the stifle joint angle and Mostafa *et al.* would underestimate these angles. Thus, when Mostafa *et al.* report that the patellar ligament has statistically constant length between 70° and 110°, they may be reporting a range of 80° to 120° if they had used the method by Johnson *et al.*

1.3.2.2 Patella Alta and Patella Baja (Infera)

Most of the research on patella alta and patella baja that exists has been performed on human subjects. According to Lancourt and Cristini, patella alta may be a contributing factor to patellar luxation and chondromalacia [61]. Using the Insall-Salvati (IS) method, they

measured patellar position in four separate groups of patients: those with no history or complaints of knee joint pain, those with chondromalacia, those with dislocating patellae, and those with apophysitis of the tibial tubercle. They found a statistically significant difference between the IS ratios of the four groups suggesting a link between patellar position and the aforementioned complications.

Johnson *et al.* relate the ratio of the patellar length to patellar ligament length and define it as 1.71 ± 0.02 (mean \pm SEM) in the clinically normal canine stifle of large breed dogs [55]. The authors further define a ratio greater than 1.97 to signify patella alta and a ratio less than 1.45 to signify patella baja. In the case of patella alta, the proximally located patella may lose the buttressing effect of the trochlear groove and thus be more susceptible to dislocation [34,55]. Further research pertaining to canine patellar luxation is needed and no reports have shown the effects of cruciate rupture or repair on patellar position in dogs.

1.3.2.3 Patellafemoral Contact

There have been several studies aimed at evaluating the role and significance of patellofemoral stabilizing components [39,52]. It is believed that any abnormality in factors such as patellar geometry, magnitudes and line of action of the quadriceps muscles, tibial rotation, etc. may lead to anomalies in the patellofemoral contact or patellar movement [52]. Jafari *et al.* [52] investigated the significance of structures such as the trochlear groove and medial and lateral retinacula on the shift and tilt of the patella in humans. Their study was restricted to two dimensions and a system of nonlinear equations based on actual geometry

with several assumptions such as a fixed femur. The results identified that differences in geometry from a normal trochlear groove have an effect on the patellar movement and cause excess tilt and rotation. Likewise, a drastic increase or decrease of quadriceps tension also had a noticeable effect on the patella. For all the combinations of trochlear groove anatomy and quadriceps force, however, no combination resulted in patellar subluxation or dislocation. Their results showed also that the retinacula, especially the medial, play a significant role to patellofemoral stability under tension from the quadriceps muscles. A study by Elias *et al.* concurred that the choice of quadriceps force distribution plays an important role in the patellofemoral biomechanics [39]. Due to the assumptions and simplifications of this research, the results should only be taken as a basic estimation. Patellofemoral articulation is a notable topic and in need of further research, especially in regards to the dog.

1.3.3 Medical Imaging

Modern medical imaging technology is used extensively in both clinical context and scientific research. Machines such as Magnetic Resonance Image (MRI), X-ray and Computed Tomography (CT) give physicians more ability to examine and diagnose a patient while giving researchers a better understanding and greater accessibility to the body.

1.3.3.1 CT technology

While several devices exist, such as those mentioned earlier, improved diagnostic capabilities of Computed Tomography (CT) make it one of the most valuable and frequently used

research tools in the medical and engineering fields. Computed tomography was first introduced in the 1970's, but has only more recently begun to be used for preventative medicine because of significant improvements to scanning technology. The introduction of helical scanning and, most recently, multi-slice technology has transformed the CT from a transaxial imaging mechanism to a fully three-dimensional technique, capable of yielding high quality images that one can manipulate through computer post-processing [88,96,107]. Moeller *et al.* [76] also promotes the use of the CT as “one of the two modalities that have the greatest practical importance in modern sectional imaging” and, similar to Prokop *et al.*, attributes its importance to the high resolution and quality of the images [88]. It has been said that CT technology may have a hand at revolutionizing other forms of medical imaging such as virtual endoscopy, colonography, angiography and cardiac imaging [76,88,107]. This is supported by the continual revisions and updates on related publications and manuals. This prediction and enthusiasm is by and large based on the most modern of CT technology: the multi-slice scanner.

While older models such as helical CT remain in high use worldwide, multi-slice CT is the forerunner in this area of medical imaging technology and has the capability of higher quality images, faster scanning time, more flexibility and comfort for the patient and overall a “more pronounced clinical impact” over helical scanning [94,107]. Multi-slice CT scanners are similar to their predecessors but contain more than one detector ring, with up to 64 rows in the latest generation of scanners [94].

1.3.3.2 Concerns with CT technology

There are those who agree with Silverman [107] and are confident that CT technology will continue to evolve and improve the medical imaging community with possible advancements like appreciably faster scanners and wholly volumetric scanning acquisitions. There are others, however, who believe the future of medical imaging lies elsewhere. An update on the policy implications of the CT scanner mentions that the Federal Government is not contributing significantly any longer to the R&D of CT technology [86].

Radiation dosage associated with high resolution CT scanning continues to be a controversial issue [96]. Since concerns regarding this issue were first raised, back in the 1990s, several surveys and studies have been done to quantify the amount of radiation the patient receives during scanning. Although it has replaced some techniques that use higher radiation exposures, CT is still a relatively high dose modality. According to both Reiser and Kachelriess, radiologists are focused on image quality, which is a function of dose, so CT images are often achieved using high radiation exposure which frequently goes unnoticed by the radiologist [92]. They furthermore state that even after surveys showed that this issue needed to be regarded with higher consideration, little has been done to remedy it. Current levels of radiation are high especially in the pediatric populace.

Rivière says several techniques and protocols are currently being explored that will cut down on radiation dosage without compromising resolution [94]. He shows support of automatic tube current modulation, calling it a “promising approach, already implemented on a number

of commercial scanners”. Introduced by Naidich *et al.* in 1990, others state that although this method yields adequate images there was a considerable increase in noise [92].

1.3.4 Finite Element Analysis

Developed in 1943 and once limited to expensive mainframe computers owned by industries such as aerospace, defense and nuclear, today Finite Element Analysis is widely used for research, product design and product refinement in almost every industry. Several books are available on the subject which is also a field of specialization for many engineers. The medical and veterinary community has also benefited greatly from this technological tool. There has been much work and research, particularly on human anatomy, that has incorporated the use of FEA in solving structural analysis problems. Fewer studies have been done with respect to canine anatomy. Some of the most useful studies regarding FEA in medical and veterinary modeling are mentioned in the following sections.

1.3.4.1 Modeling in Humans and Canines

Though little research on the canine stifle has directly incorporated finite element analysis, several studies have been done on human anatomy and other regions of the dog using this powerful modeling tool. Since the introduction of finite element based medical research, several researchers have focused on the increased accuracy of three-dimensional solid geometric models from digitized scans. Several others have added the complex nature of soft tissues, articular cartilage and structures like the menisci in the knee [38,64,83,110]. Donahue *et al.* determined, through a geometrically accurate 3D FEA model of the human

knee, that the assumption of rigid body motion to the bony structures (i.e. femur and tibia) are valid and only change the results by a small percentage [38]. Also of significance was their discovery that unrealistic rotational constraints beyond that of flexion/extension resulted in large errors for contact variables. These additional constraints had been frequently used in previous studies so this study reported important information for future endeavors. The research was limited in several ways including modeling the ligaments as nonlinear springs, neglecting the effects of the LCL and posterior cruciate ligament and excluding the patellofemoral joint contact. These simplifying assumptions were made because of the limited computational power and technological capabilities at the time of the study. Beillasa, *et al.* studied the general dynamic joint response in the human leg during strenuous activities, such as impact and showed that, although based on several assumptions which should not be used to define subject-specific response, finite element analysis makes it finally possible to illuminate this dynamic state [14]. However, some significant limitations include a lack of the lateral and medial collateral ligaments as well as the fact that the cruciate ligaments were represented by spring elements. Li *et al.* determined in their finite element model of the human knee joint that the inclusion of the meniscus is necessary for more reliable approximation of knee kinematics [63]. Their study, however, contained several limitations in the representation of this component which has since been improved upon by others [124,126].

Barink *et al.* implemented a 3-dimensional dynamic FEA model to simulate patellar movement, ligament behavior, and joint kinematics in a prosthetic human knee joint [11].

The study found a relatively linear relationship between patellar movement and knee flexion, but the model was oversimplified excluding proper nonlinear material properties as well as the proper insertion point of the lateral collateral ligament. Their predictions for varus valgus laxity may also be incorrectly estimated due to the absence of the patellar retinaculum.

Though more limited in its use on the canine stifle, finite element analysis is also being used to determine joint mechanics in dogs. A study by Shahar, Banks-Sills and Eliasy was the first report of results of finite element analyses of a clinical canine hip replacement system [101]. This study demonstrated the differences between two types of hip replacement stems commonly used in clinical veterinary practice (cementless and cemented) and proved that FEA was a useful means of approximating stress, strain and displacements for a complex geometry that would otherwise be difficult to determine. The authors assumed the bones to be linearly elastic, isotropic and homogeneous though they stated that the modulus of cortical bone varies over a large range. This is due to a lack of reliable material properties for canine anatomy. Thus, this study may not have fully and properly described the situation but approximated the circumstances to the best of their knowledge and obtained reasonable and meaningful results. In another study by Shahar, Banks-Sills and Eliasy the stress and strains in an intact canine femur for two loading conditions during mid-stance were investigated [102]. Prior to this study, information on this topic was unavailable. It was found that without the proper affects of surrounding muscle forces, stress and strains on the femur were overstated.

1.3.4.2 FEA of Ligaments

Direct measurement of the stress or strain distribution within the ligaments of the knee is a challenging task. Various techniques including strain gauges [10,46], displacements [67,93], Roentgen stereophotogrammetry [70,119], buckle transducers [13], Hyperelastic Warping [84] and robotic technology [123] have been used to describe the nature of human ligaments such as the ACL. An alternative to in vivo experimental studies is the use of computer methods, particularly the three-dimensional capabilities of FEA. Due to the similarities in material properties and function, research on human knees and ligaments is still valuable to research involving canine limbs. Research pertaining to the study of ligaments in both humans and dogs, with considerably more available for humans, is discussed in this section.

Of the primary ligaments in the knee (or canine stifle), the ACL (CCL in dogs) is by far the most researched. Several of the first studies that used FEA and involved ligaments modeled them as nonlinear springs [11,63]. Advancements in technology and computational power have allowed researchers to model ligaments as 3-dimensional nonlinear entities resulting in models that more accurately mimic these anatomical structures [122]. However, there are still comparatively few full three-dimensional finite element models that have been developed. Pioletti *et al.* developed an FEA model based on a full thermodynamic constitutive law for the ACL, incompressible isotropic hyperelastic formulation, and derived material data from uniaxial tensile tests [85]. The assumption of isotropy was later shown to severely limit the outcome of the model for a compression load directed along the collagen fibers and generate high compressive stresses that disagreed with experimental observations

[65]. An extension of the Pioletti model was seen in work by Daniel who developed a 3D orthotropic viscoelastic FEA model of the ACL [32]. This model included both the transverse isotropy and time-dependent material behavior but offered no information regarding ligament behavior during passive flexion. Limbert *et al.* expanded on a neo-Hookean incompressible isotropic hyperelastic potential constitutive model to include the application of the initial stress field within the ACL at full extension [64]. They determined that the inclusion of a pre-stress improved the prediction of the resultant force within the ACL for a passive knee flexion and supported previous assertions that the ACL in human has no stress-free position.

1.3.5 Summary

The stifle joint is one of the most complex and extensively examined joints in the dog. Due to the intricate relationships between its ligamentous components, muscle groups, articular cartilage and bony structures, injury to one of its constituents becomes a multifaceted problem requiring a thorough understanding of not only joint biomechanics but its functional anatomy as well. However, much of what is used to evaluate the stifle joint in canine models still comes from human analysis due to a scarcity of knowledge specific to canine joint mechanics and material properties. With the advent of advanced medical imaging techniques, such as Computed Tomography, a more thorough knowledge of both normal and afflicted stifle anatomy is possible.

Patella alta has been considered a significant cause of recurrent dislocation of the patella [49,55,61,81]. However, there is an apparent lack of both experimental and clinical

information regarding patellar luxation and patella alta diagnosis in the canine. Due to the differences in both geometry and joint motion, data for patellar movement in the human should not be extended directly to the dog and more species specific analysis should be done. Many researchers have used modeling as a tool to analyze the mechanical characteristics of the patellofemoral joint but most of these have been limited to 2D representation [52]. The findings by Jafari *et al.* [52] suggest that the trochlear groove and quadriceps forces are unlikely candidates for dislocation risk factors and further studies on the causes of patellar subluxation are necessary. The issue of patellar location within the trochlear groove is of clinical importance and in need of further research as it pertains to the canine stifle.

A number of experimental studies have been done to describe the forces, strains and failure of stifle ligaments and surrounding components. There are a number of limitations, however, with these experimental methods. A significant alternative to experimental studies is the use of computer models. In particular, the use of finite element analysis is popular as it allows the three-dimensional structure to be analyzed and the stress/strain distribution to be visualized anywhere within the model. Several finite element models have been developed for human anatomy and this method has been equally useful in estimating the mechanical response of canine joint structures that are difficult or impossible to measure by other means. However, there remain very few fully three-dimensional models of the canine knee and several issues that would benefit from the implementation of such technology.

Cranial cruciate rupture remains one of the most widely diagnosed and threatening conditions to stifle stability and rear limb function. By means of in vitro and in vivo experiments as well as mathematical and computer models, many researchers have focused their efforts on understanding the stifle joint mechanics and the changes and behaviors associated with cranial cruciate ligament rupture. Understanding this condition and its effect on joint mechanics will aid in future efforts to develop new methods of treatment.

1.4 STATEMENT OF THE PROBLEM

Rupturing of the canine cruciate ligament is one of the largest contributors to rear limb lameness in dogs. A CCL deficient stifle will, consequently, suffer from prolonged and deteriorating shear forces and result in continually worsening joint disease. Though much has been done to investigate the nature of this ligament in humans, very little research has focused on the biomechanics of the canine stifle joint or the effect of a ruptured CCL. The intention of this thesis project was to determine the effects of CCL insufficiency on the kinematics of the canine stifle joint and surrounding ligaments by way of developing a 3D finite element model of the entire rear limb. The results of particular interest will be resulting stress distributions on the stifle components and any other geometric anomalies that can be confirmed by stress analysis. The results from this research will help support existing literature on the canine stifle as well as provide additional insight into the effects of CCL rupture.

1.5 MATERIALS AND METHODS

1.5.1 Subject Specifics

The subject used for this study was a Doberman pinscher, age 5.5 at the time the scans were taken. His weight at time of scan was 50kg and his left hind limb had a tibial plateau, measured from mediolateral radiographs using conventional methods [12,41,91], of 28°. The subject was euthanized for reasons unrelated to this project.

1.5.2 CT to 3D Modeling: Pre-processing

Images of the subject's left hind leg were attained using computed tomography. This data was obtained prior to this study for reasons unrelated to the project. Due to proximal tibial deformities in the subject's right hind leg, it was decided that the left hind leg would be used to create all models for this study. The CT scan was chosen based on the following objective criteria: the scan was free from scatter and required minimal manual cleaning, the patient's left hind leg exhibited good physical condition representative of this type of large-breed dog, and the patient was of median age and weight as compared with other studies of large-breed dogs found in literature [26,51,89,98]. The CT data was imported and manipulated using Mimics 11.11 (Materialise, Leuven, Belgium). The threshold was set in order to highlight the dense bony structures of the leg including the femur, tibia, patella, fibula, and hock as shown in Figure 1.5.1 below. The entire left hind leg was isolated just below the acetabulum and each of the aforementioned bony structures was separated into a different mask and verified for geometric accuracy.

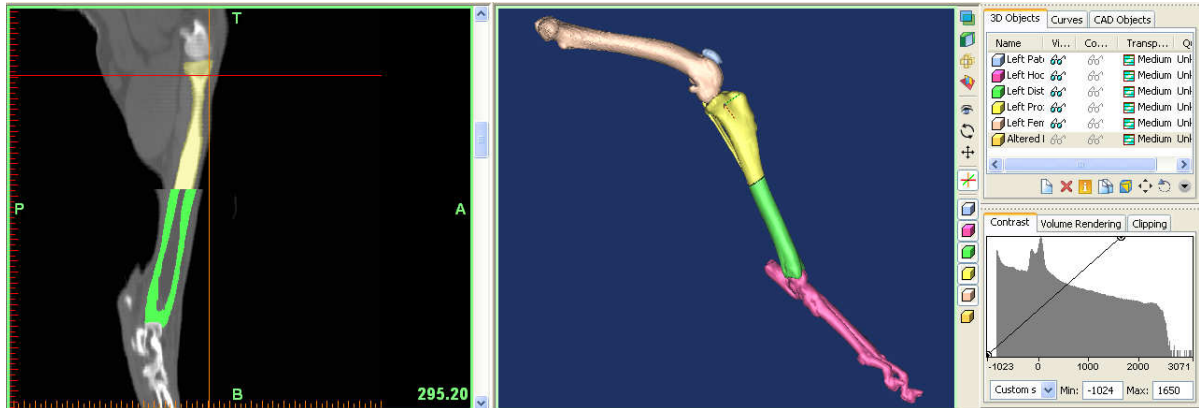


Figure 1.5.1: Isolation of bony structures in Mimics 11.11 [Materialise, Leuven, Belgium].

The files were refined in Magics 12.01 (Materialise, Leuven, Belgium) before being ready to create the FEA models. Specifics on the other processing operations done in Magics are highlighted in the following section.

1.5.3 Convergence Analysis & Final Mesh Preparation

Firstly, unwanted shells, intersecting and inverted triangles, and holes were eliminated in all model components. The Remesh module of Magics was used to achieve a custom mesh for each component obtained from CT (i.e. tibia, femur, patella, and hock). In order to determine the appropriately sized mesh for the FEA models, a convergence test was performed on the femur as seen in literature [38]. Three separate meshes were obtained by reducing the number of triangles using a pattern of triangle reduction, smoothing, and other algorithms. The articulating surfaces of the bones such as the condyles and femoral head

retained a finer mesh structure. To begin with, a *global* remesh (split based method) was performed with the parameters shown in Figure 1.5.2 in order to reduce the initial triangle count.

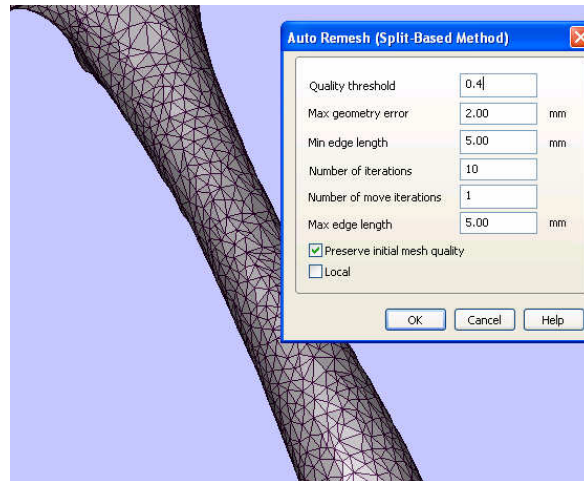


Figure 1.5.2: Global remesh parameters. [Magics, Materialise, Leuven, Belgium]

To eliminate additional elements and reduce file size, a *local* split based remesh with min and max edge length of 10mm was executed on the areas of least concern, those that do not interfere with the articular regions of the bones. Since the joint surfaces and regions experiencing contact forces were crucial to this analysis, the element sizes in these areas (mainly the most proximal and distal sections of each bone) were made much smaller by excluding them from this additional triangle reduction. This can be seen in Figure 1.5.3. Considerations such as aspect ratio and element type were also taken into account by manually manipulating troublesome triangles in order to assure an accurate representation of the system and more reliable results.

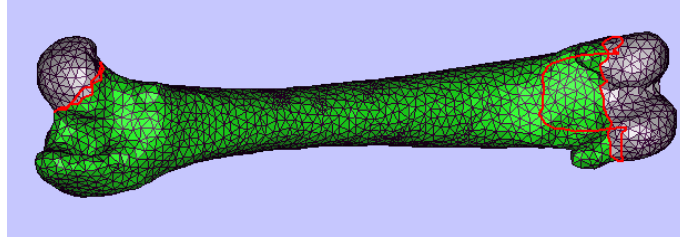


Figure 1.5.3: Selection of femoral shaft for localized re-meshing.

This method was applied two more times, varying the remesh parameters to ultimately obtain a fine, medium and coarse mesh. The final meshes are shown in Figure 1.5.4 (a-c).

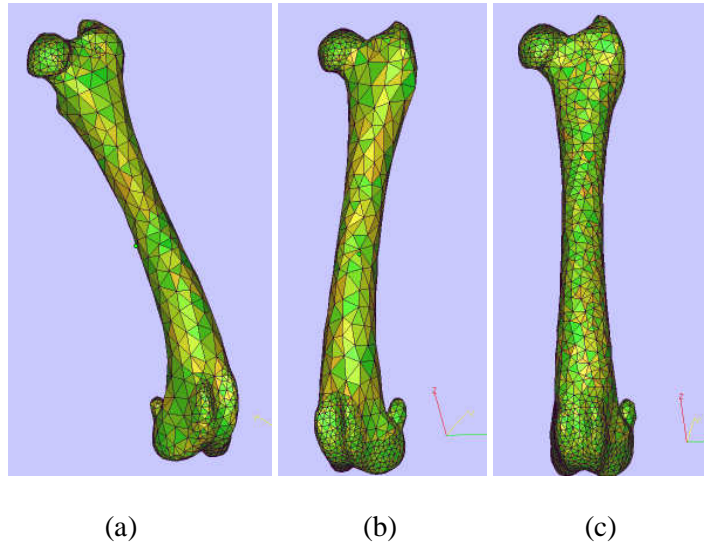


Figure 1.5.4: Variation of femur meshes for convergence test. (a) coarse (b) medium (c) fine

After being imported into the finite element package Abaqus/CAE v.6.7 (SIMULIA, Providence, RI, USA), the distal portion of the femur was fixed and a load was placed on the

femoral head equivalent to 30% of the subject’s body weight (Figure 1.5.5). A visualization of the outputs from the convergence test is shown in Figure 1.5.6 (a-c).

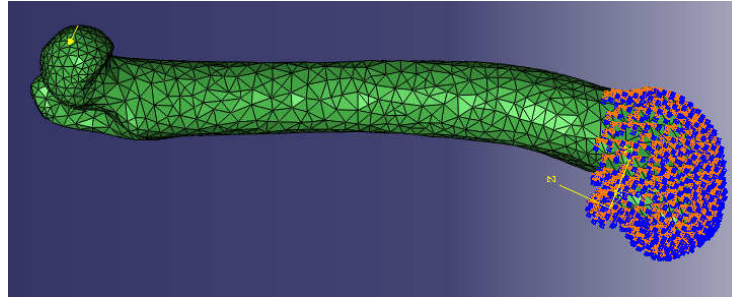
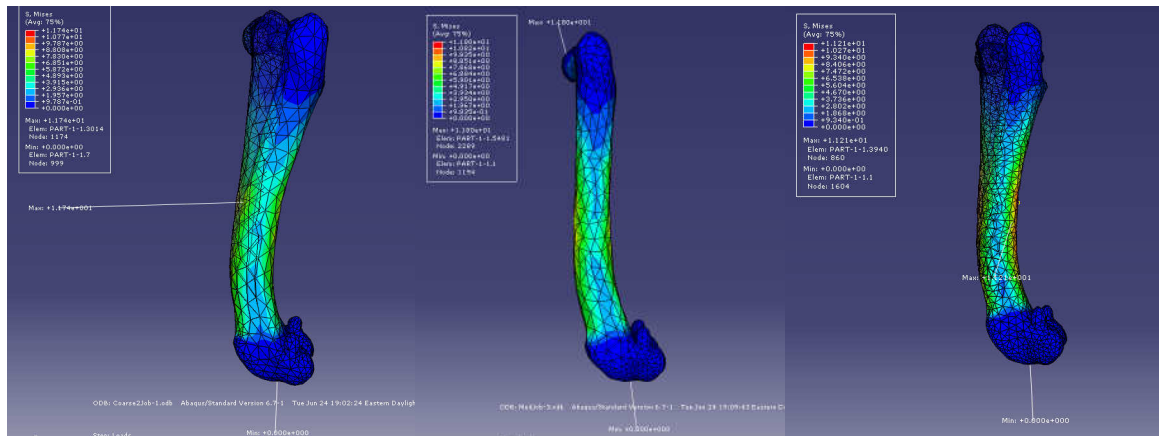


Figure 1.5.5: Load application and boundary condition for convergence test.



(a)

(b)

(c)

Figure 1.5.6: Resulting stress distribution for each mesh type. (a) coarse (b) medium (c) fine

It can be seen from Table 1.5.1 that the maximum stress values for each mesh size are very similar. The coarsest mesh, however, has over 50% fewer elements than the finest mesh, maintains the proper geometric shape and locations of the various origins and insertion points

for the ligaments and muscle but results in a maximum stress value less than 5% larger than the finest mesh. Considering that the final FEA model will include three bony components, several ligaments as well as muscles and menisci, the coarsest of the three meshes was chosen in order to save on computational power and analysis time.

Table 1.5.1: Mesh information and output maximum stresses.

	Coarse Mesh	Medium Mesh	Fine Mesh
# tet elements	7244	11008	16465
# of tri elements	1972	2382	3202
Max VM Stress (Pa)	1.17E+01	1.18E+01	1.12E+01

The meshing of the tibia was performed using the same steps as the femur with the articulating distal and proximal ends retaining a finer mesh. Figure 1.5.7 shows the final mesh and mesh quality. Although there were a few triangles with poor aspect ratios, the majority of the elements are acceptable and the mesh was deemed fit for modeling.

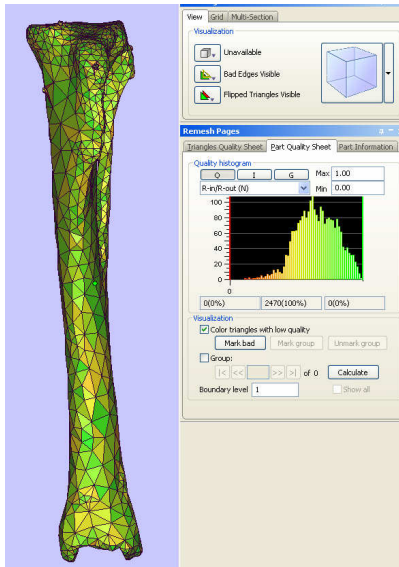


Figure 1.5.7: Final tibia mesh. Coarse tibial shaft and fine mesh around articulating surfaces.

Due to the geometric simplicity of the patella, only one global remesh was applied and no smoothing was performed. A triangle reduction was applied, however, to further minimize the number of elements (Figure A.1). Some of the other components required additional manipulation and are discussed in their own sections below.

1.5.4 Constructing the Proximal Interphalangeal Joint

The angle between the metatarsals and phalanges was chosen to be fixed at 110° for all stifle angles of this project. Since there is no literature defining the angle of the metatarsal-phalangeal joints at our specific angles of interest, this was chosen based on literature as an acceptable position for corresponding stifle angles around and during the stance phase of the gait [47]. In order to manually set this angle, the hock was separated at the proximal

interphalangeal joints. This was achieved by creating semicircular cuts at each joint using a boolean operation as shown below in Figure 1.5.8.

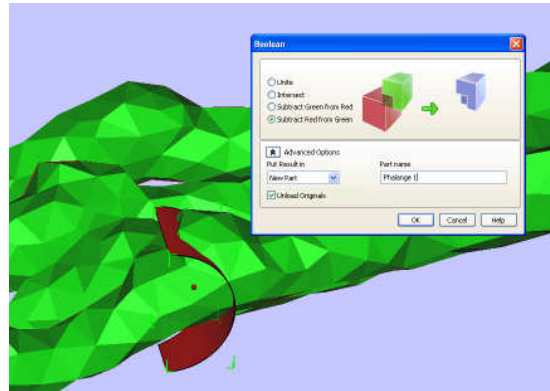


Figure 1.5.8: Boolean operation to separate phalanges at metatarsal-phalangeal joints.

After the phalanges were separated, all four digits were rotated so that when contacting a level surface the proximal interphalangeal joint would be set at 110° . The phalanges were repositioned manually and stitched to the metatarsals to create a smooth interface as shown below in Figure 1.5.9. Completion of the hock involved remeshing using the same algorithm performed on the femur and tibia. The articular surfaces were isolated and a second remesh was applied (Figure A.2).

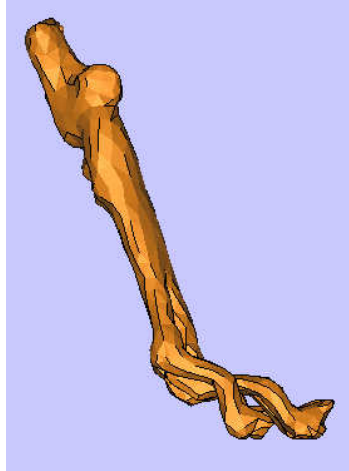
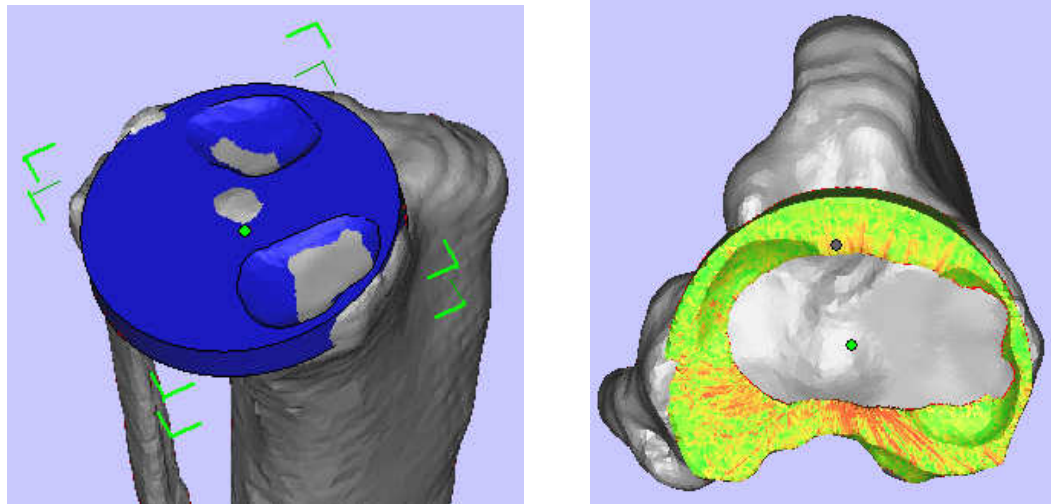


Figure 1.5.9: Illustration of angled proximal interphalangeal joint to 110°.

1.5.5 Modeling the Meniscus

In the dog, the lateral and medial menisci deepen the tibial articular surface and provide better accommodation of the femoral condyles on the tibial plateau. They help increase the stability of the stifle, act as shock absorbers to protect the articular surfaces of the tibia and femur, and aid in lubrication of the joint [27]. Injury to the meniscus is attributed to progression of degenerative joint disease [25,27,89]. It was not the intent or focus of this project to model the exact likeness or response of the menisci but it was necessary to replicate the alignment and offset between the femur and tibia in order to have an accurate model of the canine stifle. Several FEA studies have determined that the inclusion of the menisci is necessary to achieve an accurate prediction of contact pressure distribution on tibial plateau under compressive loading [124]. Using Magics, the lateral and medial menisci were created as one component through a series of boolean operations. Part of the boolean process and the resulting meniscus are shown below in Figure 1.5.10 (a-b).

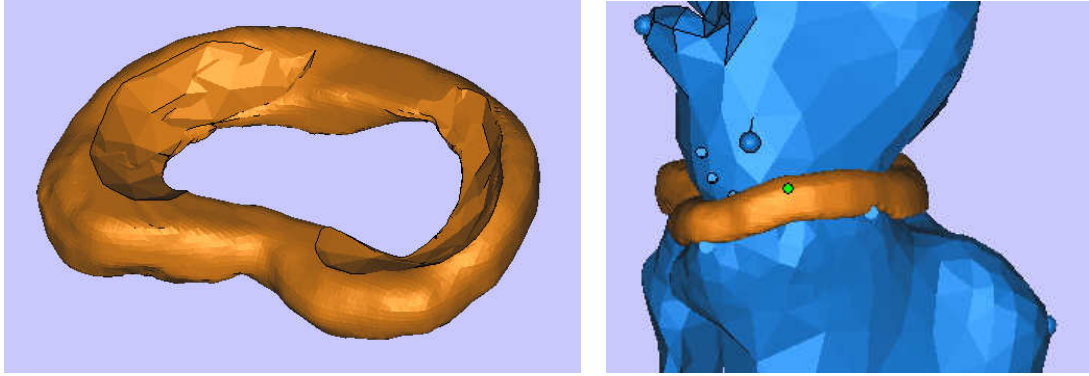


(a)

(b)

Figure 1.5.10: Meniscus created using boolean operations in Magics. (a) first boolean operation (b) further removal of interior

After performing the boolean operations, the “Shrink Wrap” function in Magics was used to thicken the general shape of the structure and make it more anatomically realistic. This was followed by performing a boolean operation with the femur in each of the angles of interest resulting in the final version of the meniscus shown below in Figure 1.5.11 (a-b).



(a)

(b)

Figure 1.5.11: Final model-ready meniscus. (a) top view of meniscus (b) meniscal boundary between articulating surfaces of tibia and femur

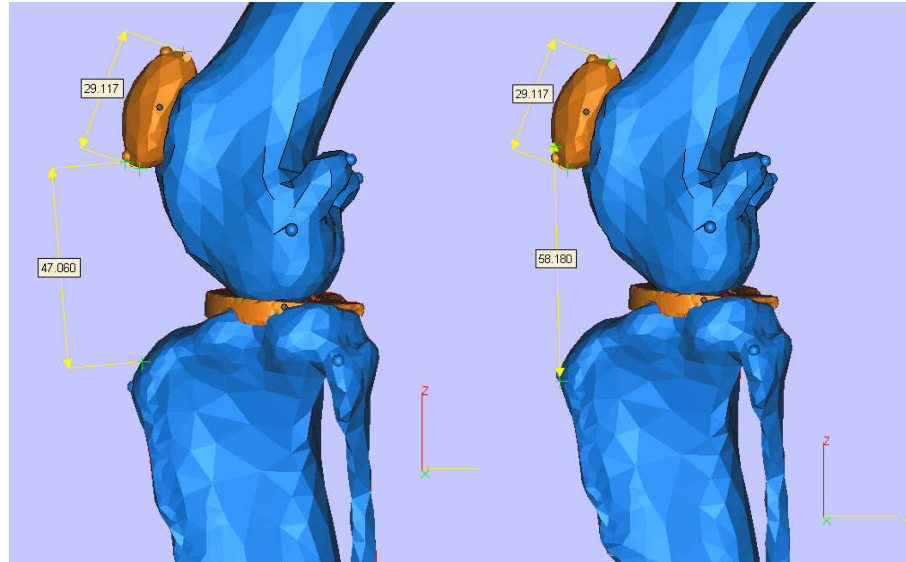
Again, the same remeshing technique was applied to minimize the number of elements (Figure A.3). In summation, the resulting component meshes were deemed minimized and ready for assembly in the FEA program. The final part information is listed below in Table 1.5.2.

Table 1.5.2: Final mesh information for hind leg components.

Component	# of elements	# of nodes
Meniscus	984	492
Tibia	2470	1235
Femur	2042	1023
Patella	216	110
Hock	1956	980

1.5.6 Measuring Patellar Location

In order to accurately position the patella in each testing orientation (stifle angles of 75°, 113°, 148°), the measurement of patellar ligament length (L) to patellar length (P) was first compared with literature and validated as a satisfactory starting position. The measurement of L:P was obtained using two separate methods [34,81] and each was found to be well within the ranges reported in the respective paper. According to Johnson *et al.* [34], the patellar ligament was measured from the caudal aspect of the ligament insertion point to the distal end of the patella, as shown in Figure 1.5.12a. This resulted in an L:P of 1.62, compared with a mean \pm SD of 1.68 ± 0.18 stated in the literature. A slightly different definition of patellar ligament was used in the paper by Mostafa *et al.* (shown in Figure 1.5.12b). Here, the ligament was measured from the cranial aspect of the area of insertion on the patella to the cranial insertion located on the tibial tuberosity. This measurement resulted in an L:P of 1.99 which was only 0.021 less than the mean value reported for that study and well within the SD of 0.2. Thus, it was concluded that the scans used for this study and original position of the patella were adequate.



(a)

(b)

Figure 1.5.12: Patellar and patellar ligament lengths via two different measurement methods.

(a) Lengths according to Johnson *et al.* [34] (b) Lengths according to Mostafa *et al.* [81]

The stifle angles used for this study are within the reported ranges for which the patellar ligament can be assumed inextensible [34]. Therefore, the original length of the patellar ligament could be used to position the patella in all subsequent orientations throughout the proposed range of motion.

1.5.7 Measuring the Stifle Angles

Three separate stifle angles were tested during this study to provide data over a range of motion. According to literature regarding typical flexion and extension angles during

walking and trotting phases of large-breed dogs [34,47] the following angles were used for this study: 75° , 113° , and 148° .

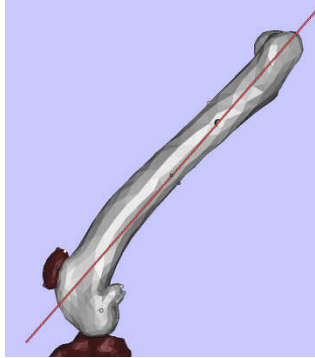


Figure 1.5.13: Illustration of the determination of the femoral long axis.

The stifle angle was defined according to literature as the angle between the tibial shaft and the longitudinal axis of the femur [51]. The femoral long axis is defined as a line that extends from the greater trochanter to the lateral femoral epicondyle (shown illustratively above in Figure 1.5.13). The original stifle angle was measured to be 128.13° , as shown in Figure 1.5.14. Using the patellar ligament length specifications, as mentioned in the previous section, the orientations for all stifle angles were constructed (Figure 1.5.15 (a-c)).

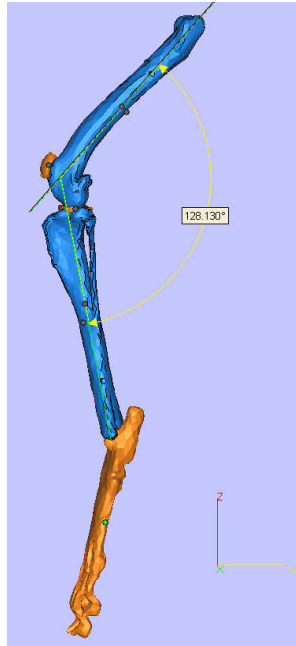


Figure 1.5.14: Lateral view showing the original stifle angle from CT data.

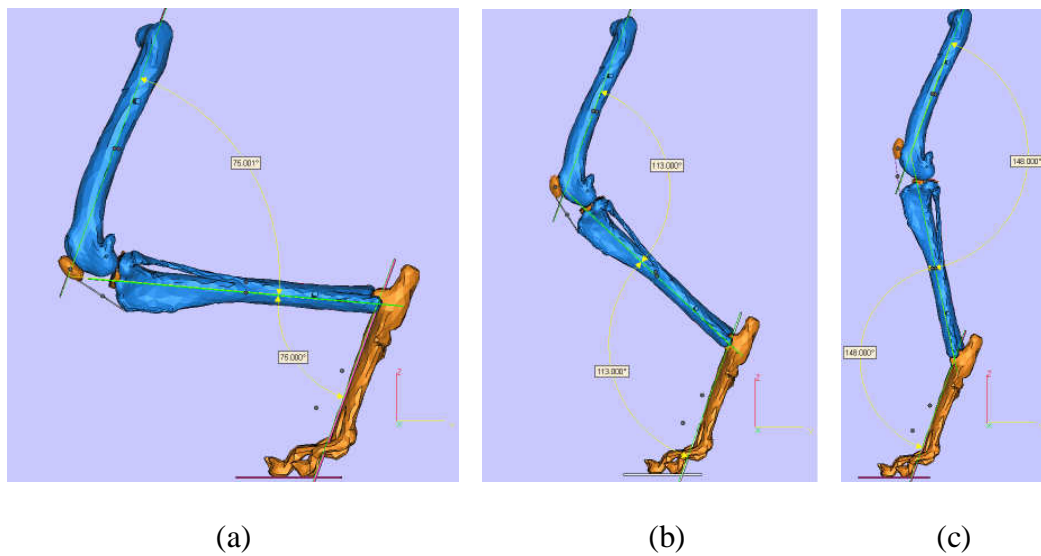


Figure 1.5.15: Stifle orientations for models. (a) stifle angle of 75° (b) stifle angle of 113°
(c) stifle angle of 148°

1.5.8 Ligaments

In order to assure that the ligaments and muscles of interest would be placed in the same position on each model, markers showing the locations of the origin and insertion points were created and placed on the computer model. Anatomical models and preserved specimens like the ones in Figure 1.5.16 (a-b) were used to determine the insertion points and CT data was used to determine the soft tissue geometry.

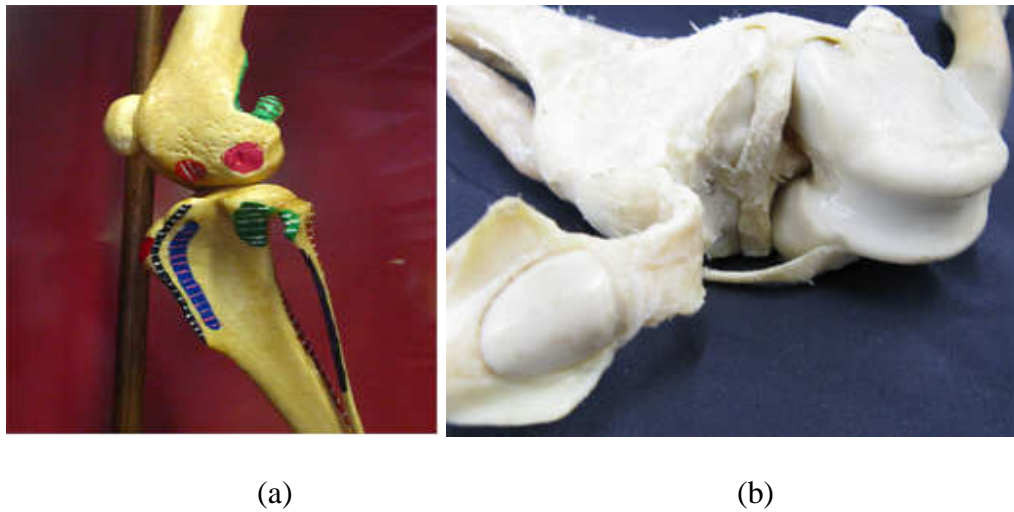


Figure 1.5.16: Anatomical models used to determine ligament origins and insertions. (a) dog leg model with painted attachment points (b) cadaver dog leg used to reproduce ligaments

Fifteen origin and insertion points in total were marked pertaining to the 5 ligaments (cruciates, collaterals, and patellar) and 2 muscles (gastrocnemius and quadriceps) being modeled. These points were marked on the model by using 3mm diameter spheres added to the bone. The ligament or muscle then attached at these points in the FEA model. Diagrams

of the origin and insertion points along with a color coded key are shown below in Figure 1.5.17 (a-d). The only points not shown are the insertion of the gastrocnemius muscle and the origin of the quadriceps.

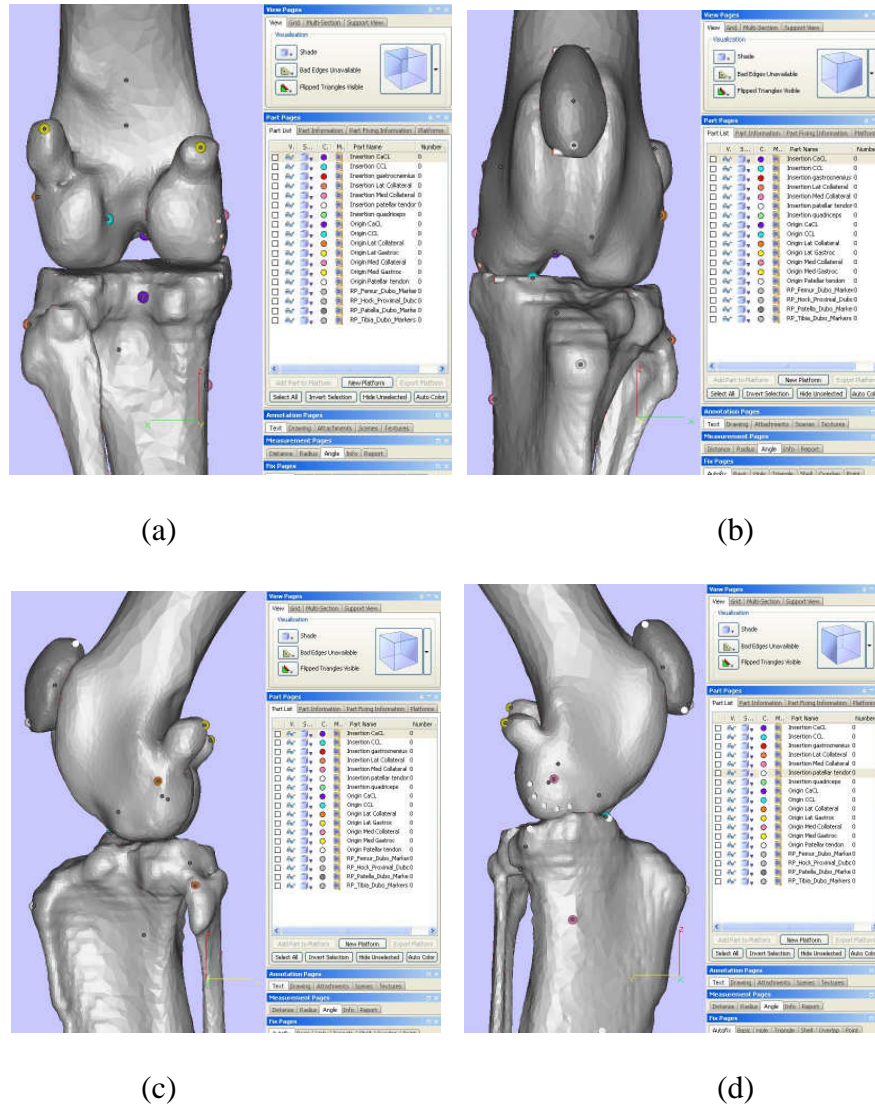


Figure 1.5.17: Origins and insertions for all stifle ligaments. (a) caudal view (b) cranial view (c) lateral view (d) medial view

According to previous research, representing ligaments by straight-line elements may not be valid due to the curve and shape of the ligaments over bony structures [18]. Therefore, CT data for the original stifle angle of 128° was used to create ligaments that fit the stifle at the three angles of interest (75° , 113° , 148°). Ligament size was obtained from CT data (shown in Figure 1.5.18 (a-b)) by measuring the cross sectional area and shape at the origin, middle, and insertion of each ligament. The final ligament geometries obtained from the CT scan can be found in Table A.2.

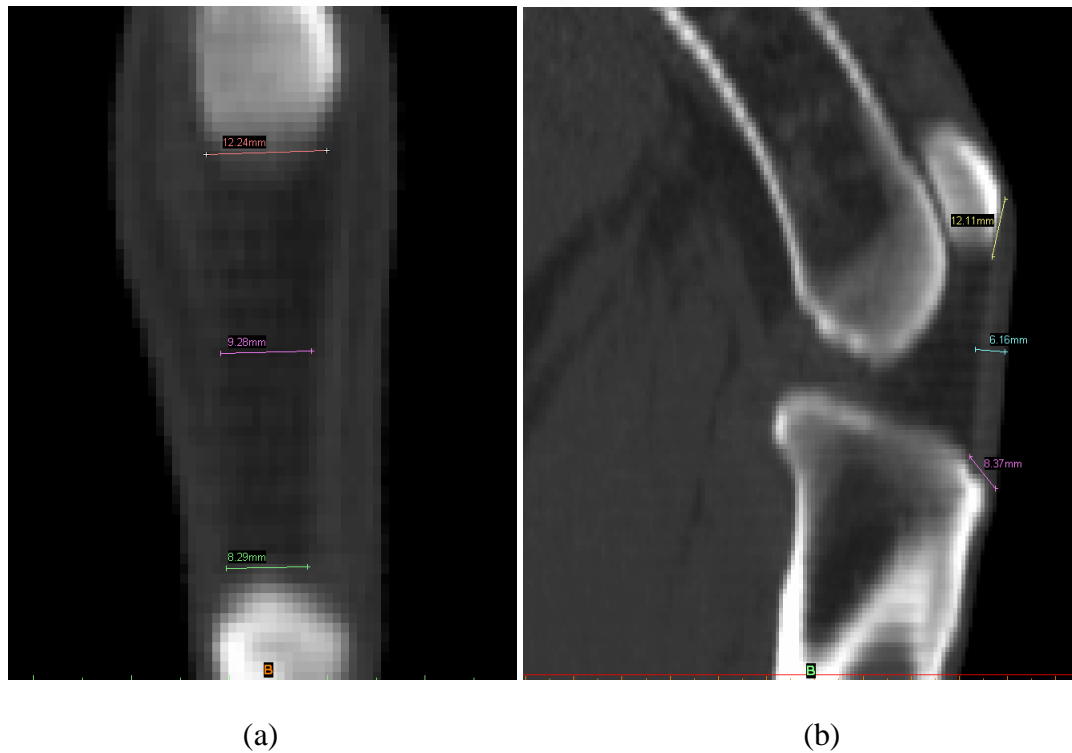


Figure 1.5.18: Measurement of the patellar ligament from CT scans. (a) craniocaudal view (b) mediolateral view

The information obtained from CT was then used to create the stifle ligaments in SolidWorks (Dassault Systemes S.A., Concord, Massachusetts, USA). Through a set of guide curves to define the ligament paths, the loft feature was used to create fully three-dimensional ligaments. An example of this process is shown below in Figure 1.5.19.

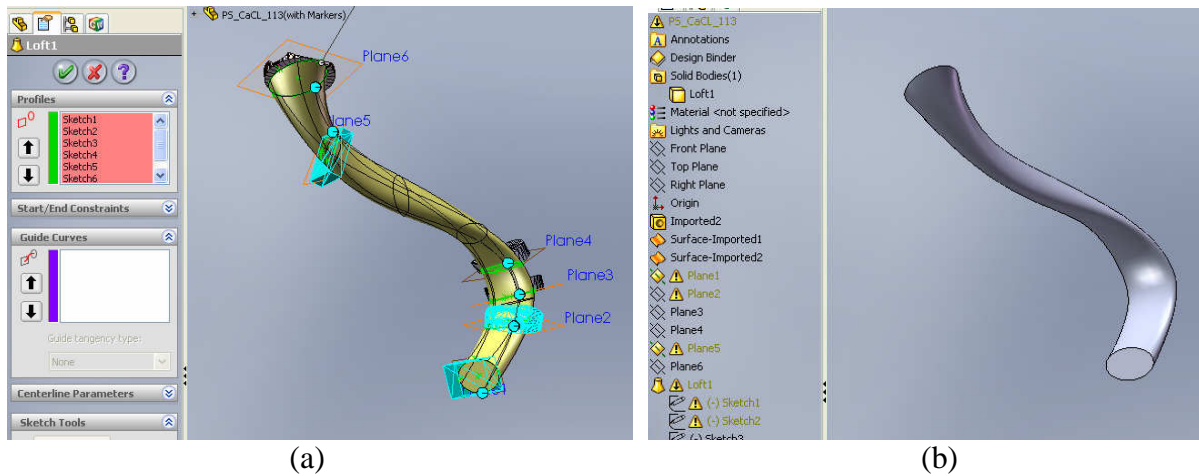


Figure 1.5.19: The creation of the CaCL in SolidWorks (Dassault Systemes S.A.). (a) using the loft feature with information from CT scans (b) final 3D CaCL

Ligaments for a specific angle, for example 75° , were used for all leg models for that stifle angle to maintain congruency. However, since the general shape and volume of the amorphous ligament shapes differ between angles (as the origins and insertions move closer or further apart), results will only be comparable between procedures at specific angles. This does not apply to the patellar ligament as it can be assumed to be of constant length throughout the range of motion examined in this study [34]. A final view of the primary stifle ligaments (with exception to the patellar ligament) is shown below in Figure 1.5.20.

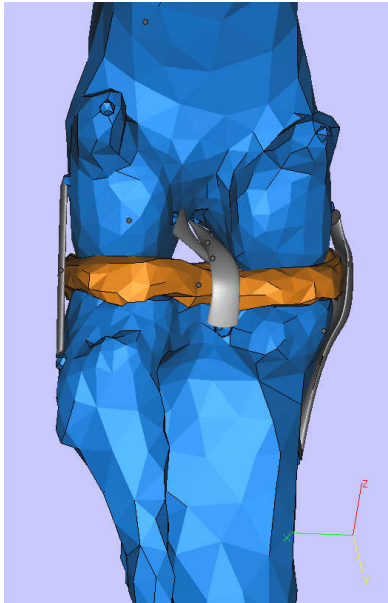


Figure 1.5.20: Caudal view of the stifle in extension with 3D ligaments attached.

1.5.9 Model Assembly in ABAQUS

The models of the three stifle orientations were imported into the FEA software program Abaqus/CAE v.6.7 (SIMULIA, Providence, RI, USA) for analysis. Once imported into Abaqus, the meshes created in Magics for the bony structures were converted to a tetrahedral mesh, consistent with previous studies found in literature [38,101]. A local coordinate system was assigned to any component whose material properties were orthotropic in nature (i.e. bones and meniscus). According to literature, direction 1 was radial, direction 2 was circumferential, and direction 3 was along the long axis of the bone [38]. An example of this assignment is shown below in Figure 1.5.21. Specifics on the material properties of the model components are discussed in the following subsection.

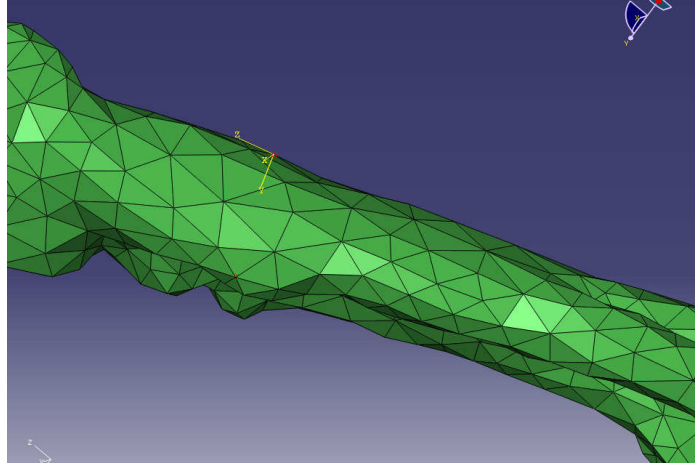


Figure 1.5.21: Local coordinate system for orthotropic property definitions of the hock.

1.5.9.1 Material Properties and Mesh Assignment

The FEA models for this study incorporated the patellar tendon and all of the major stifle ligaments (MCL, LCL, CCL, CaCL) as well as the primary contributing muscles (gastrocnemius, quadriceps). The meniscus and bony structures from hip to foot were also included. Material properties for all soft tissues and bony structures were taken from literature.

The cortical bone of the femur and tibia were defined as homogeneous, linearly elastic and orthotropic using material constants (shown below in Table 1.5.3) derived from a study of the human femur but used previously to describe the properties of canine bones [38]. Published data regarding the material properties of canine bone is sporadic and inconsistent [101].

These properties compare well with studies on canines that assume isotropy but more fully describe the physical nature of the bony components of the hind limb.

Table 1.5.3: Linearly elastic, orthotropic properties for the human femur and tibia [38].

	E_1 (GPa)	E_2 (GPa)	E_3 (GPa)	G_{12} (GPa)	G_{13} (GPa)	G_{23} (GPa)	ν_{12}	ν_{13}	ν_{23}
Femur	12.0	13.4	20.0	4.53	5.61	6.23	0.38	0.22	0.24
Tibia	6.9	8.5	18.4	2.4	3.6	4.9	0.49	0.12	0.14

Previous research has discovered a “toe region” in the elasticity curve of ligaments due to the fiber bundle behavior. The fibers begin folded and as they relax the ligaments experience an initially nonlinear strain. A linear region follows representing the fibers being fully unfolded [15,23,33]. This information is crucial in accurately representing the behavior of ligaments and thus needed to be incorporated appropriately into the model. Canine ligament data are currently unavailable and most often times taken from human literature. It is speculated that mammalian ligaments are similar in their basic characteristic and use of species-specific values will not have a considerable impact [103]. Therefore, consistent with literature on the material properties of human ligaments, this study has used a neo-Hookean, incompressible, transversely isotropic hyperelastic model [64,113]. This model has been found to adequately represent the elastic behavior and stiffening mechanical contribution of the collagen fibers of ligaments [64]. The parameters implemented for this study are shown below in Table 1.5.4 and were found from an experimental study [113].

Table 1.5.4: Neo-Hookean constants for ligament property definitions, from literature [113].

Ligament	C_{10} (MPa)
CCL	24
CaCL	15
MCL	22
LCL	15
PL	65

The ligaments were meshed as 8-node, linear hexahedral brick elements with reduced integration, finite strain and hourglass control. The use of hexahedral elements for ligaments in FEA has been found to be accurate and robust for finite deformations [122]. Some ligament mesh examples are shown below in Figure 1.5.22(a-e).

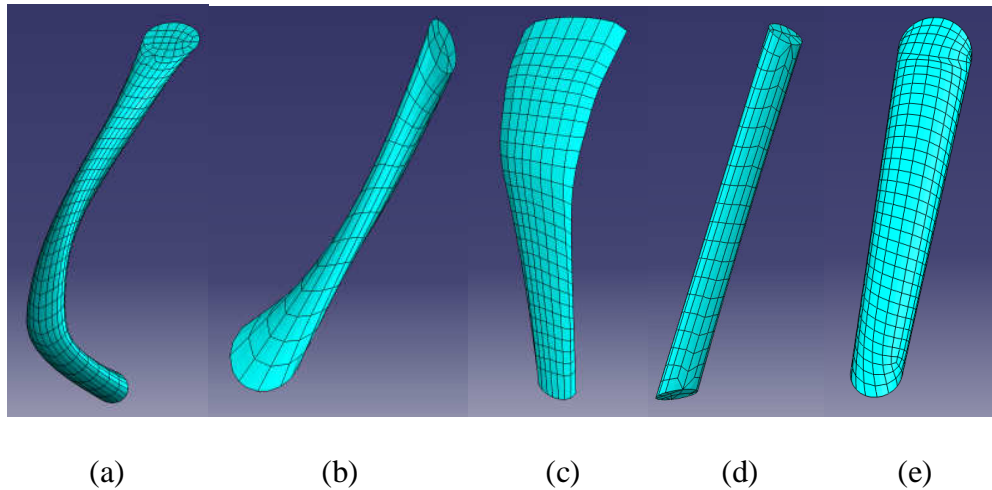


Figure 1.5.22: Ligament meshes for stifle angle of 113°. (a) CaCL (b) CCL (c) MCL
(d) LCL (e) PL

The ligaments were attached rigidly to the bone at the origin and insertion points previously noted. A rigid attachment was achieved via linear springs with nearly infinite stiffness. This

mimics the behavior of a tie constraint (which would not function with the geometry) in that the nodes of the ligament follow the same movement as the node it's attached to on the bone. A view of the attached ligaments (shown with tie constraints for visualization purposes) is below in Figure 1.5.23.

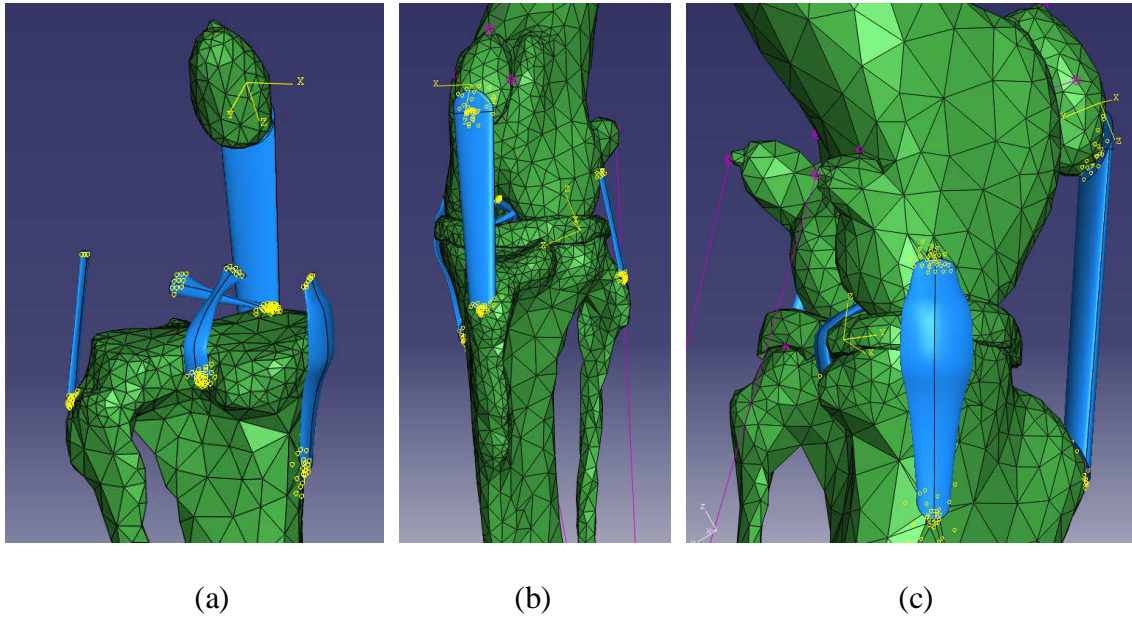


Figure 1.5.23: Views of the rigid attachment of the stifle ligaments. (a) caudal view with femur and meniscus removed (b) cranial view of intact stifle (c) medial view showing MCL

Again, very limited characterization of the material properties for the menisci in canines is available in literature. The meniscus, according to literature for humans, was modeled as homogeneous, linearly elastic, and transversely isotropic [124]. The five independent parameters required were: circumferential modulus of $E_{\theta}=125\text{MPa}$, transverse modulus $E_R=E_Z=27.5\text{MPa}$, Poisson's ratio of $\nu_{\theta R}=\nu_{\theta Z}=0.1$, Poisson's ratio within the transverse plane

of $\nu_{RZ}=0.33$ and in-plane shear modulus of $G_{\theta R}=G_{\theta Z}=2\text{MPa}$. The other parameters were calculated via the equations below (from the compliance matrix for transversely isotropic materials):

$$G_{RZ} = \frac{E_R}{2(1 + \nu_{RZ})} = 10.34\text{MPa} \quad (1)$$

$$\nu_{R\theta} = \frac{E_R}{E_\theta} \times \nu_{\theta R} = 0.022 \quad (2)$$

1.5.9.2 Contact and Surface Interaction

Contact was modeled between five contact-surface pairs (the femur and meniscus, meniscus and tibia, femur and tibia, tibia and hock and patella and femur). The contact conditions were general using finite sliding and since the coefficient of friction between cartilage surfaces in diarthrodial joints is very low, all surfaces were modeled as frictionless [103]. This assumption has been used frequently in other studies [38,63,103,124]. A contact pressure-clearance relationship of “hard” contact was defined for each contact pair. This means that no penetration was allowed of nodes from one surface (the slave surface) into the other (master) surface. Figure 1.5.24 (a-e) shows the resulting contact surfaces.

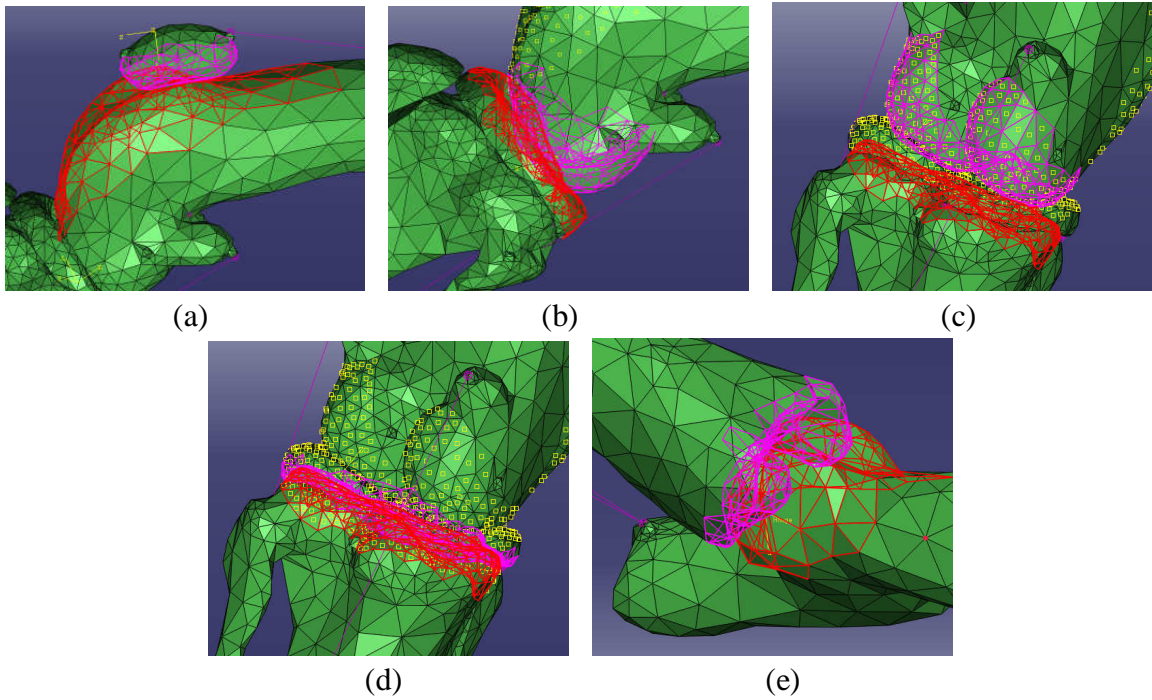


Figure 1.5.24: Contact pairs and articulating surfaces. (a) patellofemoral (b) femur and meniscus (c) femur and tibia (d) meniscus and tibia (e) tibia and tarsus

Attachment of the meniscus to the tibial plateau (Figure 1.5.25) was achieved with five linear springs with spring constants of 200N/mm, positioned on each cranial and caudal horn [38].

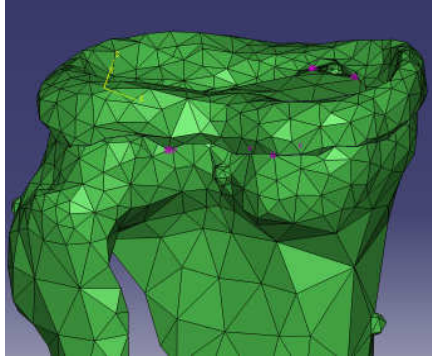


Figure 1.5.25: Attachment of the meniscal horns to the tibial plateau by linear springs.

The quadriceps and gastrocnemius muscles were included and each modeled as linear springs. The purpose of including these components was not to mimic the physiologic function of the muscle groups, but to represent the muscle-tendon units when they are loaded and opposed further elongation so as to keep the stifle and tarsal angles fixed in their testing orientations [59, 121]. The actual quadriceps muscle group includes the rectus femoris (RF), vastus intermedius (VI), vastus medialis longus (VML), vastus medialis obliquus (VMO), vastus lateralis longus (VLL), and vastus lateralis obliquus (VLO). For our study it was assumed that the entire quadriceps force was applied through the RF component [39]. Thus, the tension in the quadriceps was modeled to act along the line of action of the linear spring representing it. Figure 1.5.26 below shows both the quadriceps and gastrocnemius muscles in the model.

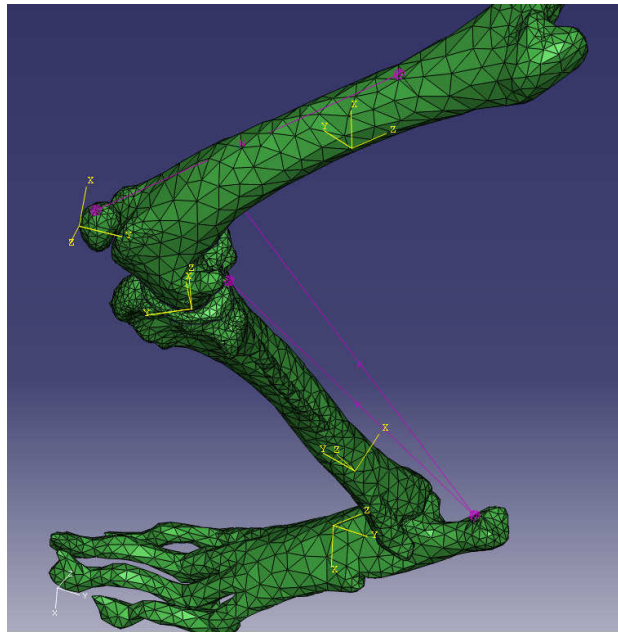


Figure 1.5.26: Gastrocnemius and quadriceps muscles modeled as linear springs.

In order to aid in an accurate prediction of patellofemoral articulation, medial and lateral parapatellar fibrocartilage were included in the model. They were designated by linear springs attached to the medial and lateral fabellae with spring constants of 22.5N/mm as found in literature [39]. The tibial and hock were also connected at the tarsal joint with linear springs of very low stiffness. Their purpose was not to influence the motion of the tibia but it was found that convergence was not attainable without this connection. Interaction between the ligaments and meniscus or adjacent bones was defined as frictionless. The muscle attachments, ligament attachments via springs, tarsal joint attachment and parapatellar fibrocartilage are shown below in Figure 1.5.27.

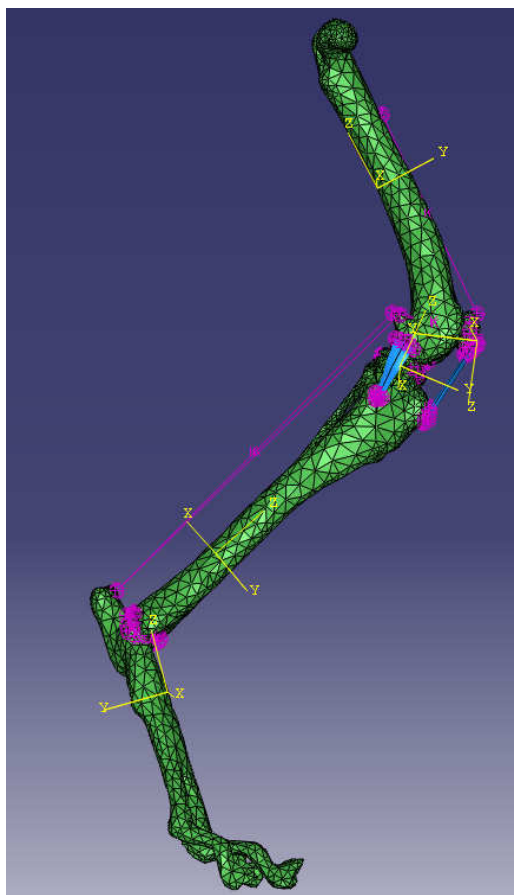


Figure 1.5.27: Final assembly of model with muscles, ligaments, and attachment springs.

1.5.9.3 Loads and Boundary Conditions

The distal portion of the hock (distal to the proximal interphalangeal joint) was fixed in translation throughout the analysis. All other components were initially fixed to allow for contact to occur and then only restrained in the transverse (x-axis) direction. This was consistent with physical testing [Crimi CS, 30]. A compressive load of 30% of the subject's body weight was applied to the femoral head and oriented along the z-axis. This is shown below in Figure 1.5.28.

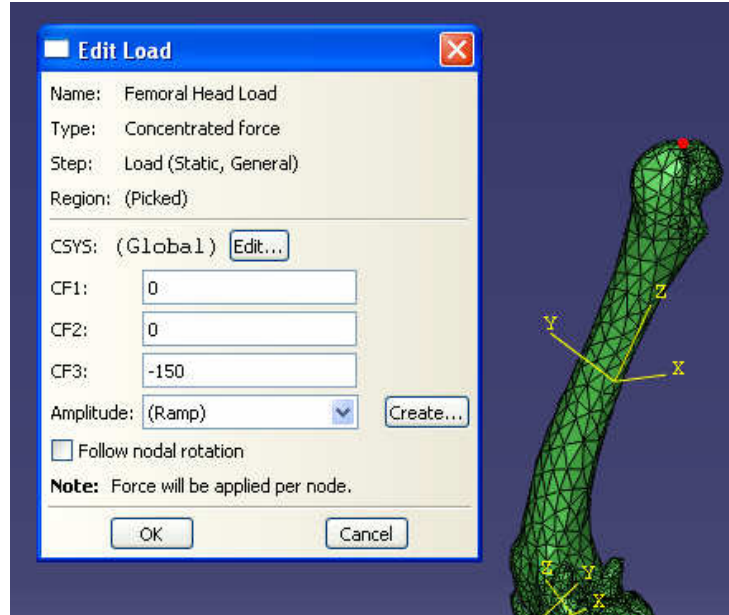


Figure 1.5.28: Application of a concentrated compressive load to the femoral head.

1.5.9.4 Testing Procedure

A fully three-dimensional, nonlinear, quasi-static model was created for both an intact and CCL deficient leg at three different stifle angle positions throughout the normal range of motion of the dog and representative of maximum and minimal angles during walking and trotting [34]. After convergence was reached, the average stress for each ligament was recorded, screenshots were taken and observations regarding drawer, subluxation, and stability were documented.

1.6 RESULTS

1.6.1 75 Degree Results

Figure 1.6.1 below shows the resulting stress distributions in all stifle angles for the intact model at 75°. Figure 1.6.2 illustrates the effects in the intact stifle model assembly.

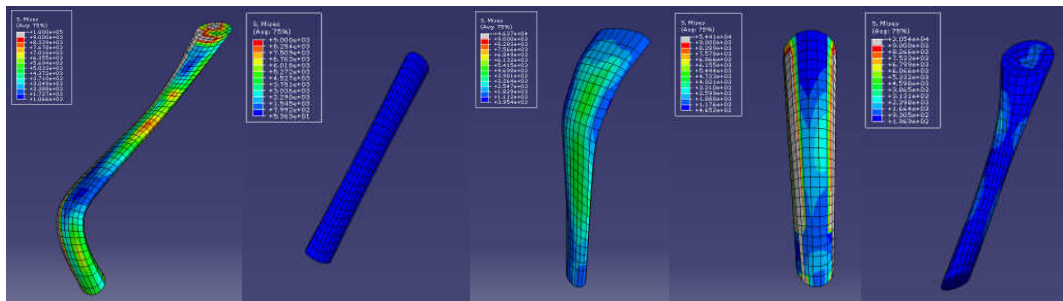


Figure 1.6.1: Visual stress output of the PS Intact stifle ligaments at 75°. From left to right:

CaCL, LCL, MCL, PL, CCL

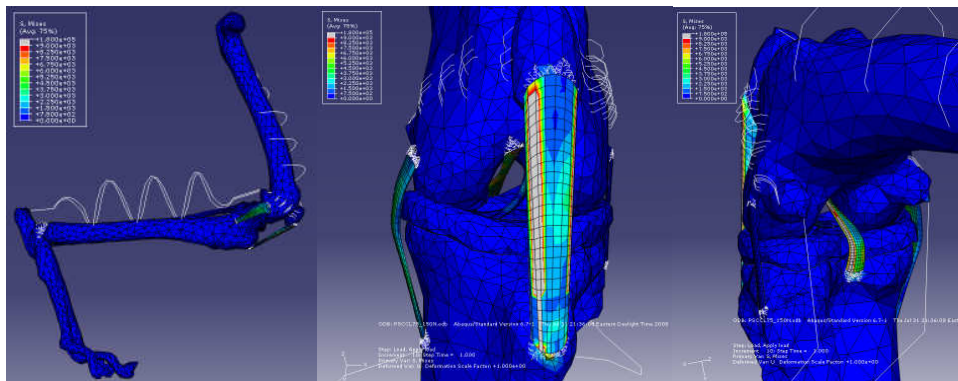


Figure 1.6.2: Several images of the PS Intact stifle joint with ligaments in place at 75°.

Figure 1.6.3 shows the post-analysis stress distributions of the major stifle ligaments in the CCL deficient model at 75°. Figure 1.6.4 displays the results in the assembled CCL deficient model at 75°.

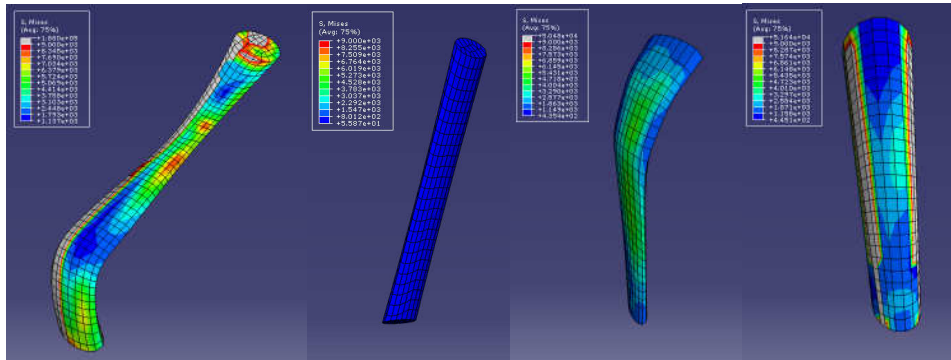


Figure 1.6.3: Visual stress output of the PS transected stifle ligaments at 75°. From left to right: CaCL, LCL, MCL, PL

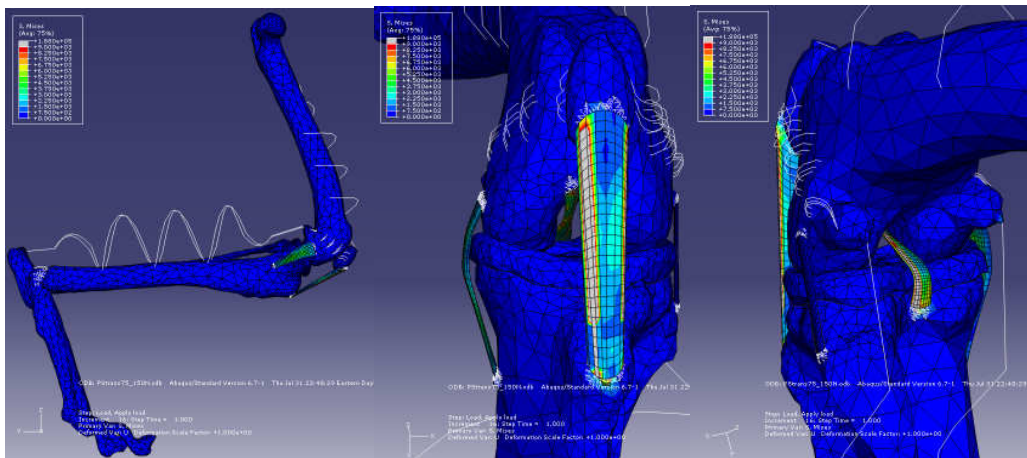


Figure 1.6.4: Several images of the PS transected stifle joint with ligaments in place at 75°.

In Figure 1.6.5 below, the plot of resulting stresses for all ligaments from the intact and CCL deficient models at 75°. Table 1.6.1 shows the percent difference calculations.

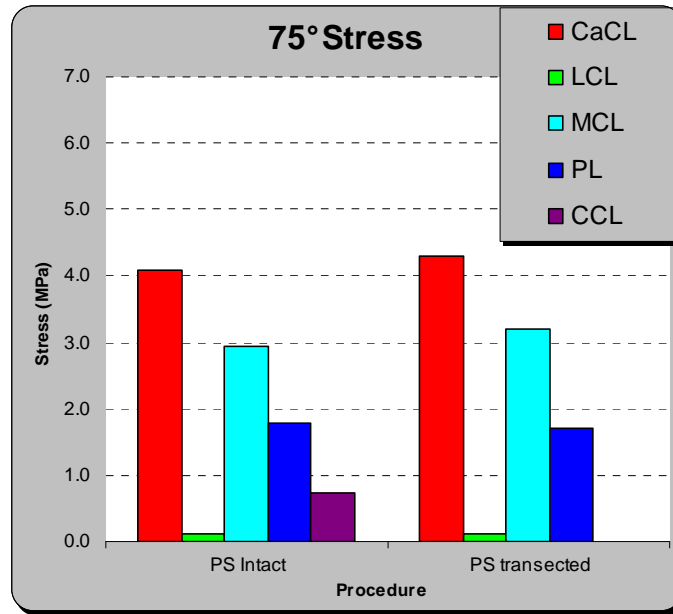


Figure 1.6.5: Graph of stress (MPa) in each of the ligaments of the PS intact and PS transected models at a stifle angle of 75°.

Table 1.6.1: Table of the percent difference between the PS intact model and the PS transected model at a stifle angle of 75°.

	75 Degrees (Percent Difference)	
	PS Intact	PS transected
CaCL	4091.32	4.90%
LCL	112.33	4.65%
MCL	2938.37	8.81%
PL	1768.93	-3.15%
CCL	731.48	

1.6.2 113 Degree Results

Figure 1.6.6 shows the output stresses in all of the ligaments of the intact model at a stifle angle of 113° . Figure 1.6.7 shows the resulting stress distributions within the model assembly. In Figure 1.6.8, the stress outputs for all ligaments in the CCL deficient model at 113° where in Figure 1.6.9 the stresses are shown in the assembly.

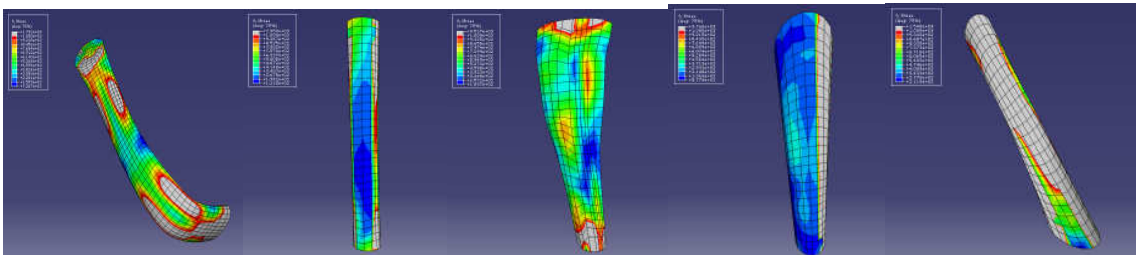


Figure 1.6.6: Visual stress output of the PS Intact stifle ligaments at 113° . From left to right:

CaCL, LCL, MCL, PL, CCL

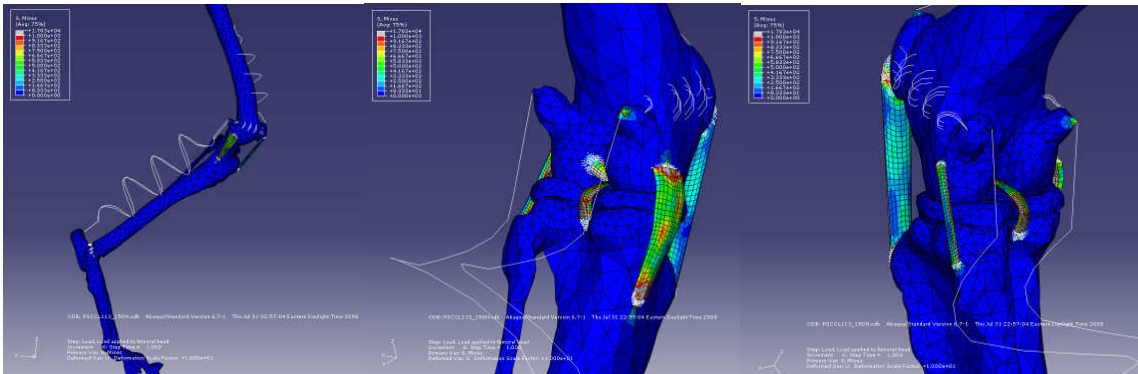


Figure 1.6.7: Several images of the PS Intact stifle joint with ligaments in place at 113° .

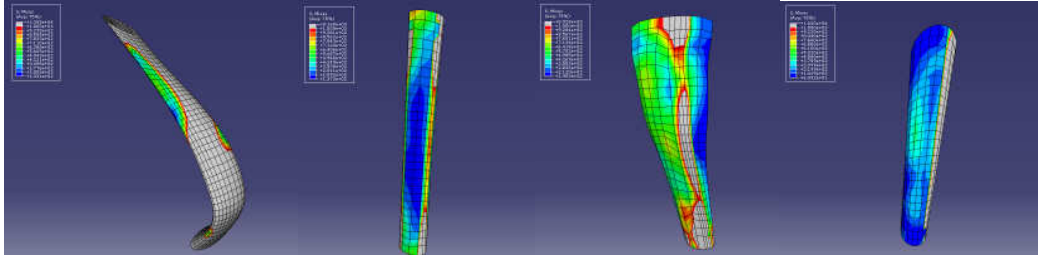


Figure 1.6.8: Visual stress output of the PS transected stifle ligaments at 113°. From left to right: CaCL, LCL, MCL, PL, CCL

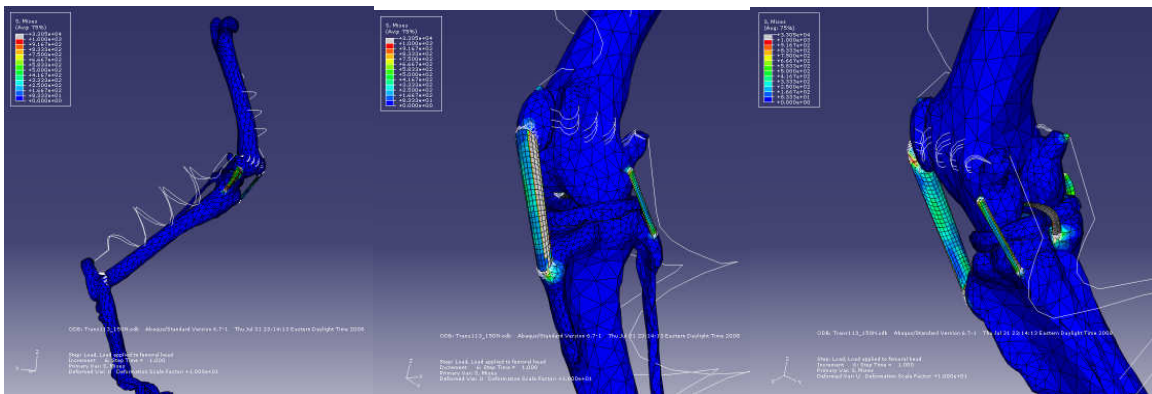


Figure 1.6.9: Several images of the PS transected stifle joint with ligaments in place at 113°.

Figure 1.6.10 below shows the comparison of stress distributions in the stifle ligaments for the intact and CCL deficient models at a stifle angle of 113°. Table 1.6.2 shows the percent difference calculations.

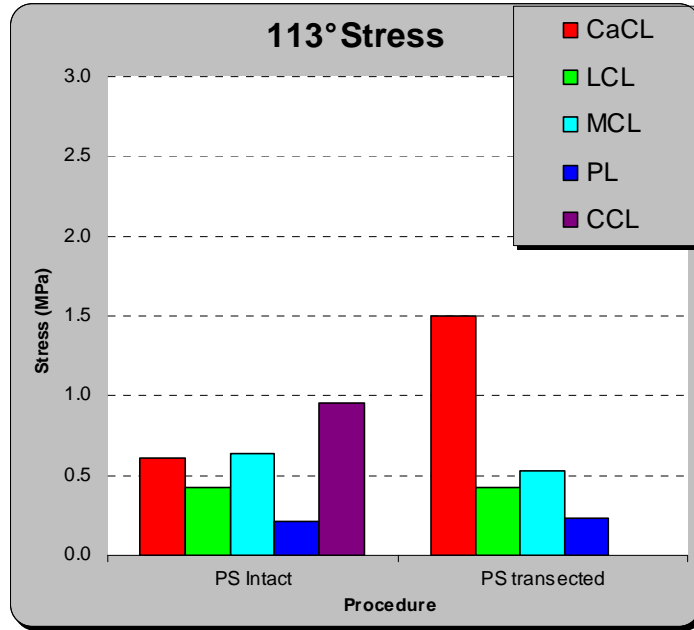


Figure 1.6.10: Graph of stress (MPa) in each of the ligaments of the PS intact and PS transected models at a stifle angle of 113°.

Table 1.6.2: Table of the percent difference between the PS intact model and the PS transected model at a stifle angle of 113°.

	113 Degrees (Percent Difference)	
	PS Intact	PS transected
CaCL	603.88	149.09%
LCL	424.82	0.79%
MCL	636.73	-17.33%
PL	217.77	8.87%
CCL	957.52	

1.6.3 148 Degree Results

The stress outputs for the stifle ligaments of the intact (Figure 1.6.11) and CCL deficient (Figure 1.6.13) models at an angle of 148° are shown below. Assembly pictures are shown in Figure 1.6.12 (intact) and Figure 1.6.14 (CCL transected).

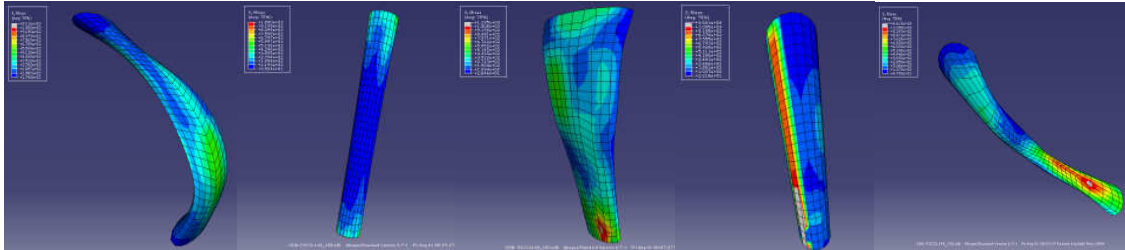


Figure 1.6.11: Visual stress output of the PS Intact stifle ligaments at 148°. From left to right: CaCL, LCL, MCL, PL, CCL

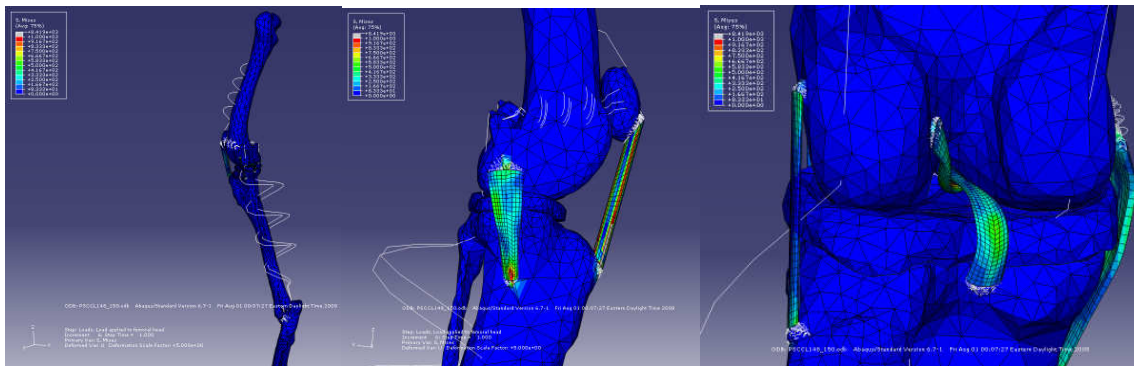


Figure 1.6.12: Several images of the PS Intact stifle joint with ligaments in place at 148°.

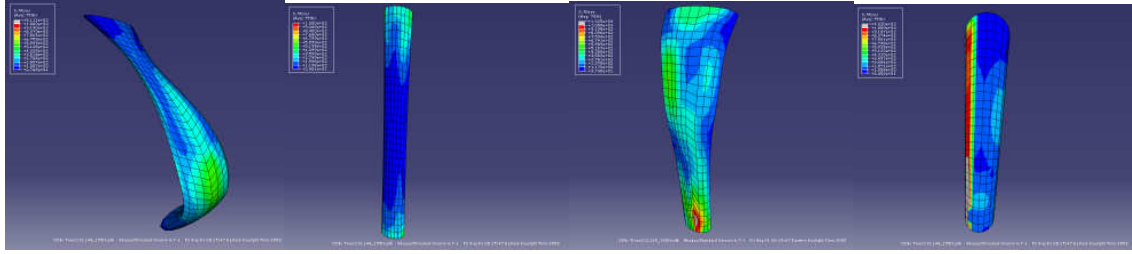


Figure 1.6.13: Visual stress output of the PS transected stifle ligaments at 148°. From left to right: CaCL, LCL, MCL, PL,CCL

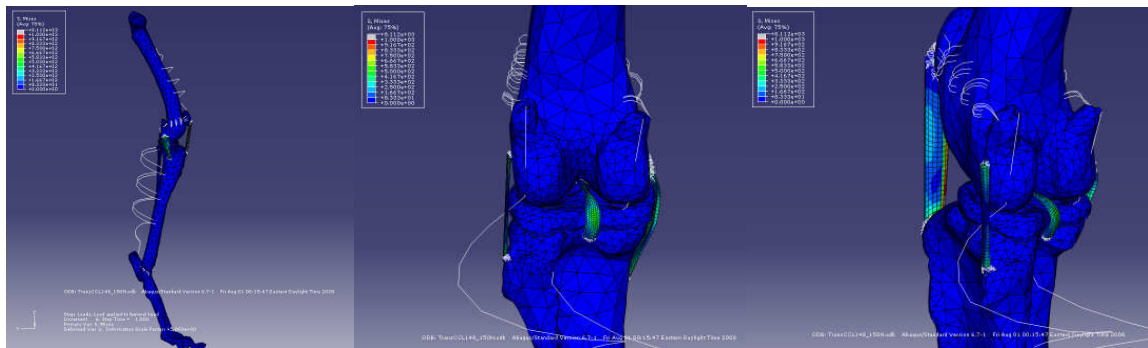


Figure 1.6.14: Several images of the PS transected stifle joint with ligaments in place at 148°.

Results for the stress analysis of the intact and CCL deficient stifles at 148° are shown below in Figure 1.6.15. The percent difference calculations follow in Table 1.6.3.

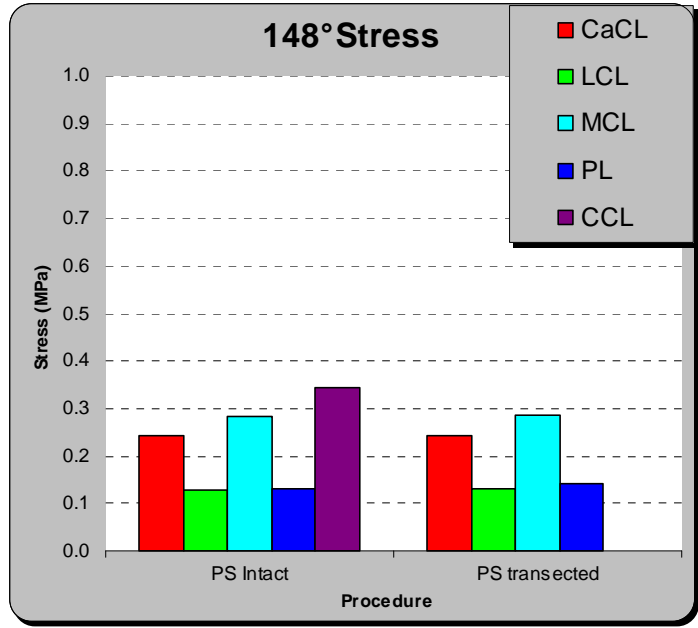


Figure 1.6.15: Graph of stress (MPa) in each of the ligaments of the PS intact and PS transected models at a stifle angle of 148°.

Table 1.6.3: Table of the percent difference between the PS intact model and the PS transected model at a stifle angle of 148°.

	148 Degrees (Percent Difference)	
	PS Intact	PS transected
CaCL	242.61	-0.05%
LCL	128.71	3.30%
MCL	281.81	1.96%
PL	132.19	7.22%
CCL	342.97	

1.7 DISCUSSION

The initial tibial plateau slope angle for this study (28°) was within ranges reported in literature. The results of the six independent FEA models that were tested agree well with previous studies and the physical testing [Crimi CS, 30].

The FE models in this study were able to mimic both normal joint function and the behavior of a CCL deficient stifle. Studies have shown that in the healthy intact stifle, a “cross-over flexion point” occurs at a patellar tendon angle (PTA) of 90° of flexion [97]. Thus, in a healthy stifle, no shear forces should exist at a stifle angle of 90° of flexion and the cruciates should be unloaded. At angles less than 90° of flexion the shear force should change to be directed caudally, thereby increasing the load on the CaCL as it becomes the primary restraint to craniocaudal motion. At angles greater than this crossover point, the load should be taken up by the CCL and the shear force should be cranially directed. According to physical testing [Crimi CS, 30], at stifle angles around and below 96° the caudally directed tibial shear force switches to a cranially directed one. The results from the finite element analysis also demonstrated this effect. For the intact model at a stifle angle of 75° , the CaCL appeared to be taking up the most amount of load and had a corresponding higher stress than the other stifle components. At 113° , significant contributions of both cruciates were apparent, but the CCL had higher resulting stress. At full extension (148°) the CCL was acting as the primary restraint mechanism with the highest stresses out of all the stifle components. However, there was a significant contribution from the CaCL present at this

angle. This may be due to the geometry of the meniscus acting as a lever against which the CaCL is being stressed.

Also important in the stability of the stifle joint are the collateral ligaments. In full extension, the stresses in the MCL were secondary only to those in the dominant CCL. The LCL was also fully taut and encountered significant stresses. At a stifle angle of 113°, the contributions of the collaterals were slightly less significant. In the flexed model (75°) of the intact stifle, the LCL was apparently slack, accruing almost no load or stress. The MCL was still a contributing factor to the load distribution at this angle however. The behaviors of the collaterals in the FE models are consistent with literature. Previous studies have found the collaterals to be fully taut and load bearing in full extension and as the stifle flexes the LCL becomes lax and the MCL remains only partially engaged [120]. This was also shown in the results from physical testing [Crimi CS, 30].

The transected models also showed good comparison to both existing literature and physical models. It has been found in literature that a cranial tibial translation results from transection of the CCL [91,121]. Only a slight subluxation was confirmed by the models in this study (specifics found in Appendix A). Upon removal of the CCL, the load on the CaCL increased during flexion, consistent with literature [91,105,121]. At 75° of flexion, a 5% increase in stress in the CaCL was noted as well as slight increases in the stress of the collateral ligaments. The patellar ligament actually resulted in a slight decrease of stress. In the transected model at 113°, a more prominent increase in CaCL stress resulted, increasing by

almost 150%. At this degree of extension the CaCL is expected to result in a substantial slackening as the tibia translates forward due to the now unrestrained cranial thrust. However, no significant tibial translation was noted for this angle and model. Therefore, it is assumed that the stifle is essentially in its starting position which would account for the unexpected increase in stress on the CaCL. Other results at this angle were that the stress in the patellar ligament decreased by 8.87%, while the stress in the MCL decreased by 17.3%. The stress in the LCL remained relatively unchanged at this angle of stifle extension. At 148° the behavior of the ligaments in the transected model was relatively unaffected when compared with the intact model. The MCL and patellar ligament were seemingly the primary means of restraint against cranial tibial thrust. The increase in load of the MCL as a result of CCL rupture is in good agreement with literature [105].

There are, as with any computer model, several limitations of the current study. This includes the assumption that the bone is linearly elastic and homogenous. This assumption is obviously not physiologic but is commonly implemented in biomechanical FE models investigating issues unrelated to the deformation of the bones. Another potential limitation of this model results from the fact that the CT data and resulting geometry was obtained from one subject. The subject was a large-breed dog of an average weight and initial tibial plateau slope similar to subjects used in previous studies.

The connection of the ligaments was made with rigid tie constraints and the surfaces of the ligaments and bones were not perfectly adjacent. As CT data was only available for one

stifle position, it was determined that manual manipulation was the only means to accurately represent the geometry and orientation of each ligament. Many 3D models found in literature continue to use straight line elements or nonlinear springs to represent ligaments, which have been found to be inaccurate for ligaments that experience warping or bending over the surfaces of the bones. It was thought, therefore, that the attachment was a reasonable sacrifice to the acquisition of anatomically accurate ligament geometries and material behaviors. Other approximations included the use of material properties from human studies. This is commonly practiced, however, for investigations of canine stifle anatomy due to the inconsistent and sporadic information concerning canine-specific material properties.

The results presented herein are subject-specific and extrapolation of this data should be done with caution. Additionally, these results cannot be compared between the three angles of interest because the ligaments used in the FE models were created specifically to fit the pre-surgical models at each angle. Also, they do not include any measure of pre-strain or pre-load to define the relationship between the geometry changes. Although it is clear that accurate representation of ligament in situ strain is critical for prediction of ligament stresses throughout the range of motion, data on ligament pre-strains for canines at each of the angles of interest in this study does not currently exist. However, comparisons between the intact and CCL deficient models within specific angles can be readily drawn since identical ligaments were used within each.

1.8 CONCLUSION

In summary, a series of 3-dimensional FEA models were created to simulate the canine stifle with and without a cranial cruciate ligament at three specific angles. These models incorporated neo-Hookean, hyperelastic ligaments, a meniscus, as well as the primary bony structures of the canine rear limb from the hip down. To our knowledge this has not been attempted before at such a level of detail. The models showed good agreement with literature and physical testing [Crimi CS, 30].

The results at 75° displayed a caudally directed shear force, in the form of an associated increase in stress in the CaCL, which increased slightly with transection of the CCL. As a secondary stabilizer, the MCL increased in load while the LCL remained lax at this degree of flexion, as is supported by previous research. At both 113° and 148° the CCL was the primary restraint against the now cranially directed shear force. An increase in stress of the CaCL following CCL transection was prominent at a stifle angle of 113° due to the apparent absence of cranial subluxation. At full extension (stifle angle of 148°) the patellar ligament and collaterals were the main stabilizers for the CCL deficient model whereas the CaCL decreased in stress slightly, as expected. The behavior of both the collateral and cruciate ligaments for both the intact and CCL deficient models are in good agreement with literature and physical testing over the range of motion. This suggests that the design and definition of the FE models in this study are an accurate representation of normal function of the stifle joint and can be used to accurately predict the effects of cranial cruciate deficiency.

2. SURGICAL PROCEDURES AND TESTING

2.1 INTRODUCTION

Because of the impact of the CCL on the stability and function of the stifle and its link to degenerative joint problems, the treatment and prevention of CCL rupture remain vital research topics in both veterinary medicine and biomedical related engineering.

Unlike humans, CCL deficiency is better treated with the use of procedures that alter the geometry and eliminate the tibial shear force rather than trying to replace the lost ligament. Among the currently available treatment options are the widely accepted and researched TPLO, and the newer TTA and TTO procedures. During a TPLO procedure, a radial osteotomy is performed on the proximal tibia and the tibial plateau is rotated so that it is nearly perpendicular to the tibial long axis, thereby reducing the tibial plateau slope and neutralizing the destabilizing cranial tibial shear force [108,109]. The tibial tuberosity advancement (TTA) procedure aims at reducing the tibiofemoral shear force by advancing the tibial tuberosity so that the patellar ligament is perpendicular to the tibial plateau when the stifle is in extension [78,79,116]. The triple tibial osteotomy (TTO) technique combines features from both the TPLO and TTA to stabilize the stifle and eliminate the harmful cranial tibial thrust. There have been several documented in vivo and in vitro experimental studies evaluating the effects of different surgical approaches such as the TPLO, TTA and TTO. In vivo experiments are difficult to conduct and nearly impossible to keep devoid of bias [104]

and in vitro studies are popular but are most often inconclusive. Because of a lack of information regarding several aspects of these procedures, a large percentage of surgeons still select a technique based on these cadaveric studies, case series and personal preferences [3]. It is believed that some surgical procedures may cause biomechanical anomalies due to a redistribution of stresses among the significant ligaments and tendons in the stifle. Increased stresses in the patellar tendon, for example, may affect the position of the patella and possibly result in patellar luxation [9]. Another theory of particular interest is that by eliminating cranial tibial thrust, the stress on the caudal cruciate ligament is increased, thereby possibly predisposing this influential ligament to rupture [121]. While post-operative findings and complications related to each surgery have been reported, there has been no known research to this date that has evaluated post-operative ligament stresses in a CCL deficient stifle treated with the TPLO, TTA or TTO let alone a valid and unbiased comparison between these three different techniques.

The objective of this research project was to utilize a previously developed 3D quasi-static finite element model of a CCL deficient stifle, simulate treatment by each of the three aforementioned surgical procedures (TPLO, TTA and TTO) and investigate the post-operative stresses in all major ligaments of the canine stifle. Since these surgical procedures are meant to rearrange load bearing surfaces, the examination of the resulting stresses and loads is a logical path for determining the true effect the surgeries have on the joint. Finite element analysis has been utilized by several researchers and proves to be an efficient tool for predicting joint kinematic responses for given parameters [38,83]. The geometric results

of the finite element model will be validated with a physical model from a parallel research experiment based on the same scans used to produce the FEA model [Crimi CS, 30].

Very little research has been done on modeling the canine stifle using FEA and no known studies have modeled the entire canine limb and examined the stifle mechanics before and after corrective surgery for a torn CCL. The models developed in this study will provide a means for determining information regarding stifle joint mechanics that is currently unavailable. It is quite possible that some of the findings of this study may explain several presently documented post-operative complications, such as osteoarthritis progression [90] and patellar luxation [9], for which the cause remains uncertain. It would be immensely beneficial to the veterinary community to ascertain the true effects of surgical procedures used to treat such a prominent and devastating condition as CCL disease. This research aims to use modern technology and reliable, recognized engineering tools to determine the post-operative effects of widely used tibial osteotomy surgeries and give veterinary orthopedic surgeons a more dependable method for determining the most suitable strategy and better predict the final outcome.

2.2 BACKGROUND INFORMATION

2.2.1 Intra-Articular and Extra-Articular Techniques

Mimicking the surgical answer for anterior (cranial) cruciate ligament deficiency in humans, the first applied treatments in the canine stifle were intra-articular and extra-articular procedures. These are still used in practice today although their popularity is declining with the advent of newer, more advanced procedures. Extra-articular techniques rely on non-absorbable, heavy gauge suture materials, wires, or transposition of periarticular tissues to provide joint stability over time. Consequences of this technique include limited tibial rotation, increased compression of the joint surfaces and possible cartilage and meniscal wear [121]. Intra-articular techniques utilize a more biomechanical approach and implement allografts, autogeneous tissues or synthetic materials to anatomically reconstruct the ruptured ligament and mimic its function and orientation. This allows for normal stifle range of motion and no limitation to tibial internal rotation. Most studies have cited good to excellent limb function in dogs that have had intra-articular procedures. However, intra-articular techniques have been found to be susceptible to early failure, even more so than extra-articular procedures. Grafting tissues undergo early avascular necrosis and encounter a considerable loss of structural and material properties after implantation. Fixing these complications is a slow and complicated process and the resulting ligament is often times left with a maximal strength that does not exceed 30% of the intact ligament [121].

If the true test of treatment for CCL rupture is the procedure's ability to restore normal joint function and prevent progression of secondary joint disease, then intra- and extra-articular techniques have failed as a treatment option. Neither extra- nor intra-articular techniques consistently preserve long-term stifle stability or prevent progression of arthritis and secondary meniscal damage.

2.2.2 Tibial Osteotomy Procedures: A Novel Approach to CCL Deficiency

The Tibial Wedge Osteotomy (TWO), proposed by Slocum and Devine, was the first of a series of new approaches for the treatment of CCL rupture. This was then improved upon by Slocum and Slocum [109] to create the Tibial Plateau Leveling Osteotomy (TPLO). Unlike intra- and extra-articular techniques, the TPLO aims to eliminate the tibial shear forces that occur in the stifle during weight bearing by reducing what they coined as cranial tibial thrust. This was a novel approach to the problem of CCL deficiency. There have been several studies on the complications after TPLO with several intra-operative and postoperative complications reported clinically. These include under- and over-rotation of the tibial plateau, incorrectly centered osteotomies, infections, implant failure, tibial crest fractures, and patellar tendinosis. Other studies have found that the procedure does not consistently prevent the progression of osteoarthritis [87,90,112]. Patellar tendon thickening is another complication that has been reviewed and confirmed in literature [9]. A caudal tibial thrust has been shown to exist accompanied by a caudal tibial translation that increases with increasing axial tibial load [91]. This has been thought to increase the load seen on the caudal cruciate ligament and potentially predispose it to failure. It has been identified that

imprecise placement of the osteotomy results in inaccurate tibial plateau leveling and if under-rotated may lead to persisting cranial subluxation. If over-rotated, an excessive caudal tibial thrust may further increase the load seen on the caudal cruciate [121].

Montavon *et al.* proposed that there are actually two possibilities for neutralizing the cranial tibial thrust in the CCL deficient stifle [115]. They stated that one option is to make the tibial plateau perpendicular to the Achilles' tendon and essentially the tibial long axis as proposed by Slocum and the TPLO. The other possibility for stabilization is to make the tibial plateau perpendicular to the patellar ligament. This second option was implemented in a new technique they called the Tibial Tuberosity Advancement technique (TTA). The TTA procedure was based upon a biomechanical model of the joint forces of the human knee. Correcting the angle of the patellar ligament is well known in human orthopedics, but had not been used to treat CCL deficiency in dogs. The TTA positions the patellar ligament perpendicularly to the tibial plateau by advancing the tibial tuberosity and eliminates the tibiofemoral shear force, stabilizing the stifle during weight bearing. The developers claim it to be a less invasive technique and clinical results have been shown to be satisfactory. However, complications have been found to occur such as failure to maintain patellar ligament advancement, implant failure, tibial tuberosity fracture, medial patellar luxation, CaCL injury because of excessive advancement, and meniscal injury [57,60]. The TTA preserves the natural tibiofemoral articulation because no rotation of the tibial plateau is induced. Natural load transmission across the stifle and menisci will also be more likely to remain unaltered. The technique is still relatively new and in depth experimental studies have yet to be done to fully define the effects and benefits.

The Triple Tibial Osteotomy (TTO) procedure is a recently developed treatment option for CCL rupture. It can be thought of as a hybrid of a Tibial Wedge Osteotomy (TWO) and TTA procedure. Similar to the intent of the TTA, this procedure aims to reposition the patellar ligament so that it is perpendicular to the tibial plateau in extension. This is achieved, however with a series of proximal tibial osteotomies that rotate the tibial plateau and subsequently advance the tibial crest cranially. Very little study based on clinical cases has been reported thus far [20]. Complications encountered included tibial tuberosity fractures, infection and meniscal injury. Advantages of the TTO procedure include the minimal change to the orientation of the tibiofemoral articulating surfaces, no loss of limb length, and low technical difficulty [57].

2.3 REVIEW OF LITERATURE AND RESEARCH

With cranial cruciate disease remaining one of the largest threats to rear limb function and a growing concern for both pet owners and orthopedic surgeons, research related to joint motion, joint function and surgical treatment for CCL disease continue to be a greatly valued area of research. Several considerations must be made when it comes to diagnosis of CCL disease, treatment selection and procedure performance. A fundamental prerequisite, however, is a thorough understanding of knee anatomy, possible complications and both existing and novel approaches to correcting a ruptured ligament. There is a vast wealth of knowledge on each of these subjects. This section aims to inform the reader of issues concerning cruciate disease, joint degeneration and corrective surgeries by providing a selection of prominent research related to the contents and purpose of the project.

2.3.1 The Cruciate Ligaments

The canine stifle is an intricate joint whose function and stability relies entirely upon the cooperation of five major ligaments, a few large muscle groups, supporting cartilaginous tissue and bony structures such as the tibia, femur and patella. There have been several who deem the cranial cruciate among the most important components in this system [4,23]. Kinematic studies in dogs were able to confirm that transection of the CCL results in substantial cranial tibial subluxation during the stance phase of the gait [58,114]. These studies demonstrated that forces from the surrounding muscle groups are unable to

compensate for the loss of stability provided by the CCL. Complications concerning the CCL are frequent and in most cases detrimental to the dog. The understanding of the role both cruciate ligaments play to the overall function of the joint is an important and valued task. De Rooster *et al.* presented a thorough investigation into the makeup, function and clinical relevance of the cruciate ligaments [33]. Their paper is a compilation of previous research and literature regarding the cruciate ligaments in order to present a concise and complete description of their attributes and roles and establish their significance in stifle joint stability. They proposed that little may actually be known about the canine cruciate ligaments because existing information is sometimes not delineated between species and they also argue that an understanding of CCL geometry and function is essential for the understanding, diagnosis and treatment of CCL rupture. Among the most important comments in this paper are that the CCL is the most important ligament in cranio-caudal stifle joint stability because it is the primary restraint against cranial drawer movement, that the importance of the Caudal Cruciate is much less understood but is known to stabilize the knee against caudal drawer motion, and that the behavior of the cruciates is largely due to their biomechanical makeup, most noteworthy being the crimped pattern of their fibril bundles which others have also attributed as a significant determinant of their structural properties [44].

Many other sources agree that the primary significance of the CCL is its restraint against cranial tibial thrust, the component of tibiofemoral reaction force that causes the tibia to translate cranially relative to the femur [104,108,109,121,125]. Mechanical tests have been

done to determine the restraining action of each stifle ligament and findings also support this assertion. One study in the 1970's, selectively cut each ligament and determined after force application the amount of increased tibial translation [23]. Researchers such as Butler found this method to be imprecise and developed a methodology that uncoupled the applied force and measure of ligament significance [23]. Using this method, they were able to identify the contribution of each ligament. Their research established the ACL as the primary ligament to knee function and contested the findings of others at that time by stating that that ACL restrains anterior movement.

2.3.2 CCL Rupture

Due to its significance to the stability of the stifle joint, as mentioned in the previous section, the causes for distress and rupture as well as the effects of cranial cruciate insufficiency have been studied in numerous papers and through various methods. Hayashi *et al.* studied morphologic features in the cranial cruciate ligament in order to identify the changes that ultimately lead to its structural failure [44]. The authors focused on identifying histologic changes in ruptured cranial cruciate ligaments. Their study was sound and they were able to quantify the alterations in ruptured canine CCL and show a correlation between rupture and changes in ligament fibroblasts, ECM, “epiligamentous reparative response”, loss of normal ligament crimp, and loss of birefringence. They agreed with the other studies they cited that these changes, which may be largely due to age, could be the reason for changes in mechanical properties and ultimate failure of the ligament. This, as mentioned in the next

section, is one argument against growing speculation that other characteristics such as steep tibial plateau slope could lead to CCL rupture.

Understanding the effects of CCL rupture on the other components of the stifle as well as the overall function of joint and limb is necessary in treatment and prevention of cranial cruciate disease. DeCamp *et al.* [35] provided a gait analysis showing the changes in flexion and extension due to the loss of the CCL in the stifle in order provide a basis for diagnosis of the treatment of cranial cruciate disease. Their results were based on experimental induction of CCL rupture in test subjects and the analysis of change in movement of the hind limb after removal of the CCL. As the authors stated, the differences in motion are likely an adaptive response to pain and the unstable joint as well as the altered biomechanics of the joint but they did find that the flexion/extension capabilities of the major joints of the hind limb changed following transection of the CCL as well as the stride length of the gait. Although this paper was titled a “noninvasive” approach, the method for procuring their results was direct manipulation of live test subjects. This method may also have lead to misleading results. For example, all dogs in the study also developed meniscal injury which could have further impaired joint movement by increasing discomfort in the dog and therefore changed the dogs’ motion. The authors even assert that there has been no correlation found between CCL rupture and eminent meniscal injury so this occurrence may not be representative of the larger population but a result of testing procedure and unnatural stresses put on the animal subjects.

Some speculation has been made regarding the effect that CCL rupture has on the caudal cruciate ligament [33,43,125]. Zachos *et al.* presented an experimental study on the morphologic effects of CCL insufficiency on the CaCL [125]. One possible effect is an increase in stress in the caudal cruciate after the loss of its cranial counterpart. Although there are always uncertainties associated with in vivo studies such as differences in specimen makeup, the researchers identified differences in the fibril diameter of the CaCL in the intact and CCL deficient stifles that show a possibility of compromised material properties in the caudal cruciate ligament after repeated cranial thrust in a CCL deficient stifle. Their research does not show enough evidence or quantification of the morphologic changes on the CaCL and the authors support further research related to this endeavor. Other research has shown that the caudal cruciate ligament undergoes a substantial increase in tensile load during weight bearing due to its change in role to prime stabilizer of craniocaudal joint motion [121]. This, as several research papers have suggested, is reason to believe that a stress increase in the caudal cruciate ligament accompanies cranial cruciate ligament insufficiency [121]. This increase in stress and tensile load may cause the CaCL to be more prone to rupture. Also mentioned is the concern that surgical procedures for correcting CCL rupture may further injure the potentially compromised caudal cruciate ligament by further increasing the post-operative tensile load and stress [104,121].

Work has also been done on the mechanical response of articular cartilage to joint instability caused from rupture or transection of the cranial cruciate ligament [100]. Osteoarthritis has been found both clinically and experimentally to follow the loss of function of the CCL [90,

100]. Setton *et al.* stated that damage to the solid matrix of the cartilage may be the most contributing factor to cartilage degeneration and conditions such as osteoarthritis [100]. The findings of their research, based on measurements of material properties as well as cartilage hydration, showed significant changes in structural properties following transection of the CCL, linking loss of this ligament and the resulting instability of the joint to the damage of the surrounding articular cartilage. Most notable of these structural changes was a decrease in the stiffness and shear as early as six weeks after removal of the ligament and which continued to decrease over time. The authors stated other studies done in a similar fashion but resulted in slightly different findings with regards to certain aspects such as changes in compression stiffness. These differences are likely due to variations in testing methods and specimens but the authors were objective in stating contrasting research and not insisting that theirs was superior or more accurate. There remains, however, an area of uncertainty regarding the correct trend in material property changes of the stifle articular cartilage and may need further investigation.

2.3.3 Tibial Plateau

The tibial plateau is defined as the bony surface of the lateral or medial condyle of the tibia that articulates against the analogous condyles of the femur [73]. The lateral and medial condyles of the tibia are separated from the corresponding femoral condyles by the lateral and medial menisci. The angle that the tibial plateau makes with a line perpendicular to the long axis of the tibia is often designated the tibial plateau angle (TPA) or tibia plateau slope (TPS). The tibial long axis is a line from the midpoint of the intercondylar eminence to the

center of the talus and the plateau is measured from the cranial aspect of the medial tibial articular surface to its caudal aspect [41,51].

2.3.3.1 Steep tibial plateaus

There are several instances in literature which state that cranial tibial thrust is directly proportional to the tibial plateau angle and would thus significantly increase, along with more severe joint instability, with CCL injury [43,82]. However, some researchers offer that increased TPA is not a common risk factor for CCL rupture and many dogs with a steep tibial plateau do not experience cruciate disease [43,44]. Through experimental testing, Havig *et al.* found no correlation between TPA and clinical outcome for dogs treated with lateral suture technique (LST), suggesting that, at least for this case, tibial plateau angle is not a means for predicting CCL injury [43]. Research by Osmond, Marcellin-Little, Harrysson *et al.* assessed the morphology of proximal tibial abnormalities that could result in a steep TPS and suggest that the abnormalities themselves could be the cause for ligament failure and the steeper slope [82]. The influence of the biomechanical properties of the stifle ligaments themselves on CCL failure has also been investigated [33,44]. De Rooster *et al.* mentioned that recent investigations discovered infiltration of the CCL by synovial fluid is possible and could lead to inflammation of the synovial membrane and CCL epiligament similar to those that typically accompany joints with CCL rupture [33]. It is unknown, as the authors stated, whether this inflammation occurs prior to rupture and they suggest this is a worthwhile research topic. Ultimately, though a correlation between cranial thrust and tibial slope has

been reported clinically, no relationship between a steep TPS and eminent CCL failure has been proven to date [82].

2.3.3.2 Tibial Plateau Measurement Concerns

Regardless of its connection to CCL failure, the tibial plateau slope remains an important element for both research and pre-surgical planning. Measurement of this slope, however, is often times subject to position and observer variability [43]. Caylor, Zumpano *et al.* [28] assessed the intra-observer and inter-observer variability in the tibial plateau slope measurement from lateral radiographs measured by three different observers of varying experience levels. Their results showed no statistical variation between intra-observer measurements, a significant difference in the inter-observer variability of the novice observer and no difference in inter-observer variability between the experienced and intermediate observers. Since their research study, others have investigated similar facets of the tibial plateau measurement concerns. Fettig *et al.* [41] used a larger sample size (40 dogs of various breeds and a mix of both right and left hind limbs) and more observers (11 observers of varied experience with measuring TPA) and investigated the correlation between observer variability and characteristics of the dog such as age and degree of joint degeneration. They found evidence of both intra- and inter-observer variability but found no correlation between the variability and dog characteristics or angle of plateau itself. Their results showed that at least one pair of points needed to measure the TPS showed significant variation and this also showed correlation to the degree of degenerative joint disease.

The variability in TPA measurements has encouraged a better description and methodology for measuring this value. Baroni, Mathias, Marcellin-Little *et al.* researched two possible methods for measuring this important reference angle [12]. They contend that known significant observer variability, supported through research such as those previously mentioned, necessitates a re-thinking of the conventional TPS measurement method. Their proposed method relies more on the articulating surface and could more accurately measure the TPS and result in less variability. The researchers also investigated the use of digitized radiographs and their effect on TPS measurement. Figure 2.3.1 below shows a diagram from their paper illustrating the two different measurement techniques.

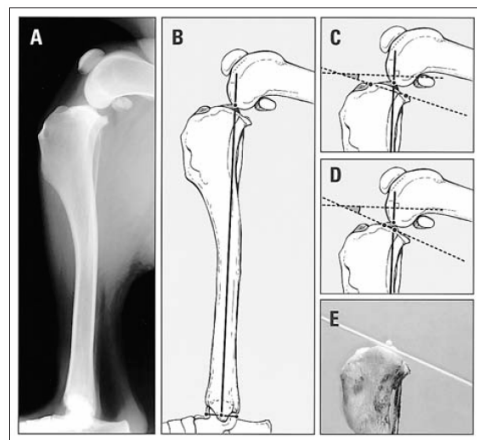


Figure 1—Mediolateral radiographic view (A), illustrations (B, C, D), and photograph (E) of a tibia and stifle joint in a dog. Femoral condyles are superimposed. Tibial plateau slope (TPS) is conventionally measured by comparing orientation of the functional axis of the tibia defined as the line joining the intercondylar eminence and a point equidistant to the cranial and caudal aspects of the trochlea of the talus (B) and the axis of the medial tibial condyle defined as the line joining the small, discreet cranial margin of the tibial plateau and the point of insertion of the caudal cruciate ligament (C). Alternatively, the axis of the medial tibial condyle may be defined as a line tangential to the cranial linear portion of the medial tibial condyle at the femorotibial contact point (D). The latter measurement more closely approximates the anatomic slope of the medial tibial condyle (E).

Figure 2.3.1: Illustrations of the conventional TPS measurement method and that proposed by Baroni, Marcellin-Little *et al.* Used with permission from the publisher [12].

The setup of their experiment kept very good control over all variables, especially observer experience with each measurement method. Those observers who measured using the alternative method were not trained in using the conventional technique and vice versa. Thus, the authors could ensure that no outside influence to measurement techniques would be included. The TPS measurements using the alternative method were not significantly different from the anatomic TPS measurements. Results for measurements taken using the conventional method were considerably lower than the anatomic measurements. For both alternative and conventional methods, the mean \pm SD for the TPS measured using digitized radiographs was closer to the actual anatomic values than those from printed radiographs. The duration for measurements using printed radiographs versus digitized was not significantly different but the inter-observer variability and mean absolute deviation decreased significantly for the measurements resulting from digitized radiographs, with the measurements using a combination of alternative TPS measuring technique and digitized radiographs giving the smallest mean absolute deviation to the anatomic TPS measurements. This research suggest that if variability and accuracy are a concern, there are alternatives to the measurement approach, such as the alternative technique proposed in their paper or use of digitized radiographs in place of conventional printed ones, that could lead to more precise and repeatable results.

2.3.4 Tibial Osteotomies

There are many currently available techniques for correcting a ruptured CCL in dogs. While surgical methods vary, the main objective of most is to eliminate cranial tibial subluxation

resulting from the loss of the ligament and limit tibial internal rotation throughout the range of motion. Extra-articular techniques rely on nonabsorbable suture materials and while joint stability may be restored, the tibia is fixed in external rotation and stifle rotation is limited to a single transverse axis whereby disrupting normal joint kinematics [7,121]. Intra-articular techniques use grafting or similar means to create a replacement ligament which can mimic the function of the CCL and allow for normal stifle range of motion [95,111,121]. Many studies have been done on the effects of intra-articular and extra-articular procedures, which have been shown to be susceptible to early failure and result in a ligament whose maximal strength is only a fraction of the normal CCL [1,5,6,22,29,36,95,106,111]. Due to the limitations offered by these methods, a new branch of preventative measure was accepted with the development of tibial plateau osteotomies. Several osteotomy procedures are available but a review of only those methods to be used in this research is outlined below.

2.3.4.1 TPLO

The Tibial Plateau Leveling Osteotomy (TPLO) was the first procedure based on an elimination of cranial tibial thrust by altering the proximal tibial geometry and remains one of the most popular surgical techniques, especially in large breed dogs, for the treatment of CCL rupture or injury [12,104,109]. The idea behind this procedure is not to replace the injured ligament, but to rearrange the loads and stresses and essentially make the absent ligament unnecessary while eliminating consequences of the rupture such as increased cranial tibial thrust or cranial tibial translation [41].

Several clinical studies and cadaver experiments have been done to determine the post-operative results of the TPLO procedure and also to contest the assertions of its proponents that it is superior to all other surgical techniques [104]. The transformation of cranial thrust to caudal thrust is one of the aspects that have been investigated [91]. Following the techniques outlined by Slocum and Slocum and using cadaver canine hind limbs, Reif *et al.* loaded the dog leg in a custom testing fixture to evaluate changes in joint stability before and after a TPLO procedure. They did not include the patella or patellar ligament in the study. Joint behavior for a CCL deficient stifle was mimicked in that the cranial tibial thrust resulted in a cranial tibial translation after severance of the CCL. Measurements confirmed that caudal tibial thrust resulted after the TPLO was performed and the authors assumed, but did not investigate further, that the forces within the CaCL also increase after the procedure. They mention that the caudal tibial thrust may be correlated to the axial load just as they showed that cranial tibial thrust was dependent upon the axial load. Though they make several predications and assumptions on the post-operative stresses of the ligaments, there was no such measurement of these variables and no quantification or validation of these assumptions. Jandi and Shulman investigated the post-operative effects of the TPLO procedure on the flexion and extension capabilities of the joint in a clinical case experiment of 412 cases [53]. The procedure performed on the stifles in their experiment was a modification to that proposed by Slocum but was performed by a board certified surgeon. The modification was not mentioned. The dogs were evaluated at two separate occurrences after surgery and lameness, flexion, and extension were recorded. The conclusion of their study reported no significant motion loss due to the TPLO but a positive correlation between

clinical lameness and extreme motion loss (>10%). Those dogs with slight motion loss (<10%) did not experience any signs of clinical lameness. The authors suggest that motion loss after knee injury and treatment is most likely related to developments such as the formation of fibrous tissue, adherence of the patella to the trochlear groove due to fibrous tissue accumulation and progression of conditions such as osteoarthritis. Complications other than motion loss due to TPLO have also been reported [87,112]. In a study from Stauffer *et al.* [112] the majority of complications found resulting from surgery (9.5%) were short-term such as swelling and tibial fracture, though long-term complications were found in nearly just as many patients (8.3%). The authors concluded that the TPLO had good overall clinical results and that the complications resulting from the TPLO procedure are not greater than any other similarly invasive orthopedic procedure. However, they do not state the complication rates or procedures to which they are referring. The overall complication rate stated in their report (18.8%) was less than a similar study by Priddy *et al.* [87], which reported a complication rate of 25%, but their sample size was considerably larger. In the latter study, the complications that did occur responded well to treatment but the authors overall were borderline disapproving of the procedure, stating that the complication rate found was higher than other surgical techniques used to treat a ruptured CCL. This was a contradictory assertion to a previous statement they made that few complication rates have been documented for other techniques and “direct comparisons of complication rates for the various surgical techniques are not possible because of differences in study designs and reporting of data.” Without adequate comparison or quantification of complication rates, the conclusions for clinical studies such as these are more of an opinion than fact.

In a study by Warzee *et al.*, a significant caudal tibial translation and associated increase in strain experienced by the CaCL following the TPLO procedure was confirmed [121]. Their findings showed that the resultant force through the weight bearing stifle was directed 6.5° more cranially than the tibial long axis. For this reason, the authors recommended an optimal plateau rotation angle of 6.5° and cautioned against over-rotation of the tibial plateau to avoid excessive increase in post-operative stress in the CaCL. They do not quantify or verify an increase in stress following the procedure. Tibial internal rotation was also investigated and a correlation was determined and illustrated below in Figure 2.3.2. As shown, tibial internal rotation was not completely eliminated after the procedure. The effect or relationship of this rotation to the CaCL was not investigated and the clinical significance of this rotation remains unknown. Testing for this study was done using a custom testing fixture and the specimens were positioned and tested at only one stifle angle. This study also failed to fully duplicate all of the muscle forces acting on the canine stifle.

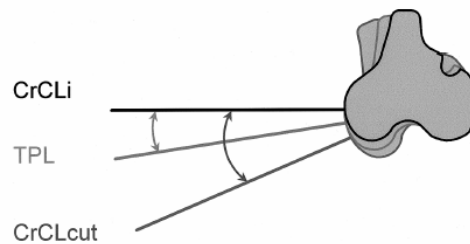


Fig 7. Schematic representation of the dorso-ventral projections of the tibial transcondylar pin used to determine tibial axial rotation. Tibial axial rotation angles were measured with respect to the pin projection in the intact specimens after: 1) CrCL transection, and 2) TPL.

Figure 2.3.2: Schematic showing tibial axial rotation. Used with permission from the publisher [Warzee *et al.*, 121].

A 3-dimensional, theoretical model of the canine stifle was examined by Shahar and Milgram in order to determine similar biomechanical effects due to altering the tibial plateau angle [104]. They were particularly interested in the forces experienced by the various stifle ligaments. Comparison of the intact stifle and the same stifle rotated through two different TPLO angles showed that the force in the CCL was greatly reduced for a TPA of 0° but only partially decreased for a 5° TPA. In order to keep the CaCL remaining unloaded the authors recommended a tibial plateau rotation to a TPA of no less than 5°. This study showed congruence with the study done by Warzee *et al.* in that the caudal cruciate ligament in the CCL deficient stifle experienced a considerable increase in tensile load as a result to a change in the TPA. The authors did mention that mathematical models such as they presented have several disadvantages and limitations. Their model included simplifying assumptions such as ignoring the effect of the menisci, limiting the movement of the patella to only rotation in the sagittal plane and material property simplifications such as modeling the ligaments as nonlinear springs. Lessening or limiting these assumptions would improve upon the theoretical model and provide a more accurate picture of joint motion in a CCL deficient stifle before and after a TPLO procedure or newer procedures such as those mentioned in the following sections.

Expanding on the effects of tibial plateau rotation on the function of the stifle and success of the TPLO procedure, a study was done to evaluate whether the center of this rotation also has an adverse effect on the clinical outcome [59]. Only one stifle angle and one loading condition was tested. The angles were readjusted after loading to assure their original

positions. The analysis was organized and the results were clear and meaningful. The study found that positioning the osteotomy too far distal resulted in an incomplete neutralization of cranial tibial thrust and when centered appropriately the osteotomy resulted in the correct and expected biomechanical effect. Another benefit this paper yields is a rethinking of the method in which tibial subluxation is measured. They offer a sound argument for using a corrected subluxation value and found, for this experimental circumstance, that the correctly centered osteotomy resulted in a subluxation value that was not significantly different from the intact stifle but the distally centered osteotomy had considerably higher tibial subluxation, similar to the value of the untreated CCL deficient stifle. There was also a positive correlation between the distal osteotomy and a shift in the tibial long axis. It may be useful to expand this research to more stifle angles.

Mattern *et al.* did a study confirming patellar ligament desmitis following TPLO and mentioned the possibility of increased stresses on the patellar ligament following the procedure [69]. They did not directly measure the stresses nor compare them with pre-operative conditions but compared the change in cross-sectional area. Confirmation of a significant change in stresses would be notable since it has been said that stress changes is suspected to be an “important factor in the development of patellar ligament desmitis” [69]. Expanding on this research to include an investigation into the occurrence of patellar tendinosis as a complication of TPLO, Carey *et al.* confirmed this patellar ligament inflammation and discovered that patellar tendinosis only occurred in dogs with severe

patellar tendon thickening [26]. Also, the pre-surgical state of the CCL was linked to the PTS in that dogs with a partial rupture were more likely to develop the condition.

The notion that TPLO prevents progression of osteoarthritis and degenerative joint disease has also been challenged [48,62,90,104]. Rayward *et al.* studied this in a clinical experiment [90]. After two post-operative reviews of the subjects' radiographs and evaluating progression of osteoarthritis based on osteophyte score, the authors discovered that while the majority of cases resulted in relatively no change in osteophyte score, nearly half of them resulted in a significant increase. This is shown below in a chart from their paper.

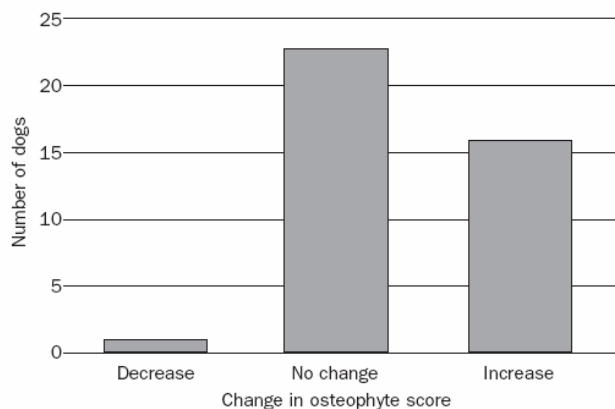


FIG 4. Change in osteophyte score from entry to six months

Figure 2.3.3: Chart showing change in osteophyte score over six months. Used with permission from the publisher [Rayward *et al.*, 90].

The authors mention the possibility that the majority of unchanged osteophyte score could be attributed to the success of the procedure or could also have been merely due to intrinsic variation in the individual patients. There were several uncertainties in their study. The

procedures varied from case to case depending on the dog's condition. Due to the fact that some of the subjects were treated differently, other variables could have been introduced that could account for different osteophyte scores. These variables should be removed in order to present a clearer picture of the post-operative effects. A longer study would also help elucidate the long-term results of a TPLO concerning osteoarthritis progression since it has been found that osteophyte score is highly correlated with the duration of the disease. Hurley *et al.* also investigated the progression of osteoarthritis and managed to eliminate some of the variation from which the previously mentioned study suffered [48]. Their study was also much shorter, reporting after only 8 weeks as compared to 6 months. A slight but measurable increase in degenerative joint disease (measured by progression of osteophytes) after the 8 week radiographic review was found. A higher number of patients resulted from a decrease in osteophytes than in the study done by Rayward *et al.* The study also investigated the change in tibial slope angle (TSA) and found that there was a considerable increase in TSA after 8 weeks for those dogs who received the smallest TPLO plate. This was also confirmed in a study by Moeller *et al.* [75]. This relationship or possible connection to DJD progression was not investigated.

As several issues concerning the TPLO procedure remain unanswered other procedures have since been developed. Information regarding one of these, the tibial tuberosity advancement technique, follows in the next section.

2.3.4.2 TTA

The Tibial Tuberosity Advancement (TTA) is a more recently developed technique for treating cranial cruciate ligament deficiency. Developed at the University of Zürich, it is based off a mechanical model of the human knee with assumptions pertaining to the canine stifle [60]. The approach maintains biomechanical considerations similar to the TPLO but rather than eliminating cranial thrust by rotating the tibial plateau, it aims to do so by positioning the patellar ligament perpendicularly to the tibial plateau [60,78,79,80,115,116]. Montavon, Damur and Tepic praise the TPLO procedure for “[reinvigorating] small animal veterinary orthopedics in an unparalleled way” but justify advancement of the tibial tuberosity as being the less invasive counterpart approach that gives greater attention to the global muscular function and takes into account the functional use of the limb instead of false loading conditions [31,80,115]. The authors and developers of the procedure rationalize that the total joint force is not, as Slocum has maintained, parallel to the functional axis of the tibia but rather approximately parallel to the patellar ligament [116]. In one of their preliminary publications of the TTA method the results from a clinical study were presented [79]. The results of 200 procedures showed mainly good outcomes with nearly all of the complications being related to poor placement of the pronged plate and a couple concerning the location of the osteotomy. All complications were successfully treated and healed normally. There also appeared to be a positive learning curve in that the last 40 patients treated with the TTA showed no complications. In an accompanying article they mention that surgeons throughout Europe, USA and Japan performing the procedure under the controlled clinical release reported reproducibility, as well as reduced complexity and

morbidity in comparison to the TPLO [116]. Also referenced in this publication were some preliminary findings such as evidence of a general reduction of all reaction forces due to increasing the lever arm of the active stifle force. They also asserted that while there is an increase in loading of the caudal cruciate, it is to a lesser extent than the TPLO. The means for acquiring this information was not stated and no quantitative evidence was reported. Several other comparisons between the TTA and TPLO were mentioned which could have been based on post-operative evaluation and not require any particular experimental testing to discover. The authors mention that TPLO often causes patellar ligament inflammation and that the TTA results in no apparent inflammation. Although they refer to experimental models which have found meniscal injury or degradation associated with TPLO, they do not mention beyond the statement of maintained joint congruency any reported findings on the effect of the TTA on the meniscus.

Since these early publications and preliminary conclusions, outside research studies have been done to evaluate the clinical outcome and effect of the TTA procedure. Lafaver *et al.* reported complications and clinical outcome from a study of 101 dogs [60]. Approximately 40% of the patients had a partial meniscal tear at time of surgery which was removed by a partial menisectomy. For 22 dogs, later in the study, a meniscal release was performed on intact menisci but the reasons for this were not mentioned and is not in the guidelines of the procedure [78,79,115,116]. Of the complications which required additional surgical intervention (12.3%) only one joint needed re-stabilization (lateral retinacular stabilization). Minor complications (i.e. chip fractures, implant failures, infection, etc) did not require

treatment in most cases. An adequate estimation of healing time was not available due to inconsistent radiographic assessments. Overall, their complication rates (~31%) were similar to findings for TPLO. They attribute many of these complications to inexperience and poor pre-surgical planning. Their findings contradict the proposal that the TTA might obviate the need for a meniscal release, as nearly 21% of the joints suffered from meniscal tears and needed debridement through meniscal release and was notably the most frequently occurring complication.

Though limited experimental results are available for this relatively new method, in vitro studies have been done [2,72]. In an experimental study by Apelt, Kowaleski *et al.* the effects of TTA on tibiofemoral shear force and cranial tibial subluxation was investigated [2]. Their study was done for one loading case and an average stifle and talocrural joint angles of $136.1^{\circ} \pm 2.01^{\circ}$ and $144.5^{\circ} \pm 2.51^{\circ}$, respectively. Results from their physical tests confirmed a cranially directed thrust at patellar tendon angles (PTA) greater than 90° , neutrality at angles around 90° and a caudally directed tibiofemoral thrust at angles less than the desired PTA of 90° . No comparisons were made directly to other methods such as TPLO but the authors mentioned that similar to TPLO, the TTA appeared to neutralize the cranial tibial thrust in the CCL deficient stifle. Miller *et al.* also confirmed a reduction in cranial tibial thrust with an in vitro cadaveric study [72]. Their study simulated only one loading case at only one stifle angle and used only the 9mm cage when performing the surgery. Their model also only included the effects of the quadriceps muscle group. They confirmed that the quadriceps force is not in itself enough to resist and neutralize the cranial tibial thrust from a

CCL deficient stifle. The TTA resulted in less CTT though it did not fully eliminate the translation in all specimens.

A study by Schwandt *et al.* focused on the determination of the ‘cross-over point’ (defined as the angle in which the PTA is 90° and no tibiofemoral shear force exists) for a canine stifle [97]. Their study agreed with previous reporting that this point occurs at a flexion angle of 90° for a healthy, intact stifle. For a stifle with a partial rupture of the CCL, the crossover point was found to be 100° and the dogs with this condition carried their limb more flexed in order to neutralize the shear force present. For angles less than this cross-over point, the force changed to a caudally directed shear force.

The expansion on techniques such as the TPLO and TTA has been seen in other recent surgical developments for the treatment of CCL deficiency. Each of the previously mentioned techniques has its benefits and limitations and one new procedure aims to combine the positive aspects of both. Literature on this procedure, the Triple Tibial Osteotomy, is outlined in the following section.

2.3.4.3 TTO

The Triple Tibial Osteotomy (TTO) developed by Dr. Warrick Bruce, combines features of both the tibial tuberosity advancement and tibial wedge osteotomy (predecessor to the TPLO) for treatment of cranial cruciate rupture in dogs. Similar to the basis of the TTA (discussed in the previous section), the TTO aims to make the angle between the tibial plateau and

patellar ligament 90° [20]. Instead of moving the patellar ligament, however, the tibial plateau is rotated following a series of proximal tibial osteotomies. In a prospective clinical study of TTO in 64 dogs with post-operative reassessment at both six-weeks and eleven months, no lameness was observed in most dogs at final examination [20]. Complications were encountered in 36% of cases, including tibial tuberosity fractures, infection, and subsequent meniscal injury. The most frequently encountered complication was intraoperative tibial tuberosity fracture while advancing the tibial crest which necessitated tension- band wire fixation. Significant increases in thigh circumference and stifle range of motion were also noted. All owners assessed their dog as being normal or near normal for all physical activities except sitting (2% mildly abnormal) and standing (4% mildly abnormal). Cranial drawer was still present in most patients after long-term follow-up. The researchers attribute this to a mean post-operative PTA that was larger than the intended 90° which may have been due to an underestimation of wedge angle, incorrectly positioned wedge osteotomy, and difficulties in measuring the TPA and patellar ligament angle. No significant increase in osteoarthritis score was presented and good clinical outcome, on the whole, was determined. As a relatively new surgical procedure more work needs to be done to fully evaluate its effect on the joint biomechanics and its comparison to other surgical techniques.

2.3.5 Summary

The admission of biomechanical considerations has had a profound effect on the treatment options for cranial cruciate deficient stifles. There remains a great need for a thorough understanding of the precise effect of CCL rupture on the function of the joint and its

surrounding counterparts, but investigation into the different surgical procedures used to correct this condition would be most valuable. Unlike humans, CCL deficiency is better treated with the use of procedures that alter the geometry and eliminate the tibial shear force rather than trying to replace the lost ligament. Among the currently available treatment options are the widely accepted and researched TPLO, and the newer TTA and TTO procedures. While there have been several clinical tests done, especially on the TPLO, in vivo experiments are difficult to conduct and nearly impossible to keep devoid of bias [104]. In vitro studies have been done but they are most often inconclusive. Because of a lack of information regarding several aspects of these procedures, a large percentage of surgeons still select a technique based on these cadaveric studies, case series and personal preferences [3]. Certainly one of the most pressing questions for veterinary surgeons and clients today is deciding which surgical option will restore joint function and which procedure is superior to others. While in vivo and in vitro experiments, clinical cases as well as mathematical models have helped identify material properties, biomechanical and histological changes after CCL transection and complications for a select few treatment options, a combination of finite element modeling with physical testing would be useful for evaluating a variety of procedures such as the TPLO, TTA and TTO. This mean of investigation would allow for joint positions to show the effects over a greater range of motion and prediction of characteristics that currently remain pure speculation. In particular, there has been no research to this date to quantify the change in stresses in the caudal cruciate ligament after CCL rupture, let alone after corrective surgery. Also, the condition of patella alta has been associated with patellar luxation, but a study into the post-operative effects on patellar

location does not currently exist. All in all, CCL rupture is the primary cause for rear limb lameness and one of the most frequently occurring injuries in dogs. Continued research into the cause and treatment of this condition is both influential and necessary to the veterinary community and pet owners alike.

2.4 STATEMENT OF THE PROBLEM

Several surgical treatment options are available today for correcting cranial cruciate ligament rupture, each with its clinical benefits and drawbacks. While much research has been focused on this area of veterinary orthopedics, no study to date has been done on the postoperative stresses in the major stifle ligaments following a TPLO, TTA or TTO procedure. The intention of this thesis project was to determine the overall postoperative condition of a CCL deficient canine stifle by way of developing a 3D finite element model of the entire limb. The results of particular interest will be areas of increased stress, evidence of subluxation or instability and any other geometric anomalies that can be confirmed by stress analysis. The results from this study will provide veterinary orthopedic surgeons, researchers and engineers with more information regarding canine stifle joint kinematics throughout a normal range of motion following commonly performed surgical procedures for the treatment of CCL insufficiency.

2.5 MATERIALS AND METHODS

The finite element analysis models created previously, as outlined in Chapter 1, were utilized to determine the effects of three different tibial osteotomy procedures. The procedures were performed in software on the intact model at each stifle angle (75°, 113°, 148°) according to the methods outlined in literature [20,78,79,109,115,116,118] and made to exactly replicate the surgical procedures performed by board certified veterinary orthopedic surgeons on a parallel study using rapid-prototyped physical models [Crimi CS, 30]. Each of these procedures is discussed in the following sections.

2.5.1 Tibial Plateau Leveling Osteotomy

To begin recreation of the tibial plateau leveling osteotomy (TPLO), a tool representing the 30mm radius of the saw blade used to perform the cut was created in Magics 12.01 (Materialise, Leuven, Belgium). This is shown below in Figure 2.5.1.

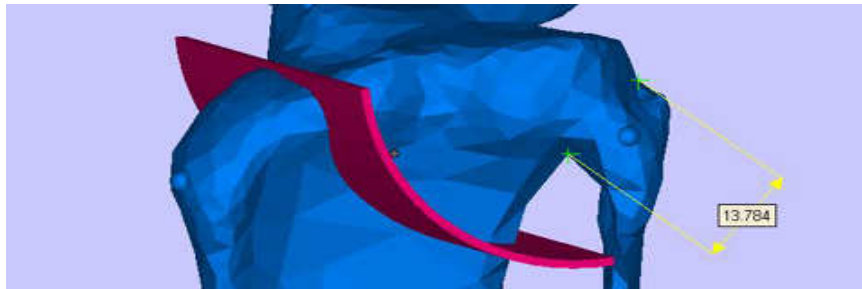


Figure 2.5.1: Tool used to Boolean a 30mm radial cut from the proximal tibial.

The center of the radial tool was located at the intercondylar eminence and the distance from the cranial aspect of the tibial tuberosity was measured and verified with the replica physical model. The distance from the tibial plateau to the caudal aspect of the cut on the physical model was verified in the computer model as well. A Boolean operation was performed to separate the proximal tibia. Since Magics does not have the ability to flex solid structures, a cut was made at the proximal junction of the fibula and tibia. The proximal tibia was then rotated ventrally by approximately 12mm. This measurement is shown in Figure 2.5.2.

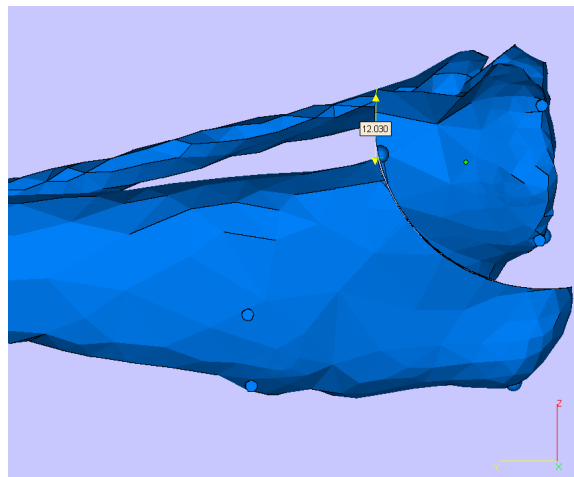


Figure 2.5.2: Ventral rotation of the proximal tibia by 12mm.

The two separate entities were fused by manually manipulating the triangles around the interface of the cuts so that the tibia became one part once again. Although a 3.5mm broad TPLO plate (Synthes, Inc., West Chester, PA, USA) was created in software, it was decided that the contact area at the osteotomy site was sufficient to assume bonding the two parts would mimic the function of the broad plate while substantially reducing the complexity of

the FE model. This procedure was performed at all three stifle angles to be tested (75° , 113° , 148°). Stifle joint angles were determined according to literature [51]. Figure 2.5.3(a-c) shows the resulting models assembled in Abaqus/CAE with ligaments and spring attachments according to Section 1.5.9. Congruency between the computer and physical model can be seen in Figure 2.5.4(a-b).

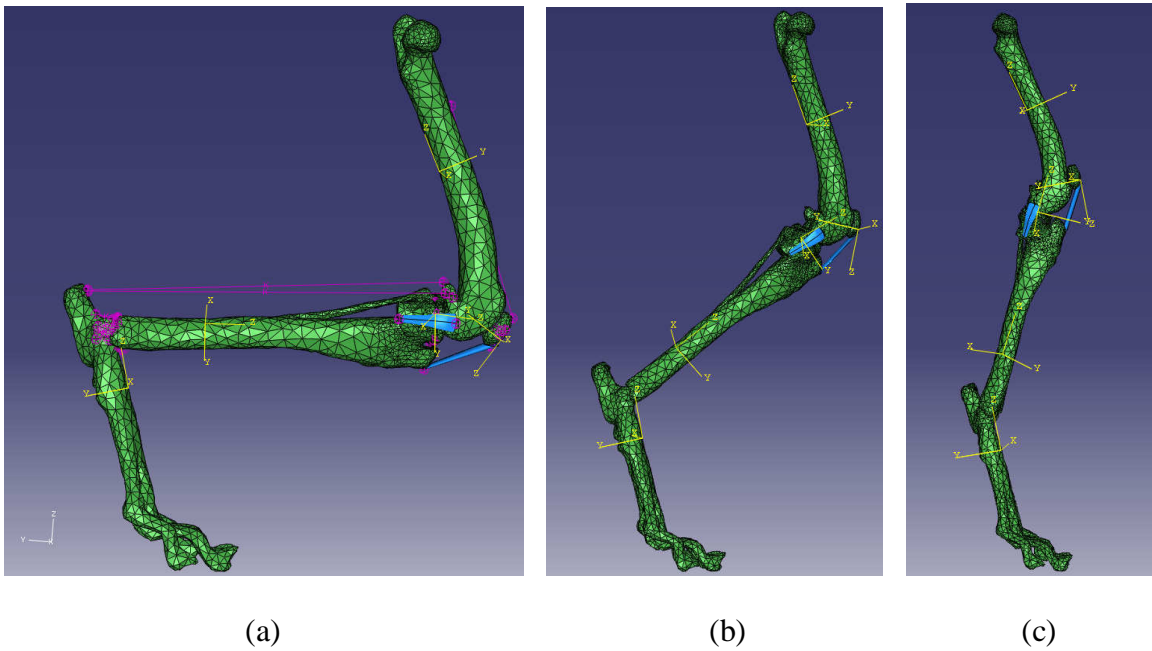
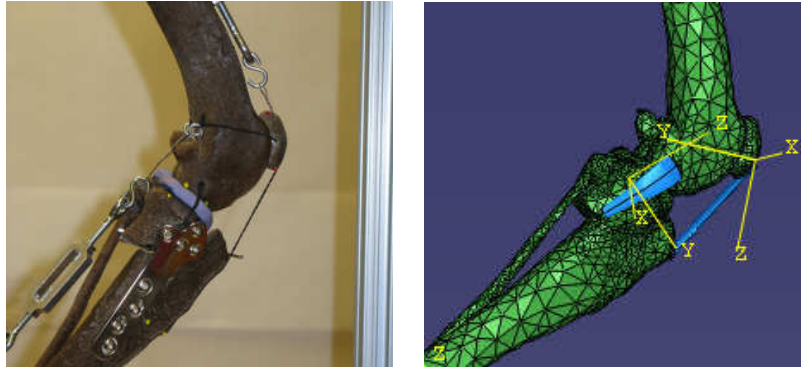


Figure 2.5.3: CCL deficient rear limb with TPLO corrective surgery at various stifle angles.

(a) stifle angle of 75° (b) stifle angle of 113° (c) stifle angle of 148°



(a)

(b)

Figure 2.5.4: Medial view of TPLO procedures for comparison. (a) physical RP model [30]

(b) FEA model

2.5.2 Tibial Tuberosity Advancement

The tibial crest osteotomy of the tibial tuberosity advancement procedure (TTA) was performed using a boolean tool created in SolidWorks (Dassault Systemes S.A., Concord, Mass., USA). This was positioned (Figure 2.5.5) according to the physical model.

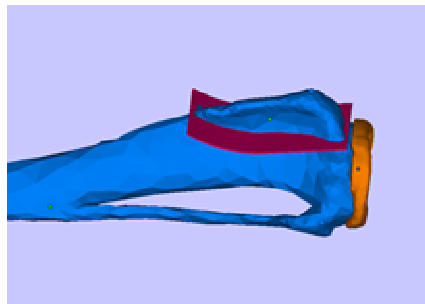


Figure 2.5.5: Boolean tool used to create tibial crest osteotomy on the proximal tibia.

The 9mm cage was modeled in SolidWorks and positioned 2-3mm from the proximal aspect of the tibia and flush against the tibial body. The tibial crest was rotated so that its caudal face lay in a plane parallel to the cranial face of the 9mm cage. A 25mm proximal translation of the tibial crest was performed to match the translation that had occurred in the physical model (Figure 2.5.6).

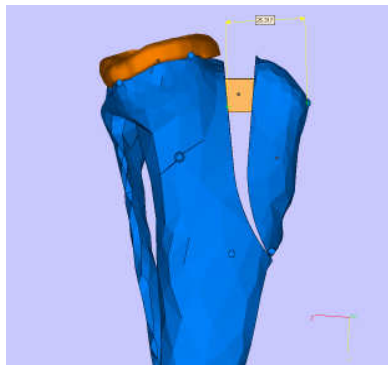
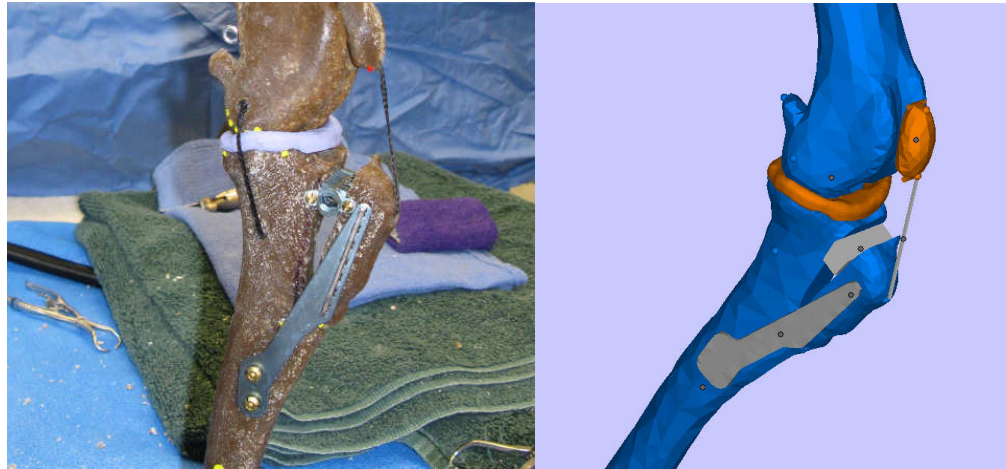


Figure 2.5.6: Proximal advancement of the tibial tuberosity with 9mm cage.

Due to the fact that the only direct contact area between the tibial crest and the tibial body occurred at the distal aspect of the crest, it was necessary to model a Kyon TTA titanium plate as a load bearing structure in the computer model. However, since the contact elements between the tibia and the plate can be modeled as rigidly fixed, there was no need to recreate the screws or prongs that the physical hardware contains. The final outcome of the TTA is shown side by side with the rapid prototyped physical model in Figure 2.5.7(a-b).



(a)

(b)

Figure 2.5.7: TTA procedure and hardware. (a) physical RP model (b) FE model

The TTA was performed on models at each of the three stifles angles to be analyzed (75° , 113° , 148°) and assembled in Abaqus/CAE. Ligaments were attached according to the methods outlined in Section 1.5.9. Additional interactions and contact constraints were necessary to model the contact between the plate and tibial body, the cage and tibial body/crest and also the contact between the tibial crest and tibial body. Tie constraints were added to the titanium parts (i.e. 9mm cage and TTA plate) to assure rigid fixation to the tibia. An example of this is shown below in Figure 2.5.8. Close ups of the stifles with ligament attachments are shown in Figure 2.5.9(a-c).

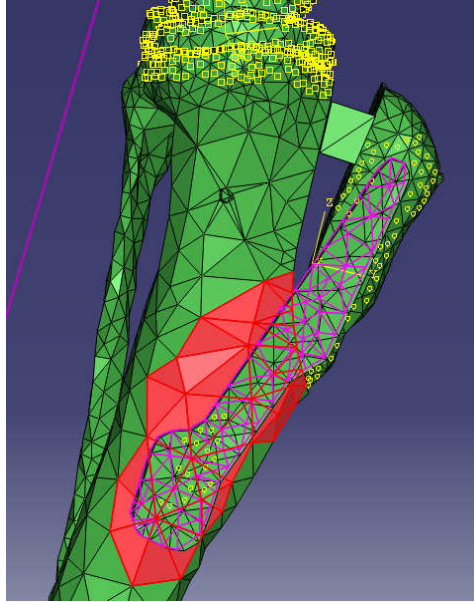


Figure 2.5.8: Tie constraint added to distal plate to rigidly attach it to the tibial body.

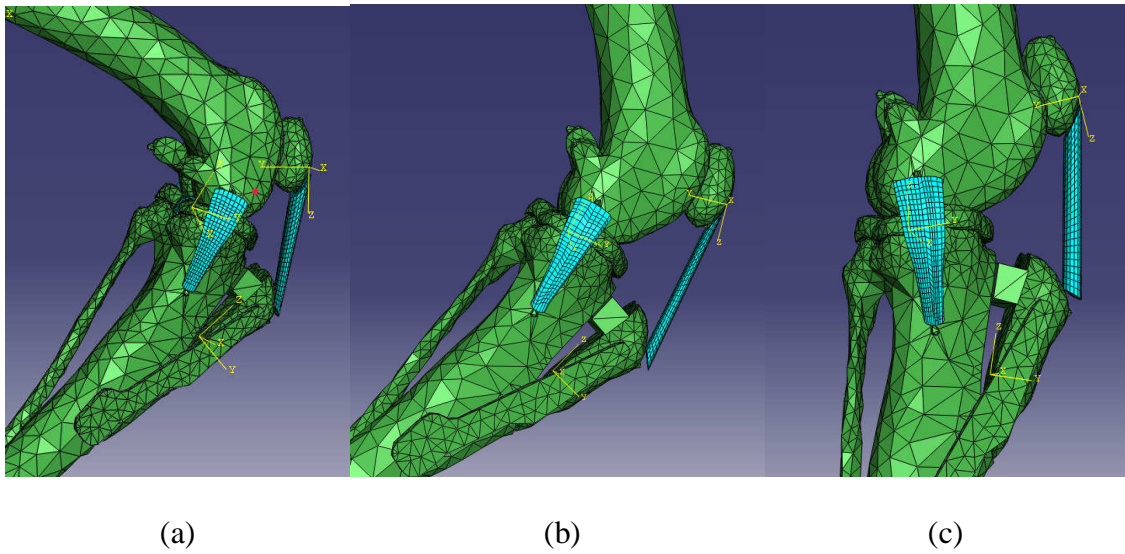


Figure 2.5.9: TTA procedure and ligament attachments at various stifle angles. (a) 75°
(b) 113° (c) 148°

2.5.3 Triple Tibial Osteotomy

The first operation of the Triple Tibial Osteotomy (TTO) procedure was a tibial crest osteotomy, performed using a vertical boolean tool as shown below in Figure 2.5.10. The crest cut was measured from proximal to distal aspect to be approximately 60mm in accordance with the physical model (Figures B.3 and B.4). The crest had to be fully separated to begin with in order to advance it as a separate body. It was then reattached at its distal aspect.

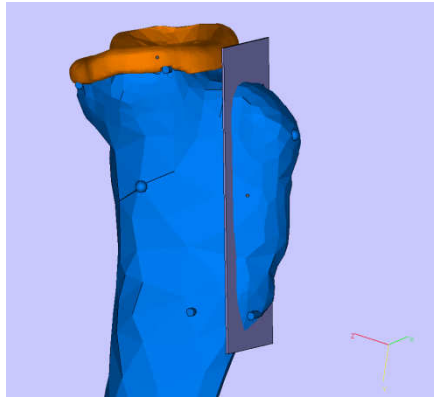


Figure 2.5.10: Boolean tool used to create tibial crest osteotomy.

Following tibial crest osteotomy, a 19° wedge was made using a tool created in SolidWorks. The tool was modeled directly from the wedge that was kept from the actual procedure performed on the physical model. The tip was placed approximately 3.81mm caudal to the insertion point of the medial collateral ligament, as was congruent with the physical model. The right plane of the wedge was set parallel to the tibial crest cut. In order to fully separate the proximal portion of the tibia and allow for full rotation of the tibial plateau, an additional

tool was used in the boolean operation. This was a 0.0001” thick sheet mimicking a transverse osteotomy from the half point of the tibial crest osteotomy and extending caudally to a location corresponding to a pre-drilled hole used in the physical surgery. Using this tool allowed the tibial plateau to become a separate entity that could then be rotated to close the gap in the tibia left by the removal of the 19° wedge. This is shown below in Figure 2.5.11(a-b).

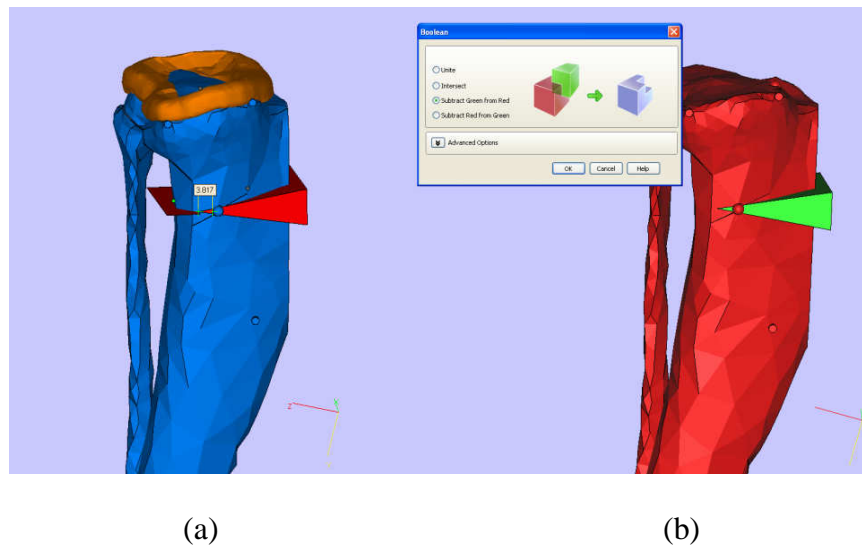


Figure 2.5.11: Performing a wedge osteotomy of FE models in software. a) boolean tools for cutting the 19° wedge b) boolean operation with wedge tool

Once the wedge osteotomy was performed, the tibial plateau was tilted cranially without displacing its caudal aspect. This motion caused the tibial crest to displace cranially as shown below in Figure 2.5.12. The distal attachment point of the crest, however, remains

attached. The proximal attachment point of the fibula was cut to allow for this rotation and reattached following the completion of the procedure.

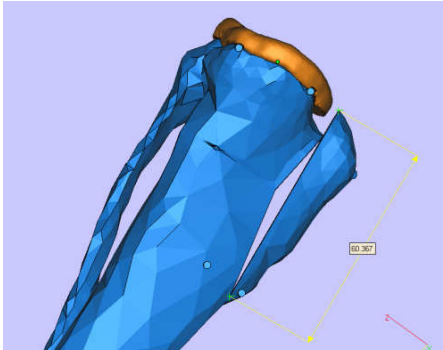
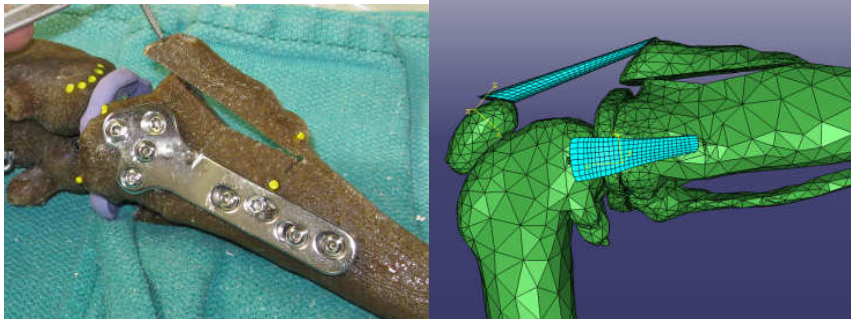


Figure 2.5.12: TTO procedure on FE model with 19° wedge osteotomy and a tibial crest osteotomy of 60mm in length.

Similar to the TPLO, the tibial plateau was fused to the tibial body by stitching the two entities together and the TPLO broad plate attachment was neglected. This minimized the number of elements, improved the poor aspect ratio caused by the various boolean operations, and reduced the complexity of the model. To ensure stability of the tibial crest, it was stitched into the tibial body at both its proximal and distal aspects. A comparison between the software model and physical RP model is shown in Figure 2.5.13(a-b).

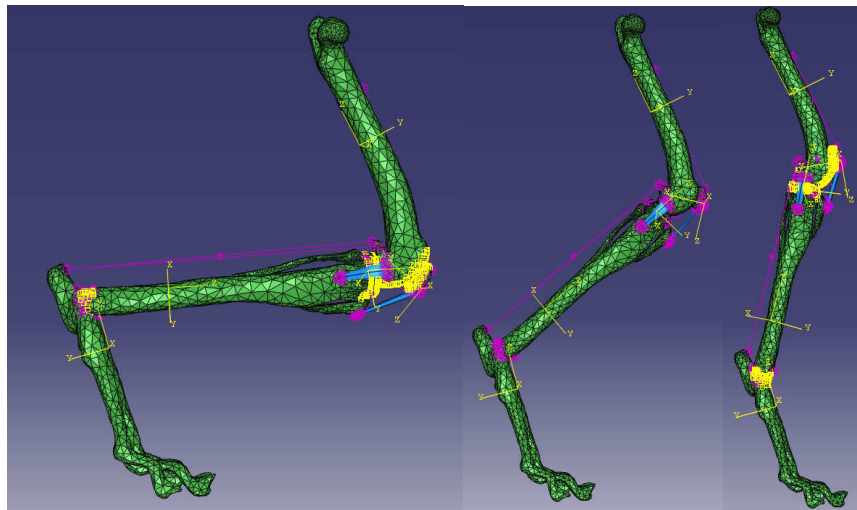


(a)

(b)

Figure 2.5.13: TTO performed on two different models. (a) RP model [30] (b) FE model

The resulting model was again positioned at each of the 3 stifle angles to be tested and imported into Abaqus/CAE. The assembled models are shown below in Figure 2.5.14(a-c).



(a)

(b)

(c)

Figure 2.5.14: Assembled TTO models at three stifle angles. (a) 75° (b) 113° (shown here without surface interactions) (c) 148°

2.5.4 Testing Procedure

A fully three-dimensional, nonlinear, quasi-static model was created for a CCL deficient leg treated with three different tibial osteotomy procedures (TPLO, TTA and TTO) and positioned at three different stifle angles throughout the normal range of motion of the dog, representative of maximum and minimal angles during walking and trotting [34]. The average stress for each ligament was recorded and observations were made regarding drawer, subluxation, and stability for each analysis.

2.6 RESULTS

2.6.1 75 Degree Results

Stress outputs for the stifle ligaments of the TPLO (Figure 2.6.1), TTA (Figure 2.6.3) and TTO (Figure 2.6.5) models at an angle of 75° are shown below. Pictures of the assemblies are shown in Figure 2.6.2 (TPLO), Figure 2.6.4 (TTA) and Figure 2.6.6 (TTO).

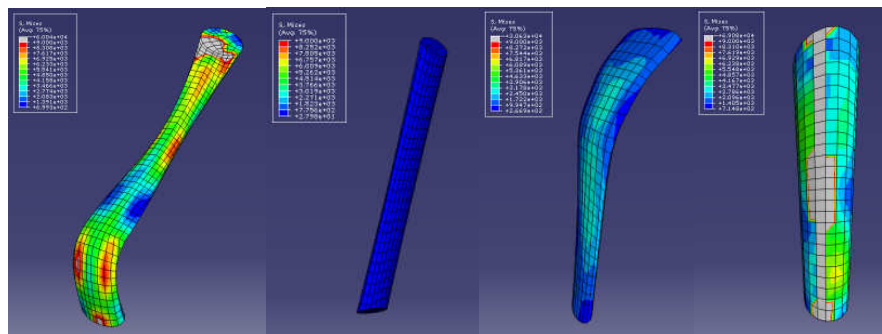


Figure 2.6.1: Visual stress output of the TPLO ligaments at 75°. From left to right: CaCL, LCL, MCL, PL

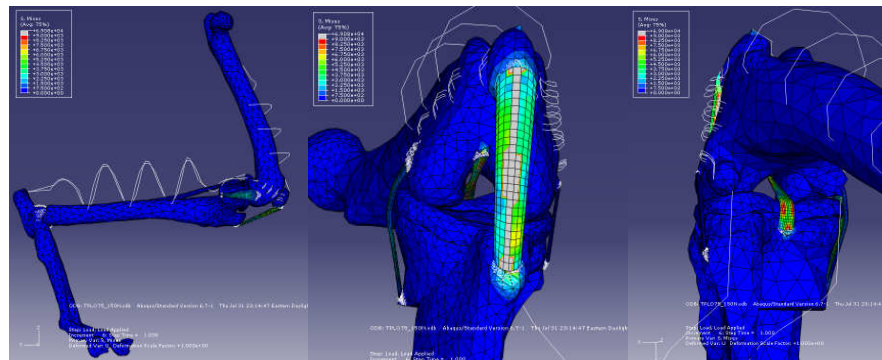


Figure 2.6.2: Several images of the TPLO stifle joint with ligaments in place at 75°.

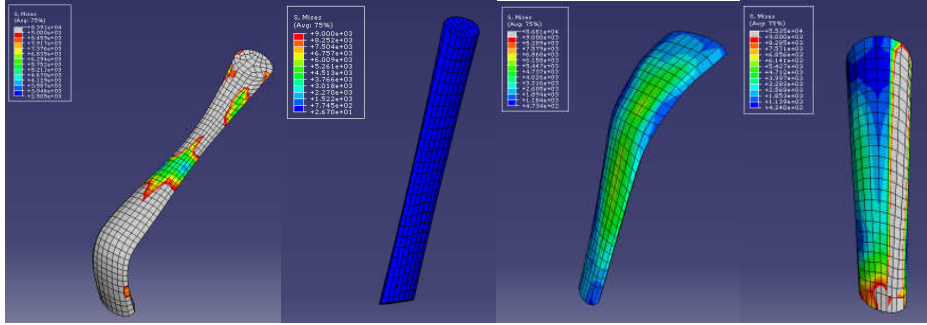


Figure 2.6.3: Visual stress output of the TTA stifle ligaments at 75°. From left to right:
CaCL, LCL, MCL, PL

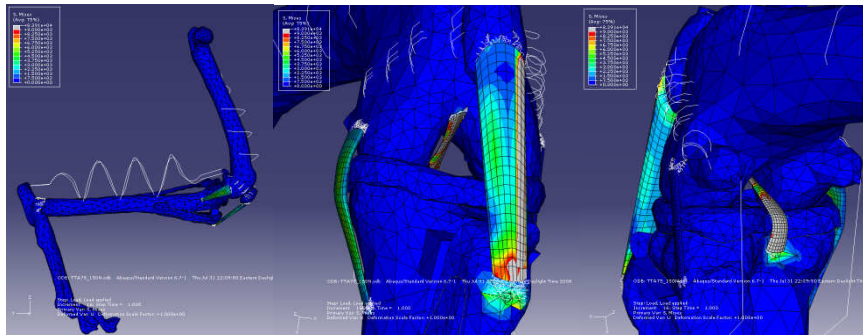


Figure 2.6.4: Several images of the TTA stifle joint with ligaments in place at 75°.

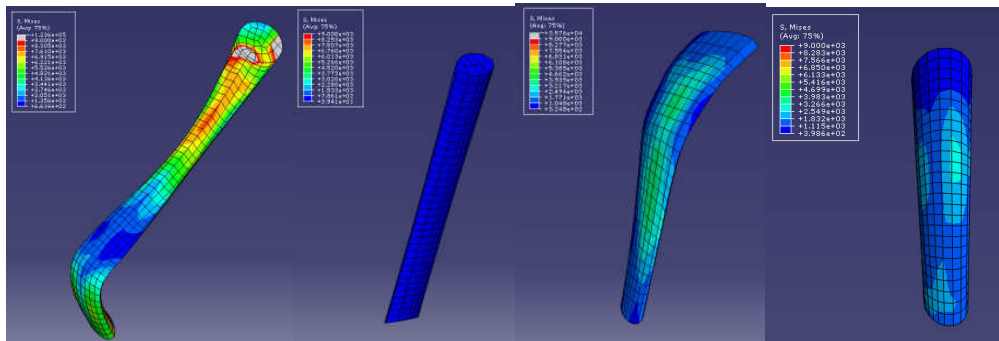


Figure 2.6.5: Visual stress output of the TTO stifle ligaments at 75°. From left to right:
CaCL, LCL, MCL, PL

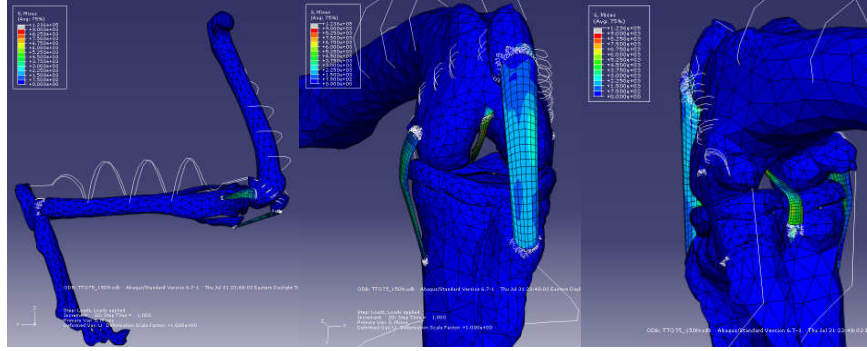


Figure 2.6.6: Several images of the TTO stifle joint with ligaments in place at 75°.

The graph in Figure 2.6.7 shows the stress output of all surgical models at 75° compared with the results from the intact and CCL deficient models. Percent differences are shown in Table 2.6.1.

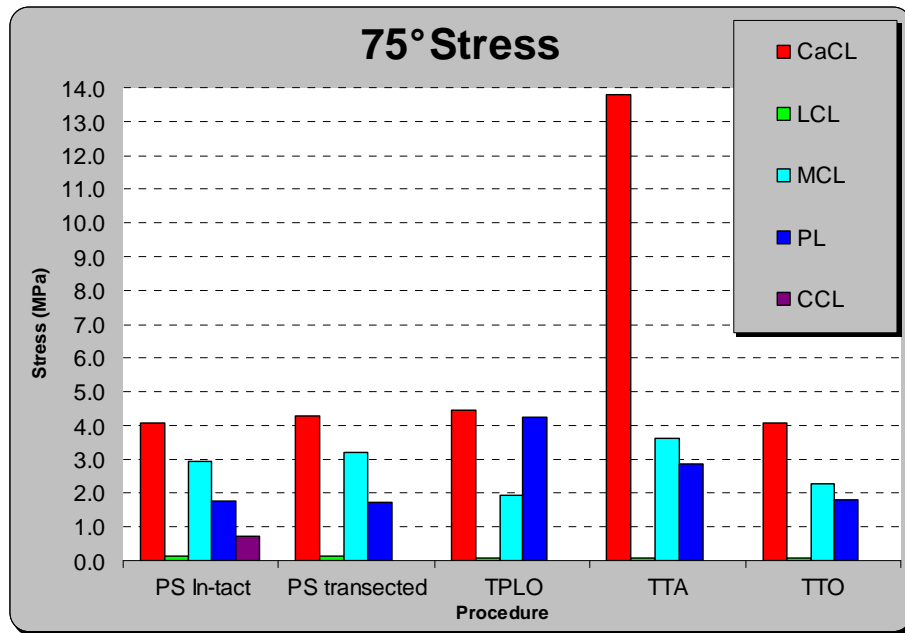


Figure 2.6.7: Graph of stress (MPa) in each of the ligaments at a stifle angle of 75°.

Table 2.6.1: Table of the percent difference between the PS intact model of the stifle and the other models at 75°.

75 Degrees (Percent Difference)					
	PS Intact	PS transected	TPLO	TTA	TTO
CaCL	4091.32	4.90%	8.68%	237.27%	-0.78%
LCL	112.33	4.65%	-40.19%	-37.02%	-37.40%
MCL	2938.37	8.81%	-33.49%	23.07%	-22.47%
PL	1768.93	-3.15%	141.01%	60.88%	2.42%
CCL	731.48				

2.6.2 113 Degree Results

Stress outputs for the stifle ligaments of the TPLO (Figure 2.6.8), TTA (Figure 2.6.10) and TTO (Figure 2.6.12) models at an angle of 113° are shown below. Pictures of the assemblies are shown in Figure 2.6.9 (TPLO), Figure 2.6.11 (TTA) and Figure 2.6.13 (TTO).

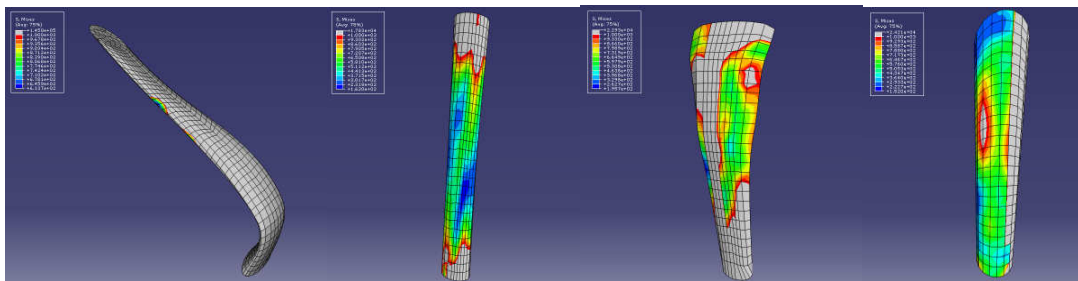


Figure 2.6.8: Visual stress output of the TPLO ligaments at 113°. From left to right: CaCL, LCL, MCL, PL

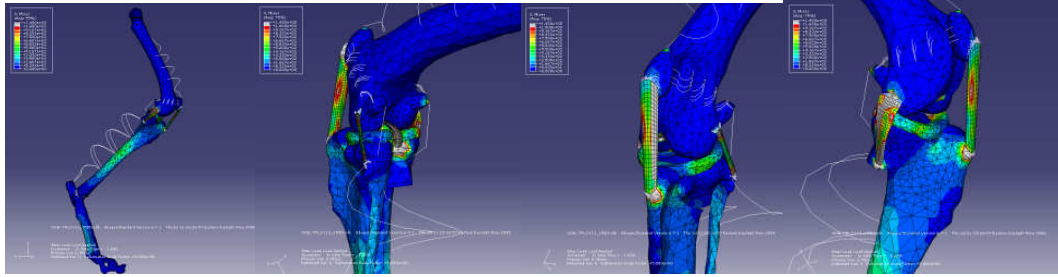


Figure 2.6.9: Several images of the TPLO stifle joint with ligaments in place at 113°.

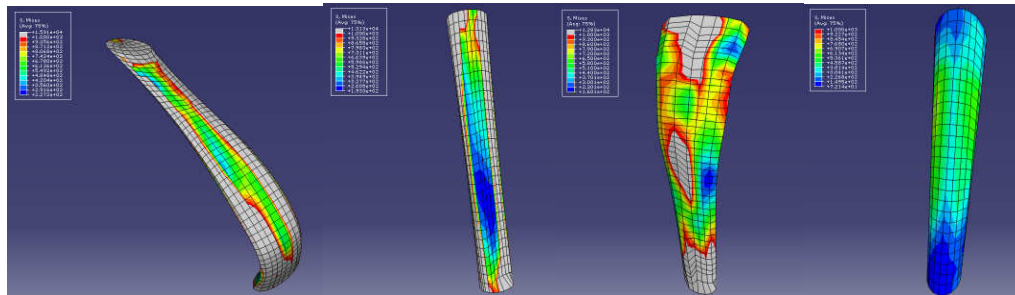


Figure 2.6.10: Visual stress output of the TTA stifle ligaments at 113°. From left to right:

CaCL, LCL, MCL, PL

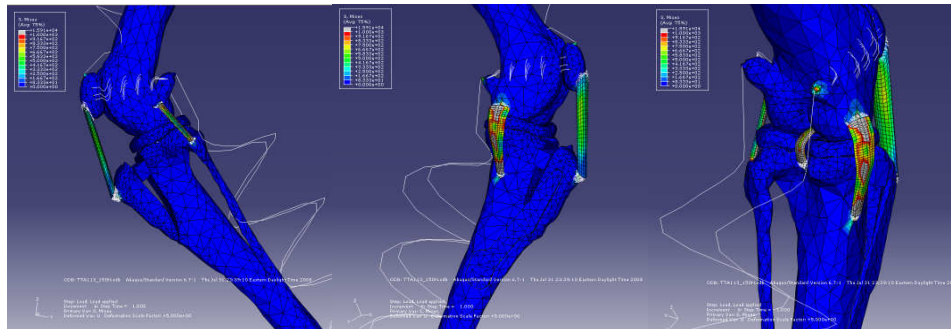


Figure 2.6.11: Several images of the TTA stifle joint with ligaments in place at 113°.

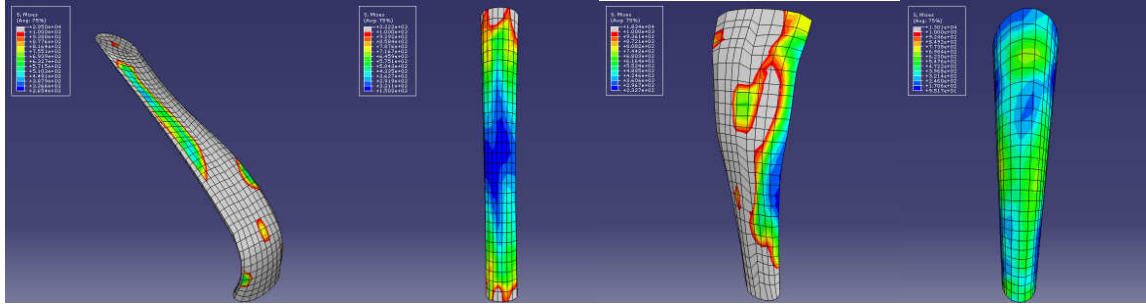


Figure 2.6.12: Visual stress output of the TTO stifle ligaments at 113°. From left to right:

CaCL, LCL, MCL, PL

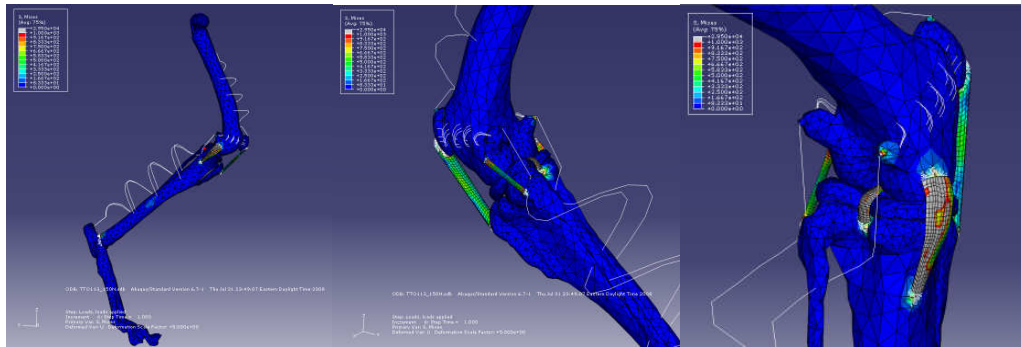


Figure 2.6.13: Several images of the TTO stifle joint with ligaments in place at 113°.

The graph in Figure 2.6.14 shows the stress output of all surgical models at 113° compared with the results from the intact and CCL deficient models. Percent differences are shown in Table 2.6.2.

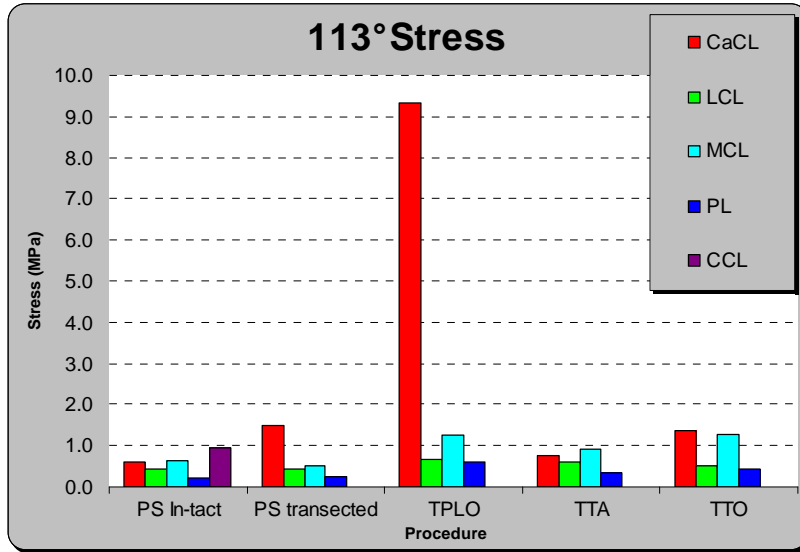


Figure 2.6.14: Graph of stress (MPa) in each of the ligaments at a stifle angle of 113°.

Table 2.6.2: Table of the percent difference between the PS intact model of the stifle and the other models at 113°.

113 Degrees (Percent Difference)					
	PS Intact	PS transected	TPLO	TTA	TTO
CaCL	603.88	149.09%	1447.15%	28.23%	126.38%
LCL	424.82	0.79%	56.06%	42.18%	21.41%
MCL	636.73	-17.33%	93.99%	41.31%	100.55%
PL	217.77	8.87%	182.70%	56.82%	98.38%
CCL	957.52				

2.6.3 148 Degree Results

Stress outputs for the stifle ligaments of the TPLO (Figure 2.6.15), TTA (Figure 2.6.17) and TTO (Figure 2.6.19) models at an angle of 148° are shown below. Pictures of the assemblies are shown in Figure 2.6.16 (TPLO), Figure 2.6.18 (TTA) and Figure 2.6.20 (TTO).

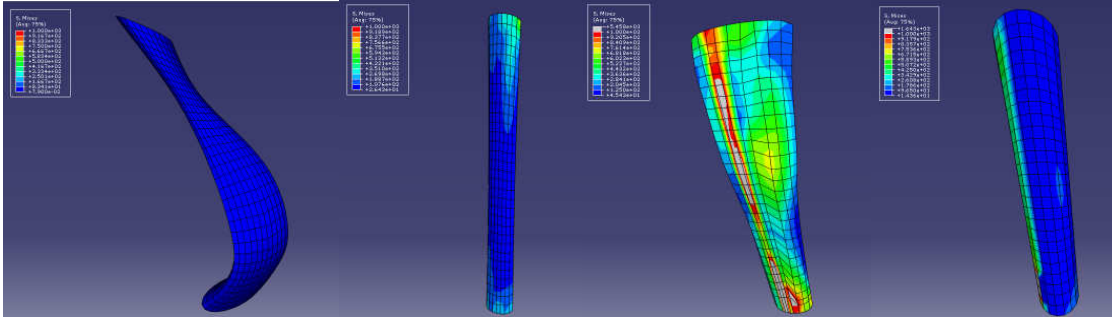


Figure 2.6.15: Visual stress output of the TPLO ligaments at 148°. From left to right: CaCL, LCL, MCL, PL

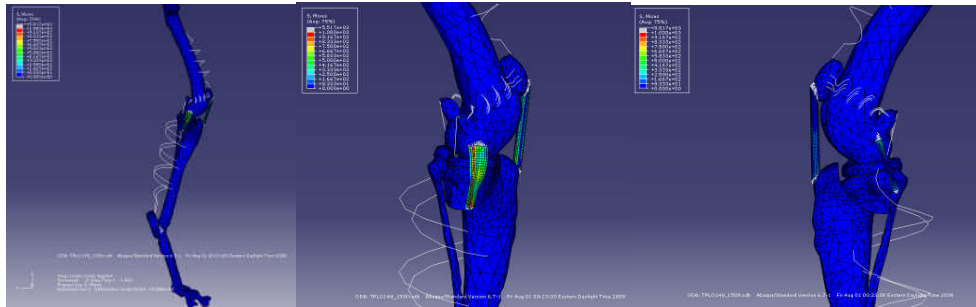


Figure 2.6.16: Several images of the TPLO stifle joint with ligaments in place at 148°.

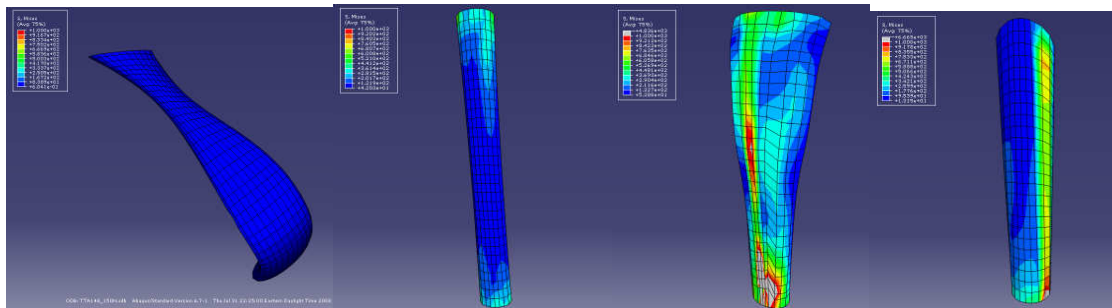


Figure 2.6.17: Visual stress output of the TTA stifle ligaments at 148°. From left to right: CaCL, LCL, MCL, PL

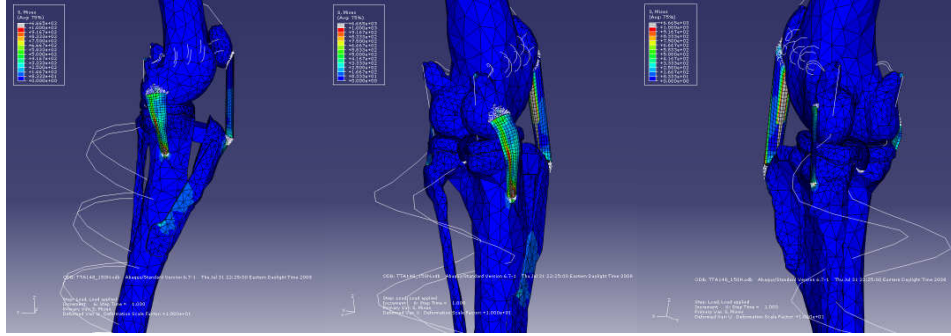


Figure 2.6.18: Several images of the TTA stifle joint with ligaments in place at 148°.

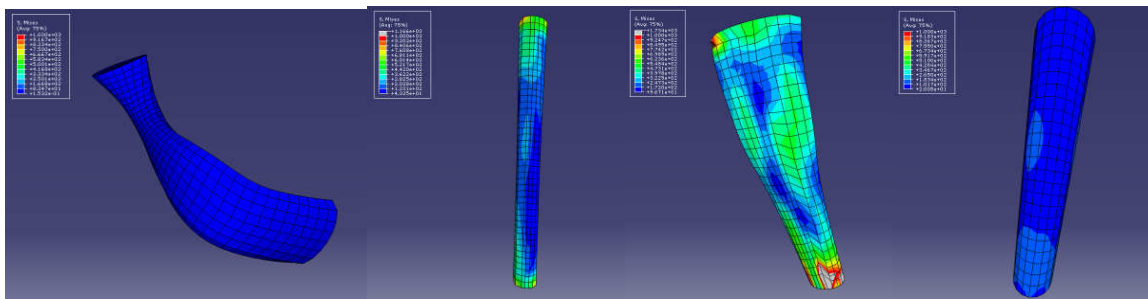


Figure 2.6.19: Visual stress output of the TTA stifle ligaments at 148°. From left to right:
CaCL, LCL, MCL, PL

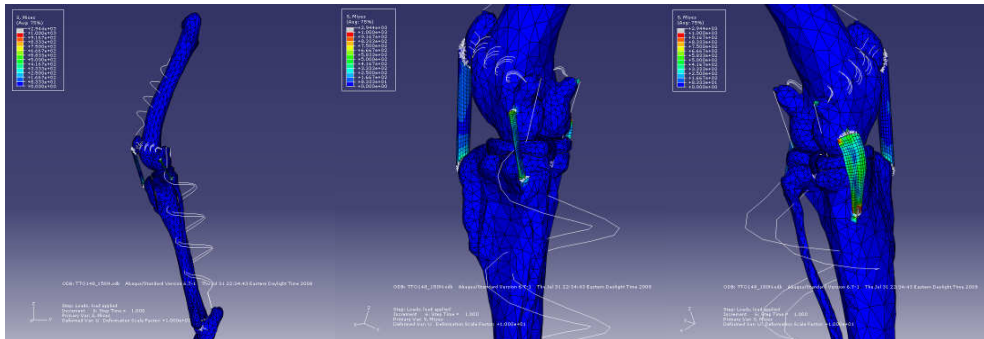


Figure 2.6.20: Several images of the TTA stifle joint with ligaments in place at 148°.

The graph in Figure 2.6.21 shows the stress output of all surgical models at 148° compared with the results from the intact and CCL deficient models. Percent differences are shown in Table 2.6.3.

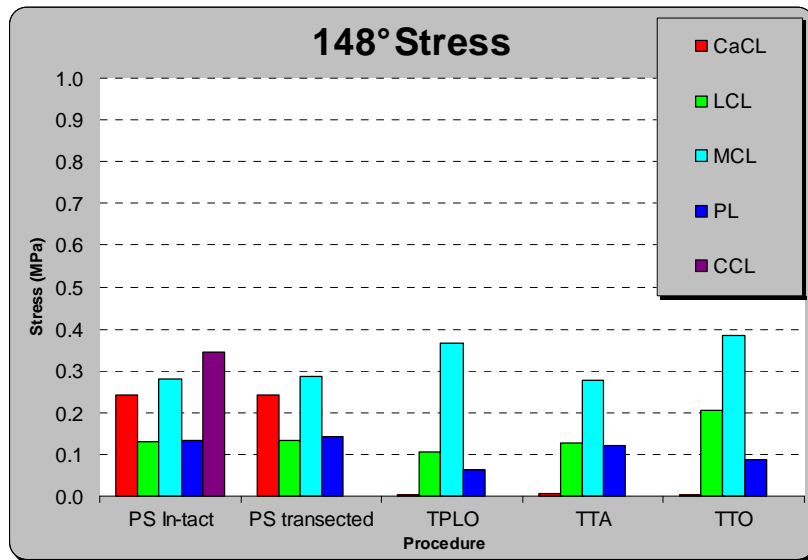


Figure 2.6.21: Graph of stress (MPa) in each of the ligaments at a stifle angle of 148°.

Table 2.6.3: Table of the percent difference between the PS intact model of the stifle and the other models at 148°.

148 Degrees (Percent Difference)					
	PS Intact	PS transected	TPLO	TTA	TTO
CaCL	242.61	-0.05%	-98.50%	-97.20%	-98.45%
LCL	128.71	3.30%	-18.10%	-1.03%	60.02%
MCL	281.81	1.96%	29.65%	-0.90%	35.72%
PL	132.19	7.22%	-53.13%	-8.51%	-32.77%
CCL	342.97				

2.6.4 Changes in Tibial Long Axis and Tibial Plateau Slope

The figures shown below illustrate the tibial slope changes for the TPLO (Figure 2.6.23) and TTO (2.6.24) as compared with the pre-surgical TPA shown in Figure 2.6.22. The TTA was not depicted because there was no change in TPA.

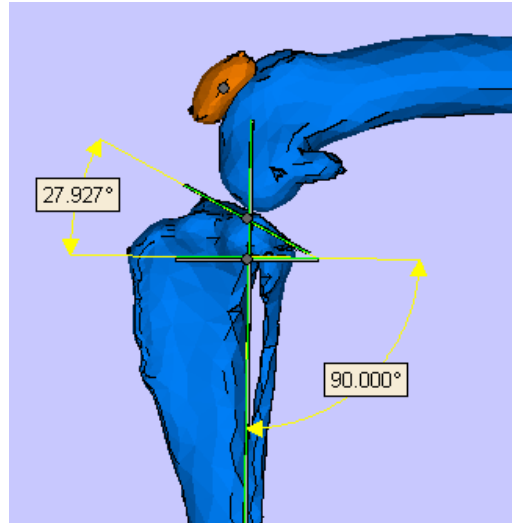


Figure 2.6.22: Pre-surgical tibial plateau slope.

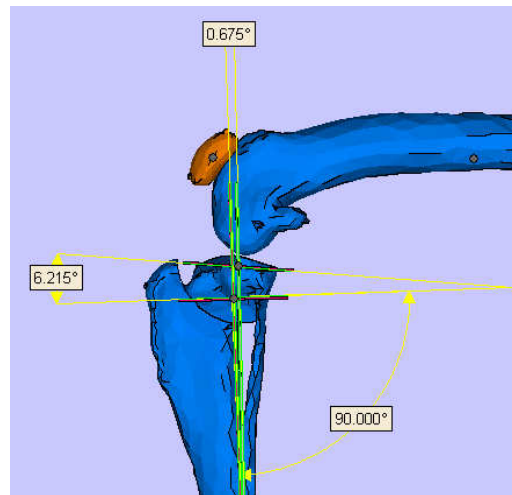


Figure 2.6.23: Tibial slope and long axis shift resulting from the TPLO procedure.

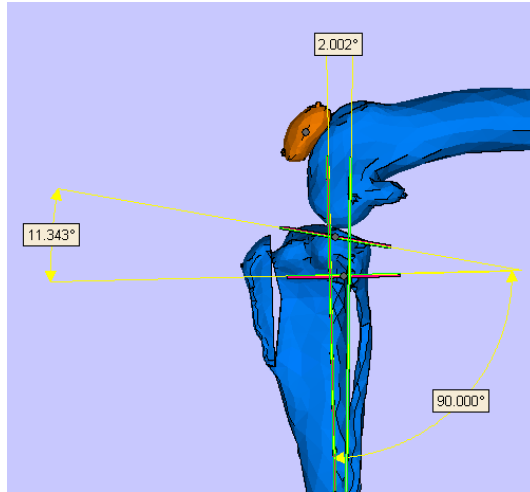


Figure 2.6.24: Tibial slope and long axis shift resulting from the TTO procedure.

2.7 DISCUSSION

Postoperative TPAs for this study were 6.2° for the TPLO and 11.3° for the TTO. The TTA resulted, as expected, in no change to TPA since no rotation of the tibial plateau occurred. These values are in good agreement with previous studies investigating the effects of these surgical techniques [20].

The TTA procedure is based on mechanics of the human knee and has been extended to canines [116]. Studies have shown that in the healthy intact stifle, this 90° “cross-over flexion point” of the patellar tendon angle (TPA) occurs at 90° of flexion [97]. At angles greater than this crossover point, the load should be taken up by the CCL and the shear force should be cranially directed. This was confirmed in the first chapter of this study (Section 1.6). A TTA aims to move this cross-over point to naturally occur at full extension, when the otherwise cranially directed shear forces are maximal and destabilize a CCL deficient stifle. Thus in a stifle treated with TTA, the point of neutrality among the cruciate ligaments should shift to occur at full extension. In order to accurately compare this study to these statements, an analysis should have been done on an intact stifle after TTA. This was not done but several observations from the analyses that were performed do support this idea. At full extension (148°) in the intact stifle the CCL carried the majority of the load and thus resulted in higher stresses. After transection of the CCL, the load in the MCL, LCL and PL increased and the CaCL remained at approximately the same load. After the TTA procedure, the load on the CaCL reduced to almost zero and most of the load was taken up by the MCL.

Although the new cross-over point cannot be directly verified, a minimized load in the CaCL and appearance of stifle stability with elimination of cranial subluxation suggests that the procedure was performed as intended. Also, at a stifle angle of 113° (which in the normal stifle should be in the range of a cranially directed shear force) the stress in the CaCL increased for both the TPLO and TTA procedures. No significant tibial subluxation following CCL transection or any of the procedures occurred at any of the three angles. Thus, results are based on an understanding that the stifle was at its initial position.

The same cross-over theory applies to both the TPLO and TTO as they all aim, by different osteotomy techniques, to eliminate the cranial shear forces by changing this cross-over point to occur at extension. By the same comparison methods as the TTA, both the TPLO and TTO functioned as intended, decreasing the load in the CaCL, at stifle extension, to nearly zero and causing the axial loads to be taken up by the other ligaments, primarily the MCL. The forces on the MCL were highest in the TTO at 148°, followed by the TPLO. The TTA actually saw a reduction in the total reaction force (and stresses) experienced by all the ligaments. This has been claimed to occur due to an increase in the lever arm of the dominant reaction force of the stifle because of the advancement of the patellar ligament insertion point on the tibia [116]. This, as is claimed, should lead to a general reduction of all reaction forces and is confirmed by the methods of this study. In particular, the load on the patellar tendon was reduced by all procedures at 148° extension. Both the TPLO and TTO reduced the stresses in the patellar ligament to a greater degree than did the TTA. This is contradictory to the reported claims that the TTA is less likely, when compared with the

TPLO, to cause patellar ligament inflammation due to a reduction in load. However, it is uncertain what degree of flexion or extension these claims are referencing.

For 75° of flexion, the TPLO increased the stresses on the patellar ligament by roughly 141%. Although the stress seen in the patellar ligament also increased for both the TTA (~60%) and TTO (~2.5%) it was much less than the TPLO. This is in agreement with literature that has shown clinical presence of patellar ligament desmitis and related complications due to a suspected increase in stress following the TPLO [20]. At 113°, the TPLO again had the most detrimental effects on the patellar ligament, increasing the stress by approximately 183% whereas the TTA and TTO increased the stresses by ~57% and 98%, respectively. With regards to the stress on the patellar ligament, the TTO was less harmful at 75° of flexion whereas the TTA faired better around 113°.

At full flexion of 75°, when the tibial shear forces are most caudally directed and the CaCL is taking up the majority of the load (as confirmed in the first part of this study, found in Section 1.6) the effect of the different surgical procedures on the behavior of the CaCL is of most importance. Experimental studies have shown that a caudal tibial subluxation exists in stifles after the TPLO procedure [121]. It has been thought that increased loads seen in the TPLO might indicate an increase in stress and imply an excessive load condition that may predispose the ligament to future failure. An increase in stress in the CaCL, during flexion, following a TPLO was confirmed during this study. However, at 75° of flexion the TTA caused the highest increases in CaCL stresses, followed by the TPLO. The TTO procedure

actually caused a decrease in CaCL stress by 0.78%. At 113°, the TPLO increased the stress on the CaCL by a substantial amount, especially compared with the effects of the TTA and TTO. Thus, when examining the stifle at 113°, the TPLO has the most negative effect of the state of the CaCL. It has been found in research [121] that the strain in the CaCL increases with an increase of rotation of the tibial slope. The postoperative TPA resulting from the TPLO for this study was found to be approximately 6.2° which is very close to the optimal postoperative angle of 6.5° reported in literature [121]. Thus, this is not believed to be the source of the excessive stress seen on the CaCL.

Again, the results presented herein are subject-specific and extrapolation of this data should be done with caution. The FE models presented in this study exhibited postoperative behaviors similar to those reported in literature and found through experiment testing of a replica physical model.

2.7 CONCLUSION

The fully three-dimensional, anatomically accurate finite element models presented in this paper were found to accurately reproduce postoperative effects of common tibial osteotomy procedures (TPLO, TTA and TTO). Use of computer models proved to be an efficient, repeatable method for simulating different surgical procedures used to treat CCL insufficiency. The results of the analyses presented in this study suggest that for a stifle angle of 75° , the loading conditions of the CaCL remain nearly constant for both the TPLO and TTO but a significant increase in stress results from the application of the TTA procedure. At 113° , the TPLO was found to substantially increase the stress in the CaCL. The TTO, at 113° , increased the stresses on the collaterals by a relatively small amount as compared with the other procedures. All stress levels for the patellar ligament were relatively low at this angle. At a stifle angle of 148° an increase in the stress of the MCL was apparent for all surgical procedures, corresponding to the nature of the MCL to take over as primary restraint against cranial tibial thrust in a CCL deficient stifle in extension. The CaCL remained relatively unloaded for all procedures, indicative of a successful transfer of the so called cross-over flexion point to extension. The stresses in the patellar ligament at extension were found to be highest for the TTA model, although all three procedures resulted in a decrease in patellar ligament stress as compared with both the intact and CCL deficient models. This suggests that if patellar inflammation occurs as a postoperative complication, such as reported for both the TPLO and TTA, the danger to this ligament lies in flexion.

Overall, the TTO resulted in the most consistent stress distributions for all stifle ligaments over the range of motion and was the less detrimental in flexion.

3. FUTURE RESEARCH

The need to acquire greater insight into the causes of CCL rupture, the effects of CCL deficiency and the resulting biomechanical changes due to proximal tibial osteotomies on the canine stifle is ever prevailing.

The FEA models created for this project could be utilized in future research to continue investigations on the effects of different surgical treatment techniques and help in developing new tibial osteotomies or making modifications to current ones. New surgeries could be developed and tested to predict excessive forces in specific ligaments that may lead to postoperative complications. Also, the 3D ligaments created in this model could help investigators study different ways of modeling these anatomical structures. Different loading conditions could be tested to determine the effects of surgical procedures during extreme physical activities such as running and jumping. The novel approach to modeling the menisci could also be extended upon in order to investigate effects on this important anatomic structure and determine possible reasons for common postoperative meniscal injuries.

4. REFERENCES

1. Amiel D, Kleiner JB, Roux RD: The phenomenon of ligamentization: Anterior cruciate ligament reconstruction with autogenous patellar tendon. *J Orthop Res* 4:162-172, 1986.
2. Apelt D, Kowaleski MP, Boudrieau RJ. Effect of tibial tuberosity advancement on cranial tibial subluxation in canine cruciate-deficient stifle joints. *Veterinary Surgery* 2007;36:170-177.
3. Aragon CL, Budsberg SC. Applications of evidence-based medicine: cranial cruciate ligament injury repair in the dog. *Veterinary Surgery* 34:93-98, 2005.
4. Arnoczky SP, Marshall JL: The cruciate ligaments of the canine stifle: an anatomical and functional analysis. *Am J Vet Res* 38:1807–1814, 1977.
5. Arnoczky SP, Tarvin GB, Marshall JL: Anterior cruciate ligament replacement using patellar tendons. *J Bone Joint Surg* 64:217-224, 1982.
6. Arnoczky SP, Tarvin GB, Marshall JL: The “over-the-top” procedure: A technique for anterior cruciate ligament substitution in the dog. *J Am Anim Hosp Assoc* 15:283-290, 1979.
7. Arnoczky SP, Torzilli PA, Marshall JL: Biomechanical evaluation of anterior cruciate ligament repair in the dog: An analysis of the instant center of motion. *J Am Anim Hosp Assoc* 13:553-558, 1977.
8. Arnoczky, SP. Cruciate Ligament Rupture and Associated Injuries. *Textbook of Small Animal Orthopaedics*. Ithaca: International Veterinary Information Service, 1985.

9. Arthurs GI, Langley-Hobbs SJ. Patellar luxation as a complication of surgical intervention for the management of cranial cruciate ligament rupture in dogs. *Vet Comp Orthop Traumatol* 2007;20:204-210.
10. Bach JM, Hull ML, Patterson HA. Direct measurement of strain in the posterolateral bundle of the anterior cruciate ligament. *J. Biomechanics* 1997;30:281-283.
11. Barink M, van Kampen A, et al. A three-dimensional dynamic finite element model of the prosthetic knee joint: simulation of joint laxity and kinematics. *J Engineering in Medicine* 2005;219:415-424.
12. Baroni E, Matthias RR, Marcellin-Little DJ, et al. Comparison of radiographic assessments of the tibial plateau slope in dogs. *AJVR* 2003;64:586-589.
13. Barry, D., Ahmed, A.M., 1986. Design and performance of a modified buckle transducer for measurement of ligament tension. *Journal of Biomechanical Engineering* 108, 149–152.
14. Beillas P, Papaioannou G, et al. A new method to investigate in vivo knee behavior using a finite element model of the lower limb. *Journal of biomechanics* 2004;37:1019-1030.
15. Bendjaballah MZ, Shirazi-Adl A, Zukor DJ. Finite element analysis of human knee joint in varus-valgus. *Clinical Biomechanics* 1997;12:139-148.
16. Berg EE, Mason SL, Lucas MJ. Patellar height ratios: a comparison of four measurement methods. *The American journal of sports medicine* 1996;24:217-221.
17. Blackburne JS, Peel TE. A new method of measuring patellar height. *The journal of bone and joint surgery* 1977;59:241-242.

18. Blankevoort L, Huiskes R. Ligament-bone interaction in a three-dimensional model of the knee. *Journal of Biomechanical Engineering* 1991;113:263-269.
19. Blankevoort L, Huiskes R. Validation of a three-dimensional model of the knee. *J Biomechanics* 1996;29:955-961.
20. Bruce WJ, Rose A, et al. Evaluation of the triple tibial osteotomy. A new technique for the management of the canine cruciate-deficient stifle. *Vet Comp Orthop Traumatol* 2007;3:159-168.
21. Burks RT, Haut RC, Lancaster RL: Biomechanical and histological observations of the dog patellar tendon after removal of its central one-third. *Am J Sports Med* 18: 146-153, 1990.
22. Butler DL, Hulse DA, Matthew DK, et al: Biomechanics of cranial cruciate ligament reconstruction in the dog: II. Mechanical properties. *Vet Surg* 12:113-118, 1983.
23. Butler DL. Anterior Cruciate Ligament: Its Normal Response and Replacement. *Journal of Orthopaedic Research* 1989;7:910-921.
24. Cabaud HE, Feagin JA, Rodkey WB: Acute anterior cruciate ligament injury and augmented repair. *Am J Sports Med* 8: 395-401, 1980.
25. Canapp SO. The canine stifle. *Clin Tech Small Anim Pract* 2007;22:195-295.
26. Carey K, Aiken SW, DiResta GR, et al. Radiographic and clinical changes of the patellar tendon after tibial plateau leveling osteotomy. *Vet Comp Orthop Traumatol* 2005;18:235-242.
27. Carpenter DH, Cooper RC. Mini review of canine stifle joint anatomy. *Anat Histol Embryol* 2000;29:321-329.

28. Caylor KB, Zumpano CA, et al. Intra- and interobserver measurement variability of tibial plateau slope from lateral radiographs in dogs. *Journal of the American animal hospital assoc.* 2001;37:263-268.
29. Christel P. Prosthetic replacement of the anterior cruciate ligament: a challenge. *Clinical Materials* 1994;15:3-13.
30. Crimi CS. Analysis of Patellar Height of the Cranial Cruciate Ligament Deficient Canine Stifle Following Three Tibial Osteotomy Procedures. (Thesis), 2008.
31. Damur DM: Tibial tuberosity advancement (TTA): Clinical results. *Proceedings of the 2005 ACVS Veterinary Symposium.* October, 2005, pp 441–442.
32. Daniel, W.J.T., 2001. Three-dimensional orthotropic viscoelastic finite element model of a human ligament. *Computer Methods in Biomechanics and Biomedical Engineering* 4 (3), 265–279.
33. De Rooster H, De Bruin T, Van Bree H. "Morphologic and Functional Features of the Canine Cruciate Ligaments." *Veterinary Surgery* 2006;35:769-780.
34. DeCamp CE, Johnson AL, Probst CW, et al. Vertical position of the patella in the stifle joint of clinically normal large-breed dogs. *AJVR* 2002;63:42-46.
35. DeCamp CE, Riggs CM, Olivier NB, et al. Kinematic evaluation of gait in dogs with cranial cruciate ligament rupture. *AJVR* 1996;57:120-126.
36. Dickinson CR, Nunamaker DM: Repair of ruptured anterior cruciate ligament in the dog: Experience of 101 cases using a modified fascia lata strip technique. *J Am Vet Med Assoc* 170:827-830, 1977.

37. Donahue TLH, Hull ML, et al. How the stiffness of meniscal attachments and meniscal material properties affect tibio-femoral contact pressure computed using a validated finite element model of the human knee joint. *Journal of biomechanics* 2003;36:19-34.
38. Donahue TLH, Hull ML, Rashid MM, et al. A Finite Element Model of the Human Knee Joint for the Study of Tibio-Femoral Contact. *Journal of Biomechanical Engineering* 2002;124:273-280.
39. Elias JJ, Bratton DR, et al. Comparing two estimations of the quadriceps force distribution for use during patellofemoral simulation. *J Biomechanics* 2006;39:865-872,
40. Feeney LC, Lin CF, Marcellin-Little DJ, et al. Validation of two-dimensional kinematic analysis of walk and sit-to-stand motions in dogs. *AJVR* 2007;68:277-282.
41. Fettig AA, Rand WM, et al. Observer variability of tibial plateau slope measurement in 40 dogs with cranial cruciate ligament-deficient stifle joints. *Veterinary Surgery* 2003;32:471-478.
42. Harner CD, Livesay GA, Kashiwaguchi S, et al. Comparative study of the size and shape of human anterior and posterior cruciate ligaments. *Journal of Orthopaedic Research* 1995;13:429-434.
43. Havig ME, Dyce J, Kowaleski MP, et al. Relationship of tibial plateau slope to limb function in dogs treated with a lateral suture technique for stabilization of cranial cruciate ligament deficient stifles. *Veterinary surgery* 2007;36:245-251.
44. Hayashi K, Frank JD, et al. Histologic changes in ruptured canine cranial cruciate ligament. *Veterinary Surgery* 2003;32:269-277.

45. Hayashi K, Manley PA, Muir P. Cranial cruciate ligament pathophysiology in dogs with cruciate disease: a review. *Journal of the American Animal Hospital Assoc.* 40:385-390, 2004.
46. Henning, C.E., Lynch, M.A., Glick, K.R., 1985. An in-vivo strain gauge study of elongation of the anterior cruciate ligament. *American Journal of Sports Medicine* 13, 22–26.
47. Hottinger HA, DeCamp CE, Olivier NB, et al. Noninvasive kinematic analysis of the walk in healthy large-breed dogs. *Am J Vet Res* 1996;57:381–388.
48. Hurley CR, Hammer DL, Shott S. Progression of radiographic evidence of osteoarthritis following tibial plateau leveling osteotomy in dogs with cranial cruciate ligament rupture: 295 cases (2001-2005). *JAVMA* 2007;230:1674-1679.
49. Hvid I, Andersen LI, Schmidt H. Patellar height and femoral trochlear development. *Acta orthop scand* 1983;54:91-93.
50. Insall J, Salvati E. Patella position in the normal knee joint. *Radiology* 1971;101(1):101-104.
51. Jaegger G, Marcellin-Little DJ , Levine D. Reliability of goniometry in Labrador Retrievers. *AJVR* 2002;63:979-986.
52. Jafari A, Faramand F, Meghdari A. The effects of trochlear groove geometry on patellofemoral joint stability - a computer model study. *J Engineering in Medicine* 2008;222:75-88.

53. Jandi AS, Schulman AJ. Incidence of Motion Loss of the Stifle Joint in Dogs with Naturally Occurring Cranial Cruciate Ligament Rupture Surgically Treated with Tibial Plateau Leveling Osteotomy: Longitudinal Clinical Study of 412 Cases. *Veterinary Surgery* 2006;36:114-121.
54. Jerram RM, Walker AM. Cranial cruciate ligament injury in the dog: pathophysiology, diagnosis and treatment. *New Zealand Veterinary Journal* 51(4):149-158, 2003.
55. Johnson AL, Broaddus KD, Hauptman JG, et al. Vertical Patellar Position in Large-Breed Dogs with Clinically Normal Stifles and Large-Breed Dogs with Medial Patellar Luxation. *The American College of Veterinary Surgeons* 2006;35:78-81.
56. Jurvelin JS, Arokoski JPA, et al. Topographical variation of the elastic properties of articular cartilage in the canine knee. *Journal of Biomechanics* 2000;33:669-675.
57. Kim SE, Pozzi A, Kowaleski MP, et al. Tibial osteotomies for cranial cruciate ligament insufficiency in dogs. *Veterinary Surgery* 2008;37:111-125.
58. Korvick DL, Pijanowski GJ, Schaeffer DJ: Three-dimensional kinematics of the intact and cranial cruciate ligament deficient stifle of dogs. *J Biomech* 27:77-87, 1994.
59. Kowaleski MP, Apelt D, Mattoon JS, et al. The Effect of Tibial Plateau Leveling Osteotomy Position on Cranial Tibial Subluxation: An In Vitro Study. *Veterinary Surgery* 2005;34:332-336.
60. Lafaver S, Miller NA, Stubbs WP, et al. Tibial tuberosity advancement for stabilization of the canine cranial cruciate ligament-deficient stifle joint: surgical technique, early results, and complications in 101 dogs. *Veterinary Surgery* 2007;36:573-586.

61. Lancourt JE, Cristini JA. Patella alta and patella infera. Their etiological role in patellar dislocation, chondromalacia, and apophysitis of the tibial tubercle. *J Bone Joint Surg Am.* 1975;57:1112-1115.
62. Lazar TP, Berry CR, et al. Long-term radiographic comparison of tibial plateau leveling osteotomy versus extracapsular stabilization for cranial cruciate ligament rupture in the dog. *Veterinary Surgery* 2005;34:133-141.
63. Li G, Gil J, et al. A validated three-dimensional computational model of a human knee joint. *Journal of biomechanical engineering* 1999;121:657-662.
64. Limbert G, Taylor M, Middleton J. Three-dimensional finite element modelling of the human ACL: simulation of passive knee flexion with a stressed and stress-free ACL. *Journal of biomechanics* 2004;37:1723-1731.
65. Limbert, G., Taylor, M., 2001b. Three-dimensional finite element modelling of the human anterior cruciate ligament. Influence of the initial stress field. In: Middleton, J., Jones, M.L., Pande, G.N. (Eds.), *Computer Methods in Biomechanics and Biomedical Engineering*. Vol. 3. Gordon and Breach Science Publishers, London, pp. 355–360.
66. Linder LH, Sukin DL, Burks RT, et al. Biomechanical and histologic properties of the canine patellar tendon after removal of its medial third. *American Journal of Sports Medicine* 1994;22:136-142.
67. Markolf, K.L., Gorek, J.F., Kabo, J.M., Shapiro, M.S., 1990. Direct measurement of resultant forces in the anterior cruciate ligament. An in vitro study performed with a new experimental technique. *Journal of Bone and Joint Surgery* 72A (4), 557–567.

68. Marsolais GS, McLean S, Derrick T, et al. Kinematic analysis of the hind limb during swimming and walking in healthy dogs and dogs with surgically corrected cranial cruciate ligament rupture. *JAVMA* 2003;222:739-743.
69. Mattern KL, Berry CR, Peck JN, et al. Radiographic and ultrasonographic evaluation of the patellar ligament following tibial plateau leveling osteotomy. *Veterinary Radiology & Ultrasound* 2006;47:185-191.
70. Meijer, R.C.M.B., Huiskes, R., Kauer, J.M.G., 1989. A stereophotogrammetric method for measurements of ligament structure. *Journal of Biomechanics* 22, 177–184.
71. Meister BR, Michael SP, Moyer RA, et al. Anatomy and kinematics of the lateral collateral ligament of the knee. *Am J Sports Med* 2000;28:869-878.
72. Miller JM, Shires PK, et al. Effect of 9 mm tibial tuberosity advancement on cranial tibial translation in the canine cranial cruciate ligament-deficient stifle. *Veterinary Surgery* 2007;36:335-340.
73. Miller ME, Evans HE, Christensen GC. *Miller's Anatomy of the Dog* (2nd edition). Philadelphia: W.B Saunders Company, 1979.
74. Miller TT, Staron RB, Feldman F. Patellar height on sagittal MR imaging of the knee. *AJR* 1996;167:339-341.
75. Moeller EM, Cross AR, Rapoff AJ. Change in tibial plateau angle after tibial plateau leveling osteotomy in dogs. *Veterinary Surgery* 2006;35:460-464.
76. Moeller TB, Emil Reif, and T.C. Telger. *Pocket Atlas of Sectional Anatomy CT and MRI* (2 ed.). New York: Thieme, 2000.

77. Monahan JJ, Grigg P, et al. In vivo strain patterns in the four major canine knee ligaments. *Journal of Orthopaedic Research* 1984;2:408-418.
78. Montavon PM, Damur DM, Tepic S: Advancement of the tibial tuberosity for the treatment of cranial cruciate deficient canine stifle. *Proceedings of the 1st World Orthopaedic Veterinary Congress; Munich Germany, September 2002*, p. 152.
79. Montavon PM, Damur DM, Tepic S: Tibial tuberosity advancement (TTA) for the treatment of cranial cruciate disease in dogs: evidences, technique and initial clinical results. *Proceedings of the 12th ESVOT Congress, Munich Germany, September 2004*, pp 254-255.
80. Montavon PM, Tepic S. Joint surgery in canine hind limb - recent contributions from the university of zurich. *European Companion Animal Health* 2006;25-28.
81. Mostafa AA, Griffon DJ, Thomas MW, et al. Proximodistal Alignment of the Canine Patella: Radiographic Evaluation and Association with Medial and Lateral Patellar Luxation. *Veterinary Surgery* 2008;31:201-211.
82. Osmond CS, Marcellin-Little DJ, Harrysson OLA, et al. Morphometric assessment of the proximal portion of the tibia in dogs with and without cranial cruciate ligament rupture. *Veterinary Radiology & Ultrasound* 2006;47:136-141.
83. Peña E, Calvo B, Martínez MA, et al. A three-dimensional finite element analysis of the combined behavior of ligaments and menisci in the healthy human knee joint. *Journal of Biomechanics* 2006;39:1686-1701.
84. Phatak NS, Sun Q, et al. Noninvasive determination of ligament strain with deformable image registration. *Annals of biomedical engineering* 2007;35:1175-1187.

85. Pioletti, D.P., 1997. Viscoelastic properties of soft tissues: Application to knee ligaments and tendons. Departement de Physique. Lausanne, Switzerland, Ecole Polytechnique Fédérale de Lausanne.
86. Policy Implications of the Computed Tomography (CT) Scanner: An Update. Washington DC, U.S. Government Printing Office, 1981.
87. Priddy II NH, Tomlinson JL, et al. Complications with and owner assessment of the outcome of tibial plateau leveling osteotomy for treatment of cranial cruciate ligament rupture in dogs: 193 cases (1997-2001). JAVMA 2003;222:1726-1732.
88. Prokop Mathias, Michael Galanski, Aart Van Der Molen, et al. Spiral and Multislice Computed Tomography of the Body. New York: Thieme, 2000.
89. Ralphs SC, Whitney WO. Arthroscopic evaluation of menisci in dogs with cranial cruciate ligament injuries: 100 cases (1999-2000). JAVMA 2002;221:1601-1604.
90. Rayward RM, Thomson DG, Davies JV, et al. Progression of Osteoarthritis Following TPLO Surgery: a Prospective Radiographic Study of 40 Dogs. Journal of Small Animal Practice 2004;45:92-97.
91. Reif U OLA, Hulse DA, Hauptman JG. Effect of Tibial Plateau Leveling on Stability of the Canine Cranial Cruciate-Deficient Stifle Joint: An In Vitro Study. Veterinary Surgery 2002;31:147-154.
92. Reiser M, Banno T, Takahashi M, et al. Multislice CT. New York: Springer, 2004.
93. Renstrom, P., Arms, S.W., Stanwyck, T.S., Johnson, R.J., Pope, M.H., 1986. Strain within the anterior cruciate ligament during hamstring and quadriceps activity. American Journal of Sports in Medicine.

94. Rivière, Patrick. *Medical Imaging Systems Technology: Analysis and Computational Methods* (Chapter 1). Singapore: World Scientific Publishing Co., 2005.
95. Rooster H, Vangheluwe L, Van Bree H, et al. Biomechanical Properties of Braided Polyester Tapes Intended for use as Intra-articular Cranial Cruciate Ligament Prostheses in Dogs. *AJVR* 2001;62:48-53.
96. Schoepf UJ, Aldrich JE, Becker CR. *Multidetector-Row CT of the Thorax*. New York: Springer, 2003.
97. Schwandt CS, Bohorquez-Vanelli A, Tepic S, et al. Angle between the patellar ligament and tibial plateau in dogs with partial rupture of the cranial cruciate ligament. *AJVR* 2006;67:1855-1860.
98. Schwandt CS, Bohorquez-Vanelli A, Tepic S, et al. Angle between the patellar ligament and tibial plateau in dogs with partial rupture of the cranial cruciate ligament. *AJVR* 2006;67:1855-1860.
99. Seil R, Müller B, et al. Reliability and interobserver variability in radiological patellar height ratios. *Knee Surg, Sports Traumatol, Arthrosc* 2000;8:231-236.
100. Setton LA, Mow VC, et al. Mechanical properties of canine articular cartilage are significantly altered following transection of the anterior cruciate ligament. *Journal of orthopaedic research* 1994;12:451-463.
101. Shahar R, Banks-Sills L, Eliasy R. Mechanics of the canine femur with two types of hip replacement stems. *Vet Comp Orthop Traumatol* 2003;3:145-152.
102. Shahar R, Banks-Sills L, Eliasy R. Stress and strain distribution in the intact canine femur: finite element analysis. *Medical Engineering & Physics* 2003;25:387-395.

103. Shahar R, Banks-Sills L. A Quasi-Static Three-Dimensional, Mathematical, Three-Body Segment Model of the Canine Knee. *Journal of Biomechanics* 2004;37:1849-1859.
104. Shahar R, Milgram J. Biomechanics of Tibial Plateau Leveling of the Canine Cruciate-Deficient Stifle Joint: A Theoretical Model. *Veterinary Surgery* 2006;35:144-149.
105. Shelburne KB, Pandy MG, Torry MR. Comparison of shear forces and ligament loading in the healthy and ACL-deficient knee during gait. *Journal of Biomechanics* 2004;37:313-319.
106. Shires PK, Hulse DA, Liu W: The under-and-over fascial replacement technique for anterior cruciate ligament rupture in the dog: A retrospective study. *J Am Anim Hosp Assoc* 20:69-77, 1984.
107. Silverman, Paul M. *Multislice Computed Tomography: A Practical Approach to Clinical Protocols*. Philadelphia: Lippincott Williams & Wilkins, 2002.
108. Slocum B, Devine T: Cranial tibial thrust: a primary force in the canine stifle. *J Am Vet Med Assoc* 183:456-459, 1983
109. Slocum B, Slocum TD. Tibial plateau leveling osteotomy for repair of cranial cruciate ligament rupture in the canine. *Vet Clin North Am Small Anim Pract* 1993; 23: 777-95.
110. Song Y, Debski RE, et al. A three-dimensional finite element model of the human anterior cruciate ligament: a computational analysis with experimental validation. *Journal of biomechanics* 2004;37:383-390.
111. Spindler KP, Murray MM, et al. The central ACL defect as a model for failure of intra-articular healing. *Journal of orthopaedic research* 2006;401-406.

112. Stauffer KD, Tuttle TA, Elkins AD, et al. Complications Associated With 696 Tibial Plateau Leveling Osteotomies (2001-2003). *Journal of the American Animal Hospital Association* 2006;42:44-50.
113. Sun Q, Dhaher Y. Three-dimensional hyperelastic model of the human knee: a parametric sensitivity study. Northwestern University and Rehabilitation Institute of Chicago, Chicago.
114. Tashman S, Anderst W, Kolowich P, et al: Kinematics of the ACL-deficient canine knee during gait: serial changes over two years. *J Orthop Res* 22:931–941, 2004.
115. Tepic S, Damur DM, Montavon PM: Biomechanics of the stifle joint. Proceedings of the 1st World Orthopaedic Veterinary Congress, Munich Germany, September 2002, pp 189–190.
116. Tepic S, Montavon PM: Is cranial tibial advancement relevant in the cruciate deficient stifle? Proceedings of the 12th ESVOT Congress, Munich Germany, September 2004, pp 132–133.
117. Thomas TM, Marcellin-Little DJ, Roe SC, et al. Comparison of measurements obtained by use of an electrogoniometer and a universal plastic goniometer for the assessment of joint motion in dogs. *AJVR* 2006;67:1974-1979.
118. Triple Tibial Osteotomy (TTO). <www.vetinst.com>
119. van Dijk, R., Huiskes, R., Selvik, G., 1979. Roentgen stereophotogrammetric methods for the evaluation of the three-dimensional kinematic behavior and cruciate ligament length patterns of the human knee joint. *Journal of Biomechanics* 12, 727–731.

120. Vasseur PB, Arnoczky SP. Collateral Ligaments of the Canine Stifle Joint: Anatomic and Functional Analysis. *Am J Vet Res* 1981;42:1133-1137.
121. Warzee CC, Dejardin LM, Arnoczky SP, et al. Effect of Tibial Plateau Leveling on Cranial and Caudal Tibial Thrusts in Canine Cranial Cruciate-Deficient Stifles: An In Vitro Experimental Study. *Veterinary Surgery* 2001;30:278-286.
122. Weiss JA, Gardiner JC, Ellis BJ, et al. Three-dimensional finite element modeling of ligaments: Technical aspects. *Medical Engineering & Physics* 2005;27:845-861.
123. Woo SLY, Debski RE, Withrow JD, et al. Biomechanics of knee ligaments. *Am J Sports Med* 1999;27:533-543.
124. Yao J, Snibbe J. Stresses and strains in the medial meniscus of an ACL deficient knee under anterior loading: a finite element analysis with image-based experimental validation. *Journal of biomechanical engineering* 2006;128:135-141.
125. Zachos TA, Arnoczky SP, Lavagnino M, et al. The Effect of Cranial Cruciate Ligament Insufficiency on Caudal Cruciate Ligament Morphology: An Experimental Study in Dogs. *Veterinary Surgery* 2002;31:596-603.
126. Zielinska B, Donahue TLH. 3D finite element model of meniscectomy: changes in joint contact behavior. *Journal of biomechanical engineering* 2006;128:115-123.

APPENDICES

APPENDIX A

Table A.1: Comparison of coarse and medium meshes to the finest mesh.

	% Diff Coarse - Fine	% Diff Medium - Fine
# of elements	56.00	33.14
Maximum Stress	4.73	5.26

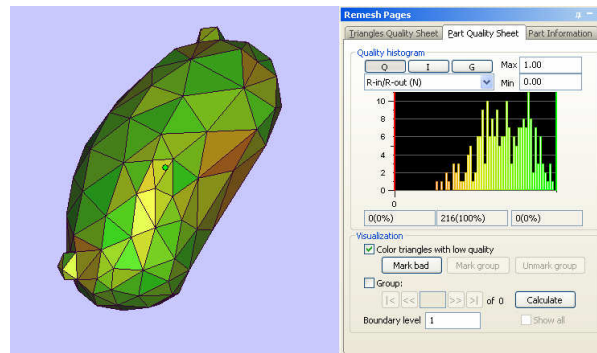


Figure A.1: Mesh quality and appearance of the patella.

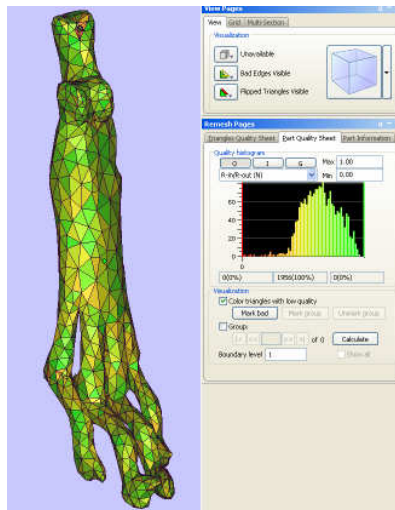


Figure A.2: Meshed hock with 110° proximal interphalangeal joint.

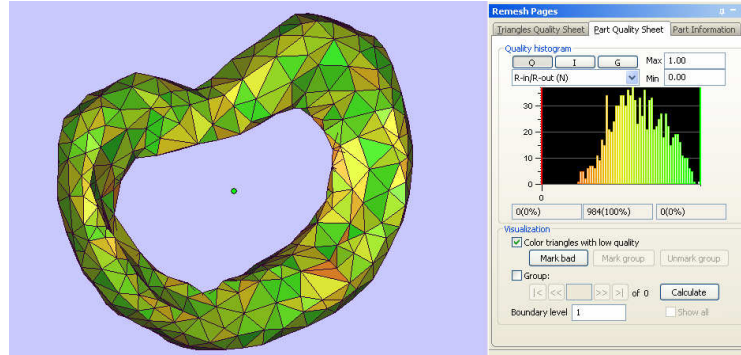


Figure A.3: Final meshed meniscus after boolean operations, shrink-wrap and remeshing.

Table A.2: Ligament geometry obtained from CT data.

	Origin	Middle	Insertion
Patellar Ligament	12.24mm x 12.11mm	9.28mm x 6.16mm	8.29mm x 8.37mm
Lateral Collateral	4.05mm x 1.78mm	3.56mm x 1.02mm	3.75mm x 1.65mm
Medial Collateral	14.00mm x 2.78mm	12.16mm x 1.25mm	5.63mm x 5.79mm
Cranial Cruciate	5.17mm x 4.93mm	2.73mm x 2.17mm	3.94mm x 2.69mm
Caudal Cruciate	4.90mm x 3.55mm	2.52mm x 1.28mm	5.50mm x 2.45mm

Table A.3: Stress (MPa) in each of the modeled ligaments of the PS intact and PS transected stifle joints at an angle of 75°.

	75 Degrees (Stress MPa)	
	PS Intact	PS transected
CaCL	4.09	4.29
LCL	0.11	0.12
MCL	2.94	3.20
PL	1.77	1.71
CCL	0.73	

Table A.4: Stress (MPa) in each of the modeled ligaments of the PS intact and PS transected stifle joints at an angle of 113°.

	113 Degrees (Stress MPa)	
	PS Intact	PS transected
CaCL	0.60	1.50
LCL	0.42	0.43
MCL	0.64	0.53
PL	0.22	0.24
CCL	0.96	

Table A.5: Stress (MPa) in each of the modeled ligaments of the PS intact and PS transected stifle joints at an angle of 148°.

	148 Degrees (Stress MPa)	
	PS Intact	PS transected
CaCL	0.24	0.24
LCL	0.13	0.13
MCL	0.28	0.29
PL	0.13	0.14
CCL	0.34	

Table A.6: Stress (MPa) in each of the modeled ligaments at a stifle angle of 75°.

	75 Degrees (Stress MPa)				
	PS Intact	PS transected	TPLO	TTA	TTO
CaCL	4.09	4.29	4.45	13.80	4.06
LCL	0.11	0.12	0.07	0.07	0.07
MCL	2.94	3.20	1.95	3.62	2.28
PL	1.77	1.71	4.26	2.85	1.81
CCL	0.73				

Table A.7: Stress (MPa) in each of the modeled ligaments at a stifle angle of 113°.

113 Degrees (Stress MPa)					
	PS Intact	PS transected	TPLO	TTA	TTO
CaCL	0.60	1.50	9.34	0.77	1.37
LCL	0.42	0.43	0.66	0.60	0.52
MCL	0.64	0.53	1.24	0.90	1.28
PL	0.22	0.24	0.62	0.34	0.43
CCL	0.96				

Table A.8: Stress (MPa) in each of the modeled ligaments at a stifle angle of 148°.

148 Degrees (Stress MPa)					
	PS Intact	PS transected	TPLO	TTA	TTO
CaCL	0.24	0.24	0.00	0.01	0.00
LCL	0.13	0.13	0.11	0.13	0.21
MCL	0.28	0.29	0.37	0.28	0.38
PL	0.13	0.14	0.06	0.12	0.09
CCL	0.34				

In Tables A.9, and A.10 below, the calculations for tibial translation based on nodal displacements are recorded for each model. Table A.11 shows a guide to understanding the calculations shown in Table A.10 and the relationships to cranial and caudal subluxation.

Table A.9: Displacement measurements between tibia and femur nodes for all models.

Model		Original Coordinates			Deformation Coords.			U: Magnitude	$\Delta U = U_{femur} - U_{tibia}$
		X	Y	Z	X	Y	Z		
Intact75	Femur	293.265	-61.7133	-539.334	293.309	-62.1882	-546.727	7.40826	0.63768
	Tibia	292.083	-49.0066	-545.866	292.085	-49.6333	-552.607	6.77058	
Intact113	Femur	293.265	16.5018	-385.806	293.264	16.257	-386.08	3.68E-01	0.02204
	Tibia	290.624	26.1736	-406.078	290.624	25.9386	-406.332	3.46E-01	
Intact148	Femur	293.719	161.019	-312.265	293.719	160.911	-312.288	1.11E-01	-0.011808
	Tibia	290.414	159.153	-340.771	290.415	159.033	-340.796	1.23E-01	
Trans75	Femur	293.265	-61.7133	-539.334	293.308	-62.2093	-547.141	7.82328	0.6987
	Tibia	290.624	-48.9682	-548.995	290.626	-49.5366	-556.097	7.12458	
Trans113	Femur	293.265	16.5018	-385.806	293.263	16.258	-386.08	3.67E-01	0.019542
	Tibia	290.624	26.1736	-406.078	290.624	25.9376	-406.333	3.47E-01	
Trans148	Femur	293.719	161.019	-312.265	293.719	160.746	-312.322	2.79E-01	0.023683
	Tibia	290.414	159.153	-340.771	290.414	158.903	-340.822	2.56E-01	
TPLO75	Femur	289.26	-60.6043	-547.174	289.276	-60.8134	-552.721	5.551	0.30718
	Tibia	286.52	-48.7214	-548.617	286.521	-49.1674	-553.842	5.24382	
TPLO113	Femur	288.706	12.8035	-391.576	288.699	12.4809	-391.958	5.01E-01	0.001794
	Tibia	286.52	26.3602	-406.094	286.52	26.0215	-406.46	4.99E-01	
TPLO148	Femur	288.746	152.1	-317.78	288.746	151.909	-317.829	1.97E-01	0.018271
	Tibia	286.479	159.097	-341.329	286.479	158.922	-341.365	1.79E-01	
TTA75	Femur	293.185	-61.0739	-540.6	293.233	-61.5548	-549.332	8.74563	0.67698
	Tibia	290.624	-48.2045	-549.58	290.624	-48.8173	-557.625	8.06865	
TTA113	Femur	293.293	16.3536	-385.395	293.289	16.0645	-385.717	4.33E-01	0.027148
	Tibia	290.624	26.0655	-405.726	290.624	25.7838	-406.018	4.06E-01	
TTA148	Femur	293.293	160.734	-312.053	293.292	160.524	-312.098	2.15E-01	0.020982
	Tibia	290.624	159.453	-340.927	290.624	159.264	-340.965	1.94E-01	
TTO75	Femur	293.945	-63.7206	-551.304	293.98	-63.863	-558.784	7.48108	0.61638
	Tibia	291.299	-50.4569	-556.385	291.299	-50.809	-563.241	6.8647	
TTO113	Femur	294.27	7.1272	-393.852	294.269	6.58154	-394.525	8.67E-01	0.056973
	Tibia	291.187	19.1677	-409.208	291.186	18.6349	-409.818	8.10E-01	
TTO148	Femur	293.851	145.509	-314.411	293.851	145.049	-314.538	4.77E-01	0.031521
	Tibia	291.187	150.413	-340.744	291.186	149.98	-340.848	4.45E-01	

Table A.10: Final calculations for subluxation measurements.

Model		Changes in position (mm)			Subluxation Measurement (mm)		
		ΔX	ΔY	ΔZ	ΔX	ΔY	ΔZ
Intact75	Femur	0.044	-0.4749	-7.393	0.042	0.1518	-0.652
	Tibia	0.002	-0.6267	-6.741			
Intact113	Femur	-0.001	-0.2448	-0.274	-0.001	-0.0098	-0.02
	Tibia	0	-0.235	-0.254			
Intact148	Femur	0	-0.108	-0.023	-0.001	0.012	0.002
	Tibia	0.001	-0.12	-0.025			
Trans75	Femur	0.043	-0.496	-7.807	0.041	0.0724	-0.705
	Tibia	0.002	-0.5684	-7.102			
Trans113	Femur	-0.002	-0.2438	-0.274	-0.002	-0.0078	-0.019
	Tibia	0	-0.236	-0.255			
Trans148	Femur	0	-0.273	-0.057	0	-0.023	-0.006
	Tibia	0	-0.25	-0.051			
TPLO75	Femur	0.016	-0.2091	-5.547	0.015	0.2369	-0.322
	Tibia	0.001	-0.446	-5.225			
TPLO113	Femur	-0.007	-0.3226	-0.382	-0.007	0.0161	-0.016
	Tibia	0	-0.3387	-0.366			
TPLO148	Femur	0	-0.191	-0.049	0	-0.016	-0.013
	Tibia	0	-0.175	-0.036			
TTA75	Femur	0.048	-0.4809	-8.732	0.048	0.1319	-0.687
	Tibia	0	-0.6128	-8.045			
TTA113	Femur	-0.004	-0.2891	-0.322	-0.004	-0.0074	-0.03
	Tibia	0	-0.2817	-0.292			
TTA148	Femur	-0.001	-0.21	-0.045	-0.001	-0.021	-0.007
	Tibia	0	-0.189	-0.038			
TTO75	Femur	0.035	-0.1424	-7.48	0.035	0.2097	-0.624
	Tibia	0	-0.3521	-6.856			
TTO113	Femur	-0.001	-0.54566	-0.673	0	-0.01286	-0.063
	Tibia	-0.001	-0.5328	-0.61			
TTO148	Femur	0	-0.46	-0.127	0.001	-0.027	-0.023
	Tibia	-0.001	-0.433	-0.104			

Table A.11: Guide for determining any present subluxation based on values in Table A.10.

		Difference= Femur-Tibia	Subluxation
Femur	positive	positive	no
Tibia	positive	negative	cranial tibial
Femur	positive	positive	caudal tibial
Tibia	negative		
Femur	negative	negative	cranial tibial
Tibia	positive		
Femur	negative	negative	no
Tibia	negative	positive	caudal tibial

APPENDIX B

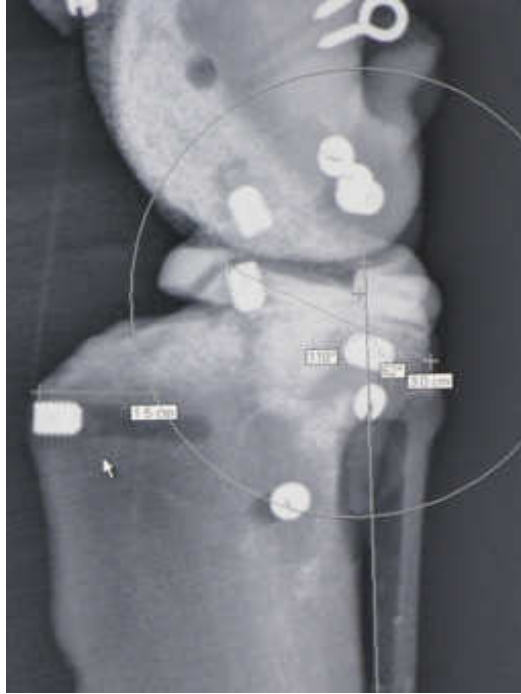


Figure B.1: Mediolateral radiograph of physical model used for TPLO pre-surgical planning [30].

Table B.1: Excerpt of TPLO ventral rotation guide for TPA of 25°-30° [30].

Tibial Angle	12mm	15mm	18mm (2.7pk)	20mm	24mm (3.5pk)	27mm	30mm
25.00	4.25	5.50	6.00	6.98	8.25	9.25	10.40
26.00	4.40	6.00	6.25	7.33	8.75	9.70	11.00
27.00	4.60	6.25	6.75	7.68	9.00	10.15	11.50
28.00	4.85	6.50	7.00	8.02	9.50	10.60	12.00
29.00	5.00	6.75	7.25	8.37	10.00	11.05	12.50
30.00	5.25	7.00	7.50	8.72	10.25	11.60	13.00

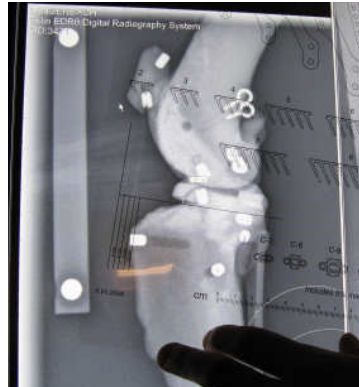


Figure B.2: Mediolateral radiograph of extended stifle and TTA plate template (Kyon).



Figure B.3: TTO cutting jig used to perform the tibial crest osteotomy.



Figure B.4: Resulting TTO, secured with 3.5mm broad TPLO plate (Synthes, Inc.)